WL-TR-90-29

(2)

BEAM AND PLASMA PHYSICS RESEARCH

Robert F. Stellingwerf
Robert E. Peterkin, Jr
Donald J. Sullivan

Mission Research Corporation
1720 Randolph Road SE
Albuquerque, NM 87106-4245

June 1990

Final Report

Weapons Laboratory
Air Force Systems Command
Kirtland Air Force Base, NM 87117-6008

This final report was prepared by Mission Research Corporation, Albuquerque, New Mexico, under Contract F29601-86-C-0216, Job Order 57972406, with the Weapons Laboratory, Kirtland Air Force Base, New Mexico. The Project Officer-in-Charge was Dr David W. Price (AWX).

When Government drawings, specifications, or other data are used for any purpose other than in connection with a definitely Government-related procurement, the United States Government incurs no responsibility or any obligation whatsoever. The fact that the Government may have formulated or in any way supplied the said drawings, specifications, or other data, is not to be regarded by implication, or otherwise in any manner construed, as licensing the holder, or any other person or corporation; or as conveying any rights or permission to manufacture, use, or sell any patented invention that may in any way be related thereto.

This report has been authored by a contractor of the United States Government. Accordingly, the United States Government retains a nonexclusive, royalty-free license to publish or reproduce the material contained herein, or allow others to do so, for the United States Government purposes.

This report has been reviewed by the Public Affairs Office and is releasable to the National Technical Information Service (NTIS). At NTIS, it will be available to the general public, including foreign nationals.

If your address has changed, if you wish to be removed from our mailing list, or if your organization no longer employs the addressee, please notify WL/AWX, Kirtland AFB, NM 87117-6008 to help us maintain a current mailing list.

This technical report has been reviewed and is approved for publication.

David W. Price

DAVID W. PRICE, PhD
Project Officer

FOR THE COMMANDER

J. DOUGLAS BEASON
Major, USAF
Chief, High Energy Plasma Division

DO NOT RETURN COPIES OF THIS REPORT UNLESS CONTRACTUAL OBLIGATIONS OR NOTICE ON A SPECIFIC DOCUMENT REQUIRES THAT IT BE RETURNED.

REPORT DOCUMENTATION PAGE

Form Approved
OMB No. 0704-0188

1. AGENCY USE ONLY (Leave blank)	2. REPORT DATE	3. REPORT TYPE AND DATES COVERED
	1990 June	Final Aug 86 to Mar 90

4. TITLE AND SUBTITLE

BEAM AND PLASMA PHYSICS RESEARCH

5. FUNDING NUMBERS

PE # 62601F
PR # 5797
TA # 24
WU # 06

C # F29601-86-C-0216

6. AUTHOR(S)

Stellingwerf, Robert F.
Peterkin, Robert E., Jr
Sullivan, Donald J.

7. PERFORMING ORGANIZATION NAME(S) AND ADDRESS(ES)

Mission Research Corporation
1720 Randolph Road SE
Albuquerque, NM 87106-4245

8. PERFORMING ORGANIZATION REPORT NUMBER

MRC/ABQ-R-1281

9. SPONSORING/MONITORING AGENCY NAME(S) AND ADDRESS(ES)

Weapons Laboratory
Kirtland AFB, NM 87117-6008

10. SPONSORING/MONITORING AGENCY REPORT NUMBER

WL-TR-90-29

11. SUPPLEMENTARY NOTES

Beams	Microwaves	HPM
Pulse power	Plasma physics	
MHD	PIC	

12a. DISTRIBUTION/AVAILABILITY STATEMENT

Approved for public release; distribution unlimited.

12b. DISTRIBUTION CODE

13. ABSTRACT *(Maximum 200 words)*

Mission Research Corporation performed analysis for ~~the Weapons Laboratory~~ in high power microwave computations and theory and high energy plasma computations and theory.

The HPM computations concentrated on generation, sources and propagation. Major codes used were the particle-in-cell codes SOS and ISIS. Topics studies were sources and antennas, propagation, relativistic klystron amplifiers, virtual cathode oscillators, magnetically insulated transmission lines, transvertrons and vircator phase/frequency locking.

High energy plasmas were analyzed with MACH2, an implicit continuous Eulerian, arbitrary Lagrangian-Eulerian nonideal magnetohydrodynamic code. MACH2 modelled a variety of high energy plasmas including plasma flow switches, imploding liners and plasmas, compact toroids, magnetic reconnection and plasma guns. A smooth particle hydrodynamics code was developed to model various conditions, including shock heating, explosions and implosions. An optical multichannel analyzer was also provided to analyze plasma emission line spectra.

14. SUBJECT TERMS

Beams	Microwaves	HPM
Pulse power	Plasma physics	
MHD	PIC	

15. NUMBER OF PAGES

128

16. PRICE CODE

17. SECURITY CLASSIFICATION OF REPORT	18. SECURITY CLASSIFICATION OF THIS PAGE	19. SECURITY CLASSIFICATION OF ABSTRACT	20. LIMITATION OF ABSTRACT
UNCLASSIFIED	UNCLASSIFIED	UNCLASSIFIED	SAR

NSN 7540-01-280-5500

Standard Form 298 (Rev 2-89)
Prescribed by ANSI Std Z39-18
298-102

ACKNOWLEDGMENTS

Mission Research Corporation wishes to acknowledge the support given by Weapons Laboratory staff members throughout the 43-month effort that is covered by this report. Special thanks are due to Dr. William Baker, Majors J. Douglas Beason, Chuck Beason, William McCullough, and Bruce Anderson, Drs. James Degnan, Ray Lemke, David Price, and Kirk Hackett, and Captains Carl Sovinec, Christopher Clouse, and Kyle Hendricks.

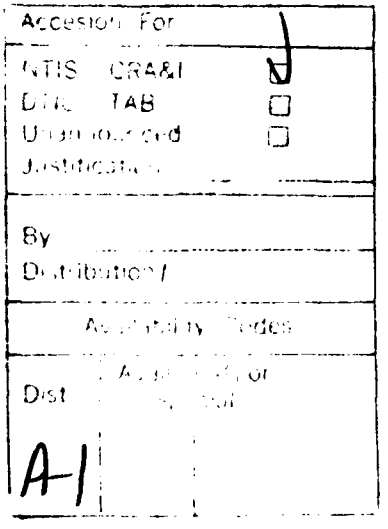

CONTENTS

CONTENTS (CONCLUDED)

FIGURES

FIGURES (CONTINUED)

FIGURES (CONCLUDED)

TABLES

1.0 INTRODUCTION

1.1 CONTRACTUAL INFORMATION

This final technical report under the Air Force "Beam and Plasma Physics Research" program, Contract F29601-86-C-0216, presents summaries of technical activities and tabulations of data items delivered for the 19 subtasks that were performed. This document has been prepared for the Weapons Laboratory (WL), Kirtland Air Force Base, New Mexico, by Mission Research Corporation (MRC).

The technical and management efforts described herein represent the accomplishment of contract and subtask objectives and fulfillment of technical requirements by the staffs of MRC (the prime contractor) and Science Applications International Corporation, Battelle Memorial Institute, and Numerex (the subcontractors).

1.2 CONTRACT OBJECTIVES

The contract objectives were to pursue fundamental physics and technology issues critical to the development of advanced weapons concepts. This was to be accomplished by conducting theoretical, computational, and experimental investigations in the areas of high-power radio frequency (RF) emission and charged-particle beams, high-energy plasma physics, and pulsed-power technologies; and by conducting developmental studies in these areas.

Two different work areas were involved: High-Power RF Emission and Charged-Particle Beam Physics Computation, Modeling and Theory; and Plasma Physics Computation, Modeling and Theory. The scope of the work included:

1. Numerical simulations of particle and field interactions using particle-in-cell codes, such as CCUBE and ISIS, to predict and analyze the performance of experiments and to provide a basis for design or modification of current and future experiments

2. Studies and analyses of high-power RF, charged-particle beam sources and source physics, and possible high-power RF weapons missions and associated high-power microwave (HPM) generation systems

3. Analysis and design of RF radiating structures for use with HPM weapons sources

4. Theoretical studies and development of models to determine key physical conditions required to successfully propagate HPM through the atmosphere and to analyze and design RF amplifier concepts for use with HPM generators

5. Evaluation and analysis of methods for phase locking multiple RF sources, including oscillators and amplifiers, to predict key experimental parameters impacting the successful development of HPM concepts

6. Theoretical studies and development of analytic models to model the dynamics of charged-particle beam generation, transport and propagation in various gases at various pressures to predict beam propagation and analyze propagation issues

7. Numerical simulations of plasma behavior to predict and analyze results and performance of current, planned, and potential experiments using existing computer codes

8. Evaluation and analysis of the effects of modifications to pulsed power systems on the system output using existing circuit, slug model, and one-dimensional response codes

9. Development of analytic models and scaling laws to isolate and predict key experimental parameters, including plasma component densities, plasma component temperatures, plasma component currents, electric and magnetic fields, and radiation output, impacting successful development of ongoing and future plasma devices

Specific projects were defined in subtask statements issued by the WL. Mission Research Corporation sometimes assisted in the work definition by recommending subtask work statements where studies indicated a need for such work. The approved subtask statements included definition of the objectives, technical requirements, delivery schedule, and level of effort.

1.3 OVERVIEW

The conduct of the Beam and Plasma Physics Research program involved the pursuit of program objectives and performance of technical requirements under 19 separate subtasks which varied in level of effort and complexity. The subtask titles, identifying numbers, periods of performance, and other information pertaining to the scheduled work are summarized in Table 1.

The contract period began on 5 August 1986 and ended on 31 March 1990. The first subtasks were issued by the WL on 4 September 1986. Technical effort continued for

TABLE 1. Beam and Plasma Physics Research Subtasks.

Subtask Number	Last Amendment	Subtask Title	Original DOA	DOA Last Amendment	Duration (Months)	Funding (%)	LOE (Hours)
TASK AREA 2—HIGH POWER RF EMISSION AND CHARGED PARTICLE BEAM PHYSICS COMPUTATION. MODELING AND THEORY							
02-01	02	Microwave Source and Antenna Scoping Study	09/04/86	12/14/87	20	2.0	709.50
02-02	01	High Power Microwave Vircator Design	01/07/87	07/14/87	12	9.2	3566.00
02-03	02	Sparse Air Breakdown Microwave Propagation Study	01/28/87	10/25/89	29	5.7	1521.50
02-04	01	Vircator Phase/Frequency Locking Studies	08/17/87	02/02/88	9.5	1.1	465.50
02-05	01	High Power Microwave Vulnerability of Space Assets	09/28/87	02/25/88	12	7.5	1867.00
02-06	00	Microwave Computer Program Enhancements	12/30/87	—	6	3.7	1610.50
02-07	01	High Power Microwave Transvertron Design	02/03/88	09/12/88	9	3.6	1417.00
02-08	00	Repetitive Pulse MITL Physics Study	07/20/88	—	9.5	4.6	1873.75
02-09	02	Microwave PIC Code Optimization and Enhancements	07/21/88	05/19/89	13.5	3.3	1532.25
02-10	02	Microwave Source Design Improvements	07/21/88	05/18/89	9.5	2.5	1101.25

TABLE 1. Concluded.

Subtask Number	Last Amendment	Subtask Title	Original DOA	DOA Last Amendment	Duration (Months)	Funding (%)	LOE (Hours)
TASK AREA 3—PLASMA PHYSICS COMPUTATION, MODELING AND THEORY							
03-01	01	SHIVA STAR Computational Physics Studies	09/04/86	09/26/86	1.5	1.1	406.00
03-02	03	SHIVA STAR Computational Physics Studies	09/26/86	07/14/87	12	13.2	4760.00
03-03	02	Coaxial Plasma Gun Physics Studies	01/14/87	08/17/87	8.5	2.0	1107.50
03-04	00	Compact Toriod Computational Physics Studies	05/15/87	—	5.5	1.7	626.00
03-05	01	SHIVA STAR Computational Physics Studies II	10/01/87	05/19/89	19.5	14.3	4712.00
03-06	01	Compact Toroid Accelerator Physics Studies	11/24/87	12/29/88	11	0.9	653.00
03-07	03	SHIVA STAR Computational Physics Studies III	10/13/88	10/25/89	16	16.9	5484.00
03-08	01	Smooth Particle Hydrodynamics	02/23/89	10/25/89	11.5	1.9	712.00
03-09	01	Plasma Jet Diagnostics	04/07/89	10/25/89	7	4.0	1312.25

29.5 months ending 15 February 1990. Throughout the contract, the total applied level of effort was 35,300 hours. The level of effort percentage breakdown by hours expended, as contrasted to the dollars breakdown shown in Table 1, in the two work areas is as follows:

Work Area 2: High-Power RF Emission and Charged-Particle Beam Physics Computation, Modeling and Theory—44.4%

Work Area 3: Plasma Physics Computation, Modeling and Theory—55.6%

The individual subtasks are summarized in the remainder of this report. For each subtask a list of technical reports completed under the subtask is given. Abstracts are included.

2.0 SUMMARY OF RESEARCH PERFORMED UNDER THE BEAM AND PLASMA PHYSICS RESEARCH CONTRACT

2.1 REPORT INDEX

Reports generated under the contract are listed in Table 2.

TABLE 2. Index of reports.

Subtask Number	Report Title	Report Number	Page
02-01	MRC Microwave and Electron Beam Computer Programs	AFWL-TR-87-69 AMRC-R-886	11
02-01	Microwave Source and Antenna Scoping Study (Simulation of the Relativistic Klystron Amplifier)	MRC/ABQ-R-1228	13
02-02	A Preliminary Study of MITL Pulse Sharpening by a Radial Magnetic Field	AMRC-R-972	14
02-02	Analytical Study and Numerical Simulation of High Power Vircator and Transvertron Microwave Source	MRC/ABQ-R-1029	14
02-03	Sparse Air Breakdown Effects on Microwave Propagation	MRC/ABQ-R-1186	18
02-04	High Power Microwave Literature Review	MRC/ABQ-R-1028	21
02-04	SOS Simulation Support for the AFWL Vircator Phase/Frequency Locking	MRC/ABQ-R-1072	21
02-06	Microwave Computer Program Enhancements: Code Conversion	MRC/ABQ-R-1081	22

TABLE 2. Continued.

Subtask Number	Report Title	Report Number	Page
02-07	Transvertron Source Design and Analysis of Experimental Results	MRC/ABQ-R-1085	24
02-08	Repetitive Pulse MITL Physics Studies	MRC/ABQ-R-1234	26
02-09	Microwave Computer Program Enhancements, Part I: ISIS and PEGASUS, Part II: CFTLIB to FORTLIB Conversion Experiment	MRC/ABQ-R-1202	27
02-10	Beam and Plasma Physics Research Microwave Source Design Improvements	MRC/ABQ-R-1177	28
03-01	Initial Simulations of the Air Force Weapons Laboratory High Voltage Switch	AMRC-N-357	31
03-02	Simulations of a Plasma Flow Switch	AMRC-R-928	47
03-02	New MACH2 Grid Specification Method	AMRC-N-371	48
03-02	MACH2: A Two-Dimensional Magnetohydrodynamic Simulation Code for Complex Experimental Configurations	AMRC-R-874	48
03-02	Task Report: SHIVA STAR Computational Physics Studies I	MRC/ABQ-R-1036	48
03-03	Subtask Report: Coaxial Plasma Gun Physics Studies	MRC/ABQ-R-957	58
03-04	Demonstration of the Poloidal Field Capability of MACH2: Compact Toroid Simulations	AMRC-R-973	65
03-05	MACH2: A Reference Manual—Third Edition	MRC/ABQ-R-1066	77

TABLE 2. Concluded.

Subtask Number	Report Title	Report Number	Page
03-05	Compact Toroid Simulations with MACH2	MRC/ABQ-R-1130	77
03-05	Enhancement of the Radiation Yield in Plasma Flow Switch Experiments	MRC/ABQ-R-1171	77
03-05	SHIVA STAR Computational Physics Studies II	MRC/ABQ-R-1173	78
03-06	Compact Toroid Accelerator Physics Studies	MRC/ABQ-R-1162	83
03-07	A Material Strength Capability for MACH2	MRC/ABQ-R-1191	98
03-07	MACH2: A Reference Manual—Fourth Edition	MRC/ABQ-R-1207	99
03-07	A Two-Temperature Model for MACH2	MRC/ABQ-R-1260	99
03-07	Can MACH2 Run Faster If We Replace Double Vector Loops with Single Vector Loops?	MRC/ABQ-N-458	99
03-07	Dynamically Changing the Logical Computational Domain of a MACH2 Physics Simulation	MRC/ABQ-N-462	100
03-07	Anomalous Resistivity Considerations for Compact TORUS Formation and Decay	MRC/ABQ-N-463	100
03-07	MACH2: A Two-Dimensional Magnetohydrodynamic Simulation Code for Complex Experimental Configurations	—	100
03-07	SHIVA STAR Computational Physics Studies III	MRC/ABQ-R-1278	101
03-08	SPHC Manual	MRC/ABQ-R-1237	103
03-09	Diagnostic White Paper Contributions	MRC/ABQ-N-451	106

2.2 TASK AREA 2: HIGH-POWER RF EMISSION AND CHARGED-PARTICLE BEAM PHYSICS COMPUTATION, MODELING AND THEORY

2.2.1 Subtask 02-01, Microwave Source and Antenna Scoping Study

2.2.1.1 Research Summary. Under this subtask MRC provided planning of analytical and computational efforts. Appropriate computer programs were identified. Modifications to these computer codes were made to address specific needs of the WL HPM program. Such modifications have included addition of more sophisticated wave transmitting boundary conditions to the ISIS code and an on-going effort to provide consultation for both ISIS and SOS.

Existing codes were documented in a 1987 report by B. Godfrey. This report includes brief summaries of their physics capabilities and limitations. When updates or modifications of the computer programs were warranted, estimated resources were identified which were necessary to complete these efforts. Separate subtasks were then let to accomplish this work.

The third technical requirement was to suggest and perform scoping analyses of alternative HPM sources and antennas. A number of HPM sources were considered for use at the WL. These included various vircators, the transvertron oscillator and amplifier. In addition, a number of antenna concepts were explored for directing VHF radiation. Each of these areas became a separate subtask. They have resulted in a number of MRC reports and publications submitted to the WL under their individual task orders. During this work, informal meetings as well as briefings were held between WL and MRC scientists to coordinate these efforts.

The one scoping study which did not result in a separate subtask is the work on evaluating and simulating the Naval Research Laboratory's (NRL) relativistic klystron amplifier (RKA). In this device the strength of the magnetic field is quite large compared to the beam current density. The beam current density is approximately 650 A/cm^2 based on a radius of 6.6 cm, annulus of 0.3 cm, and total current of 16 kA (Ref. 1). A magnetic field of 10 kG (Ref. 2) then yields a value of around 11 for a measure of the beam "stiffness" given by

$$\frac{\omega_c/\gamma}{\omega_p/\gamma^{3/2}} \qquad (1)$$

This is a large number. A decrease of at least a factor of 2 may be possible without detrimentally affecting the operation of the RKA or its efficiency. Decreasing the magnetic field will result in a thicker beam. Quantifying how the decrease in I_{SCL} and coupling to the cavity gaps changes RKA output will be important. Nevertheless, the opportunity to make the overall RKA system more compact and increasing its wall plug efficiency should be tested.

The use of a coaxial drift tube geometry may lead to an RKA of extremely low impedance (Ref. 3). This in turn could yield microwave generation at unprecedented power levels, if the tube efficiency can be maintained. An immediate concern is the possibility of multimoding in the drift region of the beam due to the density of coaxial modes allowed to propagate in such a geometry. A plot of the lowest order TM_{mn} modes for various inner-to-outer conductor separations as a function of frequency is given in Figure 1. It shows that for frequencies as low as 3 GHz, the lowest order TM coaxial mode will propagate for conductor separations larger than 5 cm. If the klystron cavities are coupled through one of these modes or the TEM mode, which does not have a frequency cut off, the operation of the RKA may be significantly different from the normal klystron interaction. Indeed, this effect may already have been witnessed in preliminary coaxial RKA experiments at NRL (Ref. 2).

This report suggests that phase locking RKA's at the 1–10 GW level per tube would be a more straightforward approach to obtaining higher power levels in the near term.

2.2.1.2 Reports. Documents prepared under this subtask are summarized here.

"MRC Microwave and Electron Beam Computer Programs"
Brendan B. Godfrey
AFWL-TR-87-69, AMRC-R-886
April 1987

ABSTRACT: This report discusses some computer programs available for addressing the physics of HPM and charged-particle beam generation and propagation. Codes range from simple lumped-parameter models to detailed multidimensional simulations. The capabilities and underlying models of the microwave source, particle beam accelerator, and particle beam propagation codes are described. Although the more powerful of these programs can also be used for microwave propagation and antenna design, other programs specifically designed for these applications are typically used instead.

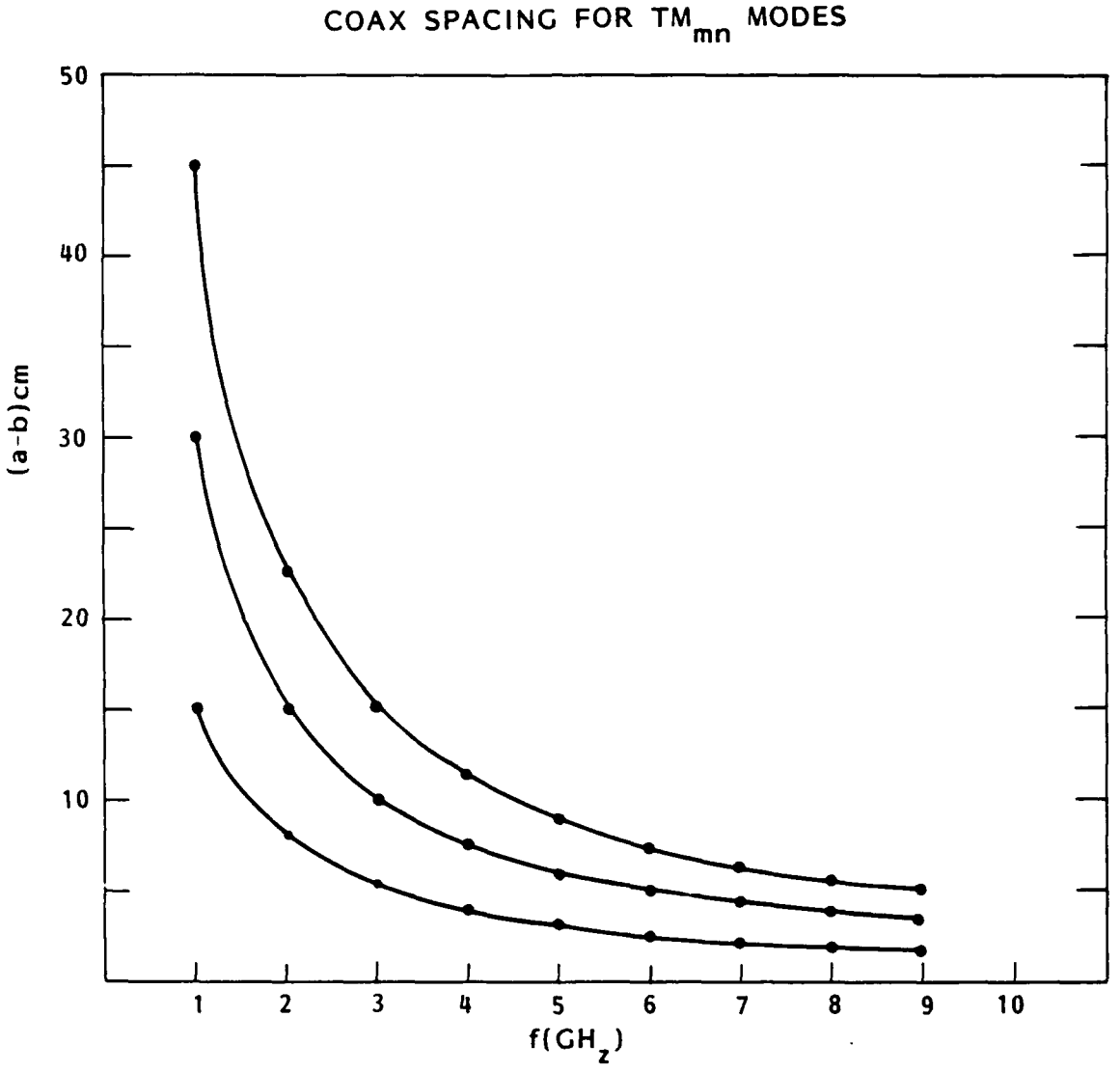

Figure 1. Coaxial spacing for TM_{mn} modes as a function of frequency.

"Microwave Source and Antenna Scoping Study (Simulation of the Relativistic Klystron Amplifier)"
Donald J. Sullivan and M. Joseph Arman
MRC/ABQ-R-1228
November 1989

See research summary for this subtask.

2.2.2 Subtask 02-02, High-Power Microwave Vircator Design

2.2.2.1 Research Summary. Ultimately, the source of all electromagnetic radiation is electrically charged particles undergoing certain nonuniform transitions in their virtual or real states of existence. Electrons, in particular, are responsible for a wide range of electromagnetic radiation from X rays to radio waves. Electrons can emit either naturally, such as in X ray and ordinary visible light, through random transitions, or coherently under controlled conditions such as in laser, maser, free electron laser, etc. All of these radiations are the result of an interaction between the electrons and their surroundings involving a change in the energy of the electrons, which determines the frequency of the emitted radiation. One means of arranging for such an energy change in the microwave range is to pass an intense relativistic beam of electrons through cavities of moderate dimensions of the order of centimeters. Under certain conditions the electrons inside the cavity can be made to radiate "coherently" at the characteristic frequencies of the cavity, thus providing for a powerful source of microwave radiation. The radiation will be coherent by the action of standing electromagnetic waves inside the cavity, which will stimulate the emission under proper conditions. For an unloaded cavity an oscillation potential equivalent to up to three times the energy of the original beam, and particle density modulations exceeding five times the original beam density become possible. At these modulation levels, nonlinear effects will play an important role which needs to be addressed in the theory of these processes.

With the advance of pulsed-power technology intense relativistic charged-particle beams of several hundred kiloamps in the multimegaelectronvolt energy range have become a reality. Use of such high-power charged-particle beams to generate intense microwave radiation is on the rise. The most successful research has emphasized simplicity, efficiency, and compatibility with advanced pulsed-power technology. Building on our WL-sponsored vircator work, we have developed a theory of a new HPM generator called the transvertron that appears to overcome the limits of vircator technology in many aspects. In particular it far exceeds the efficiency of the vircator, with the possibility of producing intense microwave beams with powers in the range of 50 GW, using the currently available machines TEMPO and PR1590 with otherwise minimal additional hardware.

2.2.2.2 Reports. Documents prepared under this subtask are summarized here.

"A Preliminary Study of MITL Pulse Sharpening by a Radial Magnetic Field"
Mark M. Campbell, Brendan B. Godfrey and Michael A. Mostrom
AMRC-R-972
December 1987

ABSTRACT: This is an investigation of the possible pulse shaping effects of imposing an external radial magnetic field (B_r) over a short region of a magnetically insulated transmission line (MITL). Computations were performed using the particle-in-cell code CCUBE, developed originally by Los Alamos National Laboratory (LANL). The analytic models were based on simple particle kinematics, circuit theory, and magnetic insulation formulae. Both approaches showed that pulse sharpening is very slight for typical parameters of interest.

"Analytical Study and Numerical Simulation of High Power Vircator and Transvertron Microwave Source"
Moossa J. Arman, Donald J. Sullivan, Brendan B. Godfrey, Robert E. Clark and John E. Walsh (Dartmouth College)
MRC/ABQ-R-1029
February 1988

ABSTRACT: This report assesses the potential capabilities of two of the WL pulse power generators, namely TEMPO and the PR1590, as sources of HPM radiation based on the virtual cathode oscillator (vircator). In addition, the effort aimed at better understanding the physics behind the vircator led MRC to discover a new electromagnetic instability. This instability forms the basis for a new source of HPM radiation (the transvertron) which is superior to the basic vircator source in efficiency by at least a factor of 10.

2.2.3 Subtask 02-03, Sparse Air Breakdown Microwave Propagation Study

2.2.3.1 Research Summary. Delivery of useful amounts of HPM energy onto targets at tactically interesting ranges is limited by typical antenna characteristics and by air breakdown considerations. From laboratory experiments, an HPM pulse is observed to break down air when the HPM power exceeds

$$P_{BD}\left(\mathrm{W/cm^2}\right) = \frac{7.2 \times 10^6}{T_p}\left(1 + 0.2T_p\right)p^2 \qquad (2)$$

where T_p is the HPM pulse duration (in nanoseconds) and p is the air pressure (in atmospheres). When breakdown occurs, the air becomes conducting and absorbs and/or reflects the HPM energy, effectively terminating transmission of the HPM pulse. For sea level pressures and pulse lengths greater than 100 ns, the breakdown power threshold is 1.4 MW/cm^2, corresponding to peak electric fields $E_{BD} = 33$ kV/cm.

If the HPM power is required to remain below these breakdown values everywhere between the source (antenna) and the target, then, using typical near-field/far-field expressions for apertures, parameterized curves for peak fluence on target may be obtained as a function of pulse width and distance to target. An example of such curves is shown in Figure 2 for 3-GHz frequency and two aperture sizes—3- and 10-m diameter (Ref. 4). For example, a 3-GHz pulse of 1-μs duration from a 3-m antenna will deliver at most 1 mJ/cm^2 on a target at 1-km range (and 10 mJ/cm^2 from a 10-m antenna). Lower frequencies will provide less energy, and higher frequencies, though propagating better, are thought to couple less well into targets of interest.

Thus, interesting fluences on targets require either short engagement ranges, large antennas, or a propagation mode which allows atmospheric propagation at a power level exceeding the experimental air breakdown limits. Since increasing antenna diameters much above 3 m becomes impractical for tactical applications, it is of interest to consider the possibility of above-breakdown propagation modes. One such mode, *sparse breakdown*, is considered here.

As is well known, gas breakdown by electromagnetic fields requires the presence of an initial electron—the seed electron—and such electrons are sparsely present in ambient air; their concentration is low, less than experimentally measurable except, possibly, by breakdown experiments. To obtain reproducibility, experimentalists who study air breakdown typically create seed electrons using an external source of ionization (Ref. 5). Recently, it has been shown experimentally at both Stanford Research Institute (SRI) and at Lawrence Livermore National Laboratory (LLNL) that propagation of HPM pulses with power substantially exceeding P_{BD} leads to breakdown in only a small percentage of the cases (a few per thousand).

Spatial sparseness of seed electrons thus leads to the possibility of propagating short HPM pulses with power substantially exceeding breakdown levels, considering the two-dimensional propagation of the HPM wave front around and between the isolated breaking-down regions centered on the isolated seed electrons. This is the concept of the *sparse breakdown* propagation mode. The achievable energy on target is determined probabilistically by free electron statistics and by the breakdown growth about isolated seed electrons. It is of interest for short pulses only, because the probability of encountering

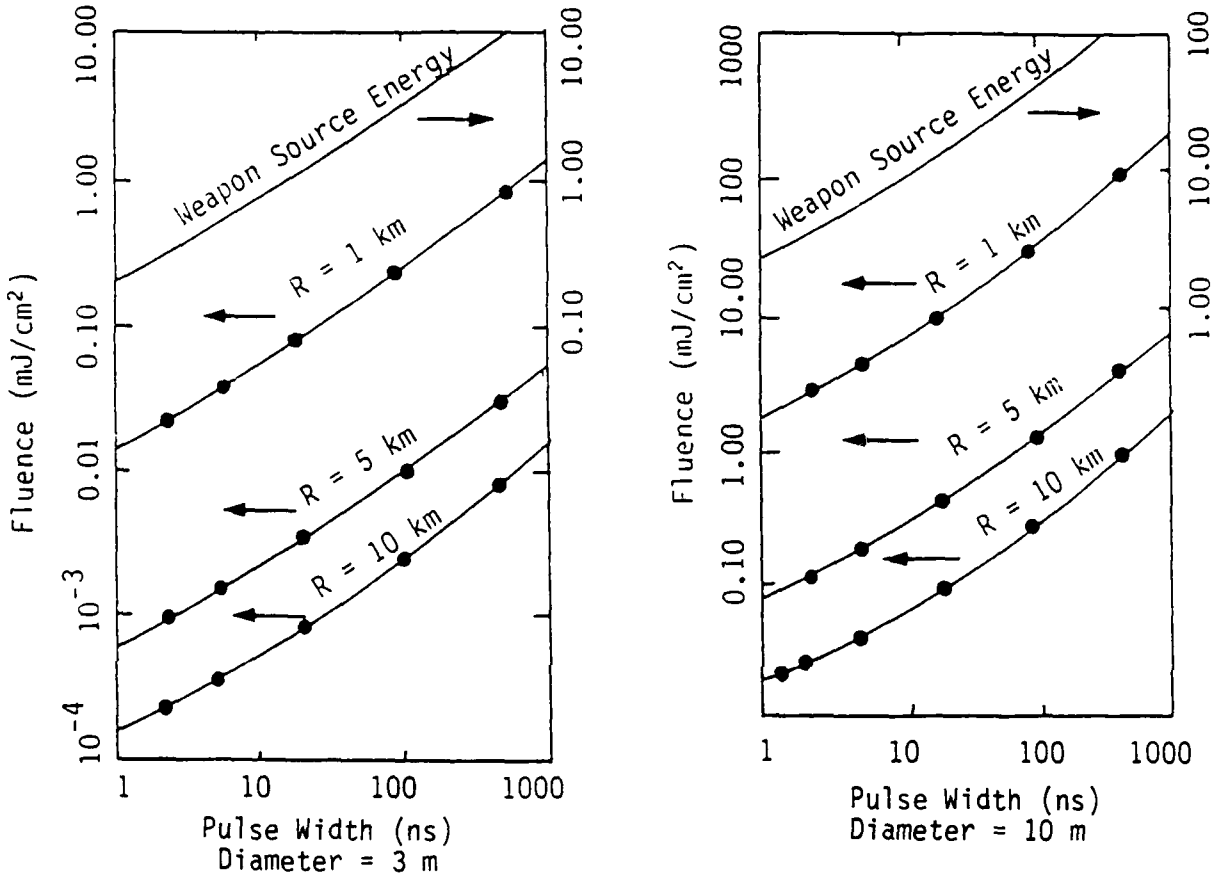

Figure 2. Upper bound for delivered fluences on targets at low altitude ($f = 3$ GHz).

a seed electron within the pulse is proportional to the pulse length, and, for sufficiently long pulses, the isolated breaking-down regions about such electrons will grow rapidly across the HPM pulse to eventually coalesce and absorb essentially all the HPM energy. A major objective of the work reported is to provide quantitative estimates of this plasma growth rate and of the achievable energy on target as functions of HPM parameters.

The viability of a sparse breakdown propagation mode depends on several physical effects only partially understood at present:

1. The number and availability of seed electrons in both ambient air and in air subjected to an HPM pulse.

2. The rate at which an air plasma generated by breakdown about such a seed electron grows in space and time, and a characterization of its HPM absorption properties.

3. The effects of such initially isolated absorbing regions on microwave propagation.

This initial study of sparse breakdown is a first-order attempt to address these issues and to provide theoretical estimates of the achievable energy on target as a function of microwave parameters. Theory alone is incapable of convincingly addressing these issues. Presently available experimental facilities lack sufficient power to provide experimental confirmation of sparse *propagation* predictions over the large volumes of ambient air required. Concurrently with this effort, sparse *breakdown* experiments in waveguides and cavities have been in progress at LLNL with theoretical support provided by Science Applications International Corporation (SAIC) (Ref. 6). A second objective of this study is thus to provide guidance to planning future experiments for confirmation of the predicted effects.

The most important conclusion of this work is that air breakdown is not expected to attenuate an HPM pulse with pulse width less than approximately 10 μs for pulsed power up to 10 times the breakdown level. This conclusion was obtained for HPM frequency 1 GHz, but partial Monte Carlo studies of frequencies up to 8 GHz indicate only small sensitivity in plasma growth rates. Higher pulsed powers would require shorter pulses but have not been quantitatively explored. Thus, the upper bound fluences of Figure 2 may be increased by an order of magnitude by similarly increasing the source power with no propagation penalties.

To address computationally such important plasma growth issues as listed above, a family of electron-air Monte Carlo codes has been developed over the past few years, under both WL and Defense Nuclear Agency support. The predictions of these codes are in good

agreement with all experimental data modeled to date. We have thus developed a set of computational tools which should be useful for other nonequilibrium air conductivity and breakdown studies.

2.2.3.2 Report. Document prepared under this subtask is summarized here.

"Sparse Air Breakdown Effects on Microwave Propagation"
Robert R. Johnston and Charles L. Yee (SAIC)
MRC/ABQ-R-1186, SAIC-U-142-PA
May 1989

ABSTRACT: The propagation of HPM in air tends to be limited by breakdown at power levels above 1.4 MW/cm^2. However, due to the sparseness of seed electrons in most ambient air situations, it may be possible to achieve propagation by using short HPM pulses. The study focuses on the availability of seed electrons and the rate of air plasma generation. Monte Carlo codes were used to investigate the probability of breakdown at various pulse lengths, power levels and frequencies. Short HPM pulses at power levels as high as 10 times the breakdown level can be propagated without attenuation due to breakdown.

2.2.4 Subtask 02-04, Vircator Phase/Frequency Locking Studies

2.2.4.1 Research Summary. During May 1988, a series of virtual cathode oscillator phase/frequency locking experiments were carried out under the direction of Capt Kyle Hendricks at the WL. To support this experiment, MRC carried out a series of numerical particle-in-cell plasma simulations using the SOS computer program. These simulations were used to evaluate several proposed virtual cathode oscillator designs as well as the final configurations actually investigated on the Gemini pulser. In addition, several virtual cathode oscillator/field emission diode concepts were investigated analytically prior to SOS simulations so that comparisons could be made between the analytic theory and the numerical simulations.

In general the numerical simulations were in good agreement with both the analytic model and, where available, with the ongoing experimental results as communicated by Capt Hendricks. Limitations on computer costs precluded a conclusive numerical demonstration of phase/frequency locking. However, an upper bound on the frequency differential, Δf, between the virtual cathode oscillator frequency and the locking frequency that will be required for phase locking dual virtual cathode oscillators connected by a rectangular waveguide was determined. A number of observations and recommendations for future analytic and numerical efforts were made and are discussed below.

The virtual cathode oscillator is a type of plasma microwave source in which a space charge oscillation is excited in an electron plasma. This is accomplished by injecting an electron beam into a cavity. If the beam current exceeds the space charge limit I_{scl} then current flow will be stopped or reversed resulting in a relaxation oscillation (Ref. 7) at a frequency comparable to the beam plasma frequency (Refs. 8–9).

Virtual cathode oscillators have been studied extensively, theoretically (Refs. 7–9), numerically (Refs. 7–12), and experimentally (Refs. 8–9, 12–15). The configuration in which the cathode is pulsed negatively and the electrons are extracted through a foil anode is called a foil diode or axial vircator configuration. The configuration where the anode is pulsed positively is called a reflex triode. Typical experimental results as summarized by Thode (Ref. 15) are shown in Tables 3 and 4.

The purpose of this task was to provide SOS particle-in-cell simulations to support the WL vircator phase/frequency locking experiments. In carrying out this task, several preliminary vircator design concepts were investigated. These simulations confirmed the validity of the analytical model in predicting diode physics and virtual cathode oscillation frequency as well as the expected observation that the TM_{021} mode is preferred for single beam configurations. In addition, attempts were made to demonstrate phase locking for the single vircator with radial extraction/radial injection of a locking signal and the double beam vircator with radial extraction. Frequency locking was not demonstrated for the single vircator with the minimum frequency resolution, Δf, constraint set by the allowable computer costs. Frequency locking was not rejected for the double beam vircator concept. In addition, it was demonstrated that a TM_{022} mode could be generated with a double beam concept. The predicted mode pattern and frequency for the double beam concept was in reasonable agreement with the experimental results.

In addition to the above results, a number of observations were made that should be pursued to develop a better understanding of the virtual cathode oscillator and phase/frequency locking. The first observation was that present particle-in-cell codes lack the capability to satisfactorily model the secondary electron and plasma flux driven off of the wall of the vircator cavity by the oscillating electron beam. This shortcoming is due to both an inadequate theoretical/experimental base and the lack of appropriate tested models in SOS and other codes. A closely related problem is the lack of a tested anode-cathode gap closure model. This model would be particularly useful in that gap closure can cause a significant shift in the diode current density and the vircator frequency/power output.

The second observation was that lowering the resonant cavity Q by opening up the waveguide outlet had the effect of suppressing the virtual cathode oscillation. This effect

TABLE 3. Summary of axial vircator experiments (Ref. 9).

Experiment	V (keV)	I (kA)	t_b (ns)	f (GHz)	P (MW)	T_μ (ns)	ϵ (%)
VC1:Buzzi, et al.	350	220	150	9–14	1000	50	1.3
VC2:Clark	900	40	35	6–8	1000	30	2.7
VC3:Sze, et al.	1000	60	65	8–12	1000	50	1.7
VC4:Scarpetti, et al.	500	40	35	7–9	300	50	1.5
VC5:Davis, et al.	1800	90	80	15–19	500	12	1.2
VC6:Clark, et al.	400	40	80	2–3	170	60	1.1
VC7:Saunders, et al.	500	50	150	0.5–0.8	600	120	2.4
VC8:Burkhardt	1750	111	60	5–7	4000	40	2.1
VC9:Clark, et al.	1500	300	40	2-4	4000	5	0.9
VC10:Davis, et al.	1800	90	80	4–6	3500	20	2.1
VC11:Bromborsky, et al.	8000	250	120	0.7–1.0	40000	50	1.8

TABLE 4. Summary of reflex triode experiments (Ref. 9).

Experiment	V (keV)	I (kA)	t_b (ns)	f (GHz)	P (MW)	T_μ (ns)	ϵ (%)
RT1:Mahaffey, et al.	335	22	50	8–12	100	50	1.5
RT2:Brandt, et al.	1000	20	25	9–13	150	10	0.8
RT3:Didenko, et al.	450	25	80	2–5	1400	60	12
RT4:Didenko, et al.	83	2.3	700	2–3	87	600	46
RT4B:Didenko, et al.	250	6	400	2–3	550	300	37
RT5A:Zherlitsyn, et al.	93	3.5	1700	2–3	120	1300	37
RT5B:Zherlitsyn, et al.	270	14	110	2–3	800	50	21

is not predicted by the analytic model and could set a limit of how many vircators could be connected together in an attempt to build a bank of phase-locked vircators. It would be useful to further investigate this suppression effect and develop a practical model.

A third observation was the fact that the usual theory of phase locking used to explain phase/frequency locking in vircators and gyrotrons uses a free-running nonlinear oscillator in the presence of a locking frequency. The actual situation for the vircator considered here is analogous to two (or more) free-running nonlinear oscillators. In this case, it is not clear what the locking frequency is or whether the simple locking formuia given by $\Delta f \leq (f_0/2Q)\sqrt{P_i/P_0}$ is still valid. It should be straightforward to extend the electrical analogue used by Van Der Pol (Refs. 16, 17) and others to the more general case.

2.2.4.2 Reports. Documents prepared under this subtask are summarized here.

"High Power Microwave Literature Review"
W. R. Zimmerman
MRC/ABQ-R-1028
January 1988

ABSTRACT: This is a review of the HPM literature with an emphasis on virtual cathode oscillators (vircators) and phase/frequency locking studies. The literature on gyrotrons, free electron lasers, slow wave devices, plasma microwave devices and phase/frequency locking phenomena is reviewed. It is seen that phase/frequency locking has been observed in conventional magnetrons and gyrotrons. It is expected that phase/frequency locking phenomena should also be observed in vircators subject to a general equation relating input power and frequency to vircator frequency, power and cavity Q. No previous successful vircator phase/frequency locking experiments or demonstrations were found.

"SOS Simulation Support for the AFWL Vircator Phase/Frequency Locking Experiment"
William R. Zimmerman, Robert E. Clark and Donald J. Sullivan
MRC/ABQ-R-1072
June 1988

ABSTRACT: During May 1988, a series of virtual cathode oscillator phase/frequency locking experiments were carried out under the direction of Capt Kyle Hendricks at the WL. To support this experiment MRC carried out a series of numerical particle-in-cell plasma simulations using the SOS computer program. These simulations were used to evaluate several proposed virtual cathode oscillator designs as well as the final configurations actually investigated on the Gemini pulser. In addition, several virtual

cathode oscillator/field emission diode concepts were investigated analytically prior to SOS simulations so that comparisons could be made between the analytic theory and the numerical simulations.

2.2.5 Subtask 02-05, High-Power Microwave Vulnerability of Space Assets

The primary results of this subtask are classified.

2.2.6 Subtask 02-06, Microwave Computer Program Enhancements

2.2.6.1 Research Summary. The ISIS code is a 2 1/2-dimensional, electromagnetic, relativistic, particle-in-cell simulation code (Ref. 18). It models collisionless plasma dynamics by moving discrete charged particles through a fixed Eulerian spatial grid. Currents from the particles are accumulated and Maxwell's equations are solved on the fixed grid. The fields from the grid are then used to accelerate the particles (Ref. 19). Diagnostics are available through the graphics postprocessor.

The PEGASUS is a multipurpose plotting and editing code that postprocesses output dump files created by ISIS. The types of output files processed include field or "grid" dumps of physical variables over the Eulerian spatial grid, particle dumps of physical variables for an arbitrary number of particles, and time history dumps of physical variables versus time. Available plotting capabilities encompass profile or x-y plots, scatter or particle plots, number distribution function plots, contour plots, isocontour three-dimensional plots, and vector plots. Built-in analysis capabilities include differentiation and integration, spatial and temporal fast Fourier transform, time autocorrelation analysis, etc. (Ref. 20).

Modification of these programs for operation on the Cray-2 computer was performed for the WL under this subtask.

2.2.6.2 Report. Document prepared under this subtask is summarized here.

> "Microwave Computer Program Enhancements: Code Conversion"
> Judith E. Sturtevant, M. Joseph Arman and Brendan B. Godfrey
> MRC/ABQ-R-1081
> June 1988

ABSTRACT: The ISIS code is a 2 1/2-dimensional, electromagnetic, relativistic, particle-in-cell plasma simulation code. The PEGASUS is a multipurpose plotting and editing code that postprocesses output dump files created by ISIS. Section 2.0 describes how to access

and initialize ISIS and PEGASUS on the WL Cray-2. Section 3.0 includes information on CFT77, FORTLIB (including BASELIB), and the Cray-2 operating system, relevant to the modifications. The Appendices include an example COSMOS command file and definitions of ISIS and PEGASUS variables.

2.2.7 Subtask 02-07, High-Power Microwave Transvertron Design

2.2.7.1 Research Summary. Mission Research Corporation has recently developed a new class of potentially high-efficiency HPM sources with the single- and dual-cavity transvertron. This scheme is based on a transit time instability associated with an Intense Relativistic Electron Beam (IREB). Mission Research Corporation was directed by the WL under this subtask to design a diode for the WL PR1590 Pulse Power Machine. This diode would drive a transvertron source and demonstrate the viability of this new approach. A study of multiple-cavity concepts was also conducted under this subtask as a possible means of obtaining higher instability growth rates and improved efficiencies.

The $m = 0$ transvertron is an unmagnetized annular electron beam driven cavity resonator. It is in effect a negative resistance oscillator which produces high levels of monochromatic radiation at frequencies near the TM_{onp} resonances of the cavity. Unlike the elementary monotron, the energy exchange process depends essentially on the oscillatory radial motion of the beam electrons, and this leads to a number of interesting characteristics. Among these are the comparatively short cavity lengths required to start the oscillation and high saturation levels.

A transvertron instability will grow on a high voltage ($\gtrsim$ 0.5 MV) low impedance (50–100 Ω) intense electron beam when it traverses a properly optimized cavity. To obtain the maximum beam current without exceeding the space-charge limited current of the cavity, the beam must have an annular profile and be injected near the cavity wall. The location of an annular beam at the radial cavity wall also maximizes the instability growth rate. Simulations were performed with a 45-kA beam injected at 4.0 MV into a cylindrical cavity with a TM_{011} frequency of 1.3 GHz and an L/R ratio on the order of unity. These simulations showed the instability saturating in about 28 ns from the time the beam current peaked. It grew from noise without the injection of microwave power to prime the cavity. Injecting slightly larger currents does tend to increase the growth rate somewhat. However, injecting significantly larger currents (say a factor of 2) triggers the growth of higher order TM_{onp} modes in the cavity. A detailed description of the transvertron theory can be found in References 21–23.

2.2.7.2 Report. Document prepared under this subtask is summarized here.

"Transvertron Source Design and Analysis of Experimental Results"
Donald J. Sullivan, M. Joseph Arman, George Z. Hutcheson and John E. Walsh
(Dartmouth College)
MRC/ABQ-R-1085
August 1989

ABSTRACT: The transvertron is a new HPM source based on a transit time instability present in simple pill box cavity configurations. A specific version was designed for the PR1590 pulse machine at the WL. The results of an experiment based on this design are analyzed and compared with the theoretical predictions. Possible sources of inconsistencies are determined and solutions devised. A two-cavity configuration of the transvertron source is studied and found to have significantly higher efficiency than the single cavity geometry. A preliminary study of the dual-cavity efficiency shows that rms efficiencies on the order of 20 percent are possible. The dual-cavity transvertron is also investigated as a possible HPM amplifier and found to be promising.

2.2.8 Subtask 02-08, Repetitive Pulse MITL Physics Study

2.2.8.1 Research Summary. Recent research has introduced a new type of HPM device called the magnetically insulated transmission line oscillator, or MILO (Ref. 24). Its successful operation in repetitively pulsed mode (approximately 10–100 Hz) depends upon the ability of the diode to reproducibly withstand applied voltages until space-charge-limited electron field emission is achieved, and continue to operate magnetically insulated for the duration of the applied power pulses (typically 1–10 μs). Since the device is normally operated in vacuum, voltage hold would not normally be a problem, provided the diode power is low. However, the MILO is intended for extremely high-power operation. Under intense field emission, regions of the cathode can be expected to heat and liberate adsorbed gases from the surface, or boil off cathode material, resulting in localized transient pressure surges or even ionized plasma expansion and eventual arcing. Although this problem is of special concern for MILOs, it is generic to all high-power long-pulse or repetitively pulsed diodes. The debris generated during operation may persist until the next pulse, degrading the withstand ability, or even shorten individual pulses because of diode shorting.

The purpose of the research was to investigate the problem of plasma/gas generation in repetitively pulsed magnetically insulated transmission line (MITL) diodes to better understand the physics involved. Additionally, methods of eliminating or reducing the problem for MILOs could be investigated.

The conclusions based on these experiments can be summarized quite succinctly as follows.

Typical existing vacuum pumping systems are inadequate for removing high-power diode debris on millisecond time scales. Effective pumping time constants are of the order of 1 s. Enhancements in the form of larger pumps or cryogenic traps may bring the pumping speed down to as low as tenths of a second.

The number of particles produced in a single pulse has been shown to scale linearly with total transferred diode charge up to 10 C. The mass per coulomb transferred is approximately the same as that for metal-vapor vacuum arc erosion, or of the order of 10^{-4} g/C. This amount of material, distributed uniformly over a given vessel volume may or may not cause Paschen breakdown of high-voltage gaps or disruption of subsequent pulse physics.

There is strong evidence for nonuniform plasma production. In fact, all of the data taken together suggest that material erosion in high-power MITL diodes is remarkably similar to that in conventional metal-vapor vacuum arcs.

The lifetime of ionized (plasma) species appears to be of the order of tens of microseconds or of the diode current pulse, whichever is longer. This observation is consistent with vacuum arc recovery experiments.

The incorporation of transparent (screen) anodes does not significantly affect the plasma/neutral production. It appears that most of the material is evolved at the cathode. The transparent anodes may enhance the evacuation rate from the diode interelectrode gap.

By far, the most significant improvement in material generation was due to damping the current waveform. Because of the linear relationship between transferred charge and mass erosion, reducing late-time current can significantly reduce the volume material inventory.

The above conclusions point toward some obvious recommendations for minimizing the problems associated with high-power diode operation. Foremost among these recommendations is to limit the power pulse to the diode to coincide with the intended load interaction. Expressed another way, eliminate long leading or trailing current waveforms. In some cases this may necessitate designing the pulsed-power driver to incorporate a pulse forming network or other means of controlling the pulse length. Adding critical damping resistance to existing underdamped systems may significantly reduce the problem. Unless the application calls specifically for it, current reversal should be avoided for two reasons. First, many diodes rely on magnetic insulation for

successful operation; at current zero all magnetic insulation is lost. Second, insulators generally exhibit enhanced failure for bipolar stresses. Associated with the requirement for effective magnetic insulation, diode load inductance should be minimized. Ideally, total load impedance should be purely resistive, so that current and voltage are in phase and maximum magnetic insulation is realized.

Should the phenomenon of repetitive pulse degradation in high-power diodes be studied further, high-voltage conditioning techniques, common in dc charging of high-voltage systems, should be examined. Since most models of vacuum breakdown incorporate surface desorption, it might prove fruitful to examine the effects of gradual and controlled removal of adsorbed species. Future experimental studies should include an extra effort to eliminate unwanted arcing, so that the evolved material under investigation can be localized with confidence to the interelectrode region. Detailed (time- and space-resolved) spectroscopy should be a good diagnostic for studying the temperature and density evolution in the diode gap. Finally, any thorough investigation of repetitively pulsed phenomena should incorporate a repetitively pulsed driver for realistic assessments of operational thresholds.

2.2.8.2 Report. The document prepared under this subtask is summarized here.

"Repetitive Pulse MITL Physics Studies"
Gerald F. Kiuttu, Robert J. Richter-Sand and Raymond D. Brown
MRC/ABQ-R-1234
September 1989

ABSTRACT: The purpose of this research was to investigate the problem of plasma/gas generation in repetitively pulsed MITL diodes to better understand the physics involved. Additionally, we propose and test means of eliminating or reducing the problem for MILOs.

2.2.9 Subtask 02-09, Microwave PIC Code Optimization and Enhancements

2.2.9.1 Research Summary. See Subtask 02-06 summary.

2.2.9.2 Report. Document prepared under this subtask is summarized here.

"Microwave Computer Program Enhancements, Part I: ISIS and PEGASUS,
Part II: CFTLIB To FORTLIB Conversion"
Judith E. Sturtevant and M. Joseph Arman
MRC/ABQ-R-1202
September 1989

ABSTRACT: The CFT to FORTLIB (BASELIB) conversion library, CFTFRT2, was created to provide an interface transparent to the user, replacing LANL CFTLIB routines with corresponding WL FORTLIB routines.

2.2.10 Subtask 02-10, Microwave Source Design Improvements

2.2.10.1 Research Summary. The objective of this subtask was to research possible improvements in the operating characteristics of an MRC RF source which emits in the VHF range. Specifically, this subtask addresses the design of an end-fire antenna in order to maximize the radiation in a single forward directed lobe. In addition, a high pressure gas switch to replace the current intermediate stage switch was investigated and a design produced.

The WL is responsible for developing HPM sources and antennas for weapon applications and for lethality and vulnerability testing. Microwave production must be efficient and the radiation pattern directed in such a manner as to be useful in practical applications such as testing. To illuminate a test object uniformly and maximize the area subjected to radiation for a given source power, a pencil beam radiation pattern is optimal. In most microwave sources, this requires that the radiation be coupled out in the fundamental mode of either rectangular or circular waveguide to an appropriate antenna. In the MRC source it requires that the antenna be end-fire.

In the previous 2 yrs MRC developed a VHF source under Air Force sponsorship which has certain desirable characteristics such as high power, compactness and efficiency. However, the utility of this device would be improved by substituting the current antenna configuration with one which would create a solid radiation pattern. In addition, higher powers can be obtained by making the pulsed power system more efficient. One method of attaining this goal is to replace the present intermediate storage switch with an SF_6 filled spark gap. The switching medium would be less resistive than at present resulting in a more efficient transfer of energy to the RF source.

A model has been developed with the three-dimensional, time-dependent electromagnetic code SOS for an antenna which has many unique features. The antenna is end-fire, stores the energy to be radiated in its capacitance, and converts this energy to a VHF plane wave by means of an integral self-break high-voltage switch. Incorporated into this model are realistic time-dependent inductance and resistance effects due to the switch. Simulations have shown, for a 2-MV charge voltage:

76 percent stored electrical to radiated RF energy efficiency

50 GW instantaneous peak power

2 MV/m instantaneous peak electric field (at 1 m)

100 MHz nominal frequency.

Due to the low frequency and resulting large structure, mesh-size limitations have prevented a determination of the radiation pattern or antenna gain. However, a minimum of 33 percent of the total radiated energy is projected axially through a maximum of 16 percent of the available radiated surface area. Only 9 percent of the total radiated energy is projected to the rear of the structure through the same size area. Due to the aperture proximity to the mesh boundary some of the main beam is clipped by the upper horizontal boundary. The forward energy density divided by the total energy density is probably significantly greater than two.

A unique design for a repetitive high-voltage switch has been produced. The switch is capable of 2 MV at 25 Hz. The switch design results from an atypical philosophy which allows a more compact, robust structure and alleviates the need for complicated grading structures and bulky fluid insulation volumes. State-of-the-art features in switch design developed by Sandia National Laboratories (SNL) have been included which improve reliability and performance (Ref. 25).

2.2.10.2 Report. Document prepared under this subtask is summarized here.

"Beam and Plasma Physics Research Microwave Source Design Improvements"
Gary R. Hess and M. Joseph Arman
MRC/ABQ-R-1177
May 1989

See research summary for this subtask.

2.3 TASK AREA 3: PLASMA PHYSICS COMPUTATION, MODELING AND THEORY

2.3.1 Subtask 03-01, SHIVA STAR Computational Physics Studies

2.3.1.1 Research Summary. A series of high-voltage switch experiments were performed on the SHIVA STAR fast capacitor bank at the WL in 1986 to generate hard X rays (Refs. 26, 27). The experiment used an open-ended Plasma Flow Switch (PFS) to generate a large voltage that created high-energy electrons.

Calculations were performed using the magnetohydrodynamics (MHD) code MACH2 (Ref. 28) to investigate the development of high voltages and intense electric fields in a high-voltage switch configuration suitable for application on the SHIVA STAR capacitor bank. The high-voltage switch under study is a variation of the PFS (Refs. 29–31). The initial configuration uses the PFS hardware with an open muzzle and no load. As the plasma from the wire array leaves the end of the coaxial barrel there is a significant increase in the inductance L and in $\dot{L}$. In the MHD model, the magnetic field propagates to the axis at the Alfvén speed of the low density region between the end of the gun and the axis. Any plasma that is carried to the axis forms a "pinch."

Initial calculations were performed on a coarsely zoned grid which had conducting electrodes at the muzzle end. The open region of the proposed experiments was terminated numerically with a screen electrode. See Reference 31 for a discussion of the boundary conditions associated with a screen electrode. Following an initial test, a series of short calculations were carried out to check zoning, boundary conditions, screen location, and bank polarity. These initial calculations indicated that the MACH2 code could be successfully used to study the MHD flow and that high voltages could be developed from the MHD behavior of the plasma. The calculations with reverse polarity showed no differences in the flow or in the switching as expected from the MHD code. They did show that when the inner electrode is negative (standard polarity) the fields were high enough at the surface to allow field emission of electrons from the surface. With the outer electrode negative, however, the geometric effects reduce the fields below the normal field emission level.

After the completion of these test problems, a simulation was performed with circuit parameters and plasma masses which were used in the SHIVA STAR experiment. In this experiment, the inner conductor was a hollow cylinder 0.2 cm thick, and the outer conductor was a hollow shell 0.2 cm thick. The other dimensions were the same as in the PFS experiments. The inner conductor was the cathode. Nine blocks were used in the simulation. Figure 3 shows the movement of the plasma and magnetic field down

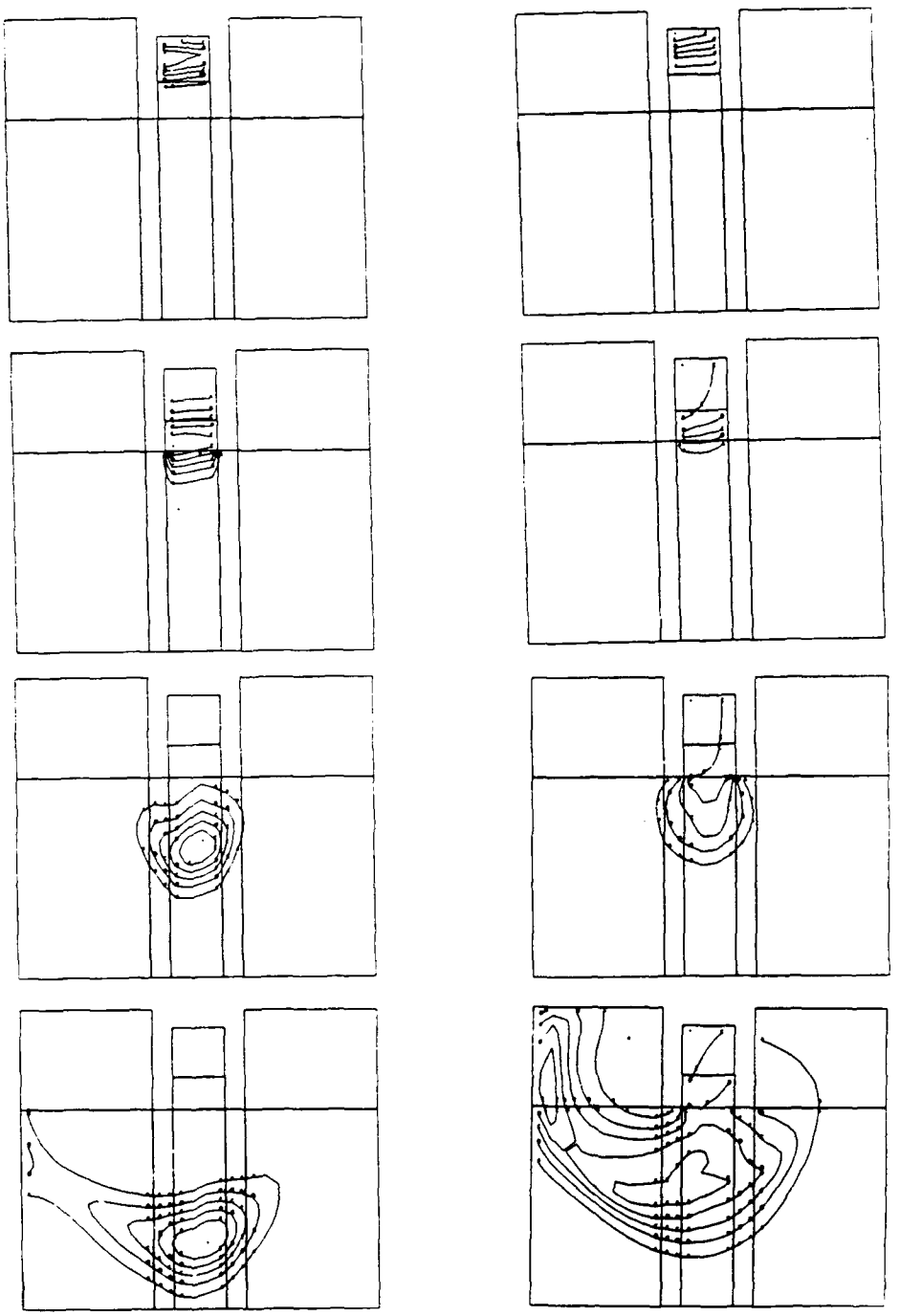

Figure 3. Density contours (left) and magnetic field contours (right) in the MACH2 simulation of the high-voltage switch.

the barrel and into the open region. The voltage developed at the 5-nH voltage monitor location and at the muzzle is shown in Figure 4. The simulation predicted a voltage spike of 153 kV at the monitor at 4.19 μs after bank firing. This prediction was in excellent agreement with the preliminary experimental data of 150 kV at 4.2 μs. It is worth emphasizing that the simulations were completed before the experiment was performed.

2.3.1.2 Report. Document prepared under this subtask is summarized here.

"Initial Simulations of the Air Force Weapons Laboratory High Voltage Switch"
N. F. Roderick, J. Buff, M. H. Frese and R. E. Peterkin, Jr.
AMRC-N-357
January 1987

ABSTRACT: A switch that is in principal capable of producing extremely high voltages is the subject of intense study by researchers at the WL. This switch is driven by the SHIVA STAR fast capacitor bank. The experimental configuration uses hardware from the PFS, but has an open muzzle and has no load. Numerical simulations of this system were performed with the 2 1/2-dimensional MHD code, MACH2, and are discussed in this report. The code predicted a 153-kV spike at the location of a voltage probe, and that agrees well with the subsequent experimental value of 150 kV. The MHD model is sufficient to study high-voltage production as long as field emission of electrons from the cathode is not substantial.

2.3.2 Subtask 03-02, SHIVA STAR Computational Physics Studies

2.3.2.1 Research Summary. Mission Research Corporation provided theoretical guidance for a number of high energy plasma experimental efforts under this subtask. During this effort, most of the attention focused on the PFS that was designed by P. J. Turchi and coworkers (Refs. 32–35). The PFS can be used to drive fast plasma liner and direct-drive solid liner implosions, and to produce hard X rays. The principal computational tool used for the majority of subtasks performed in task area 3 was MACH2. MACH2 is a 2 1/2-dimensional MHD simulation code written for problems with complex shapes. It is available for use on the Cray supercomputers running the Cray Time-Sharing System.

MACH2 is an Implicit Continuous Eulerian, Arbitrary Lagrangian Eulerian (ICE-ALE) nonideal MHD code. Developed by MRC, it is a direct descendant of MOQUI (Ref. 36), written by Jeremiah U. Brackbill of LANL. MACH2 is an MKSA code with temperature in electronvolts.

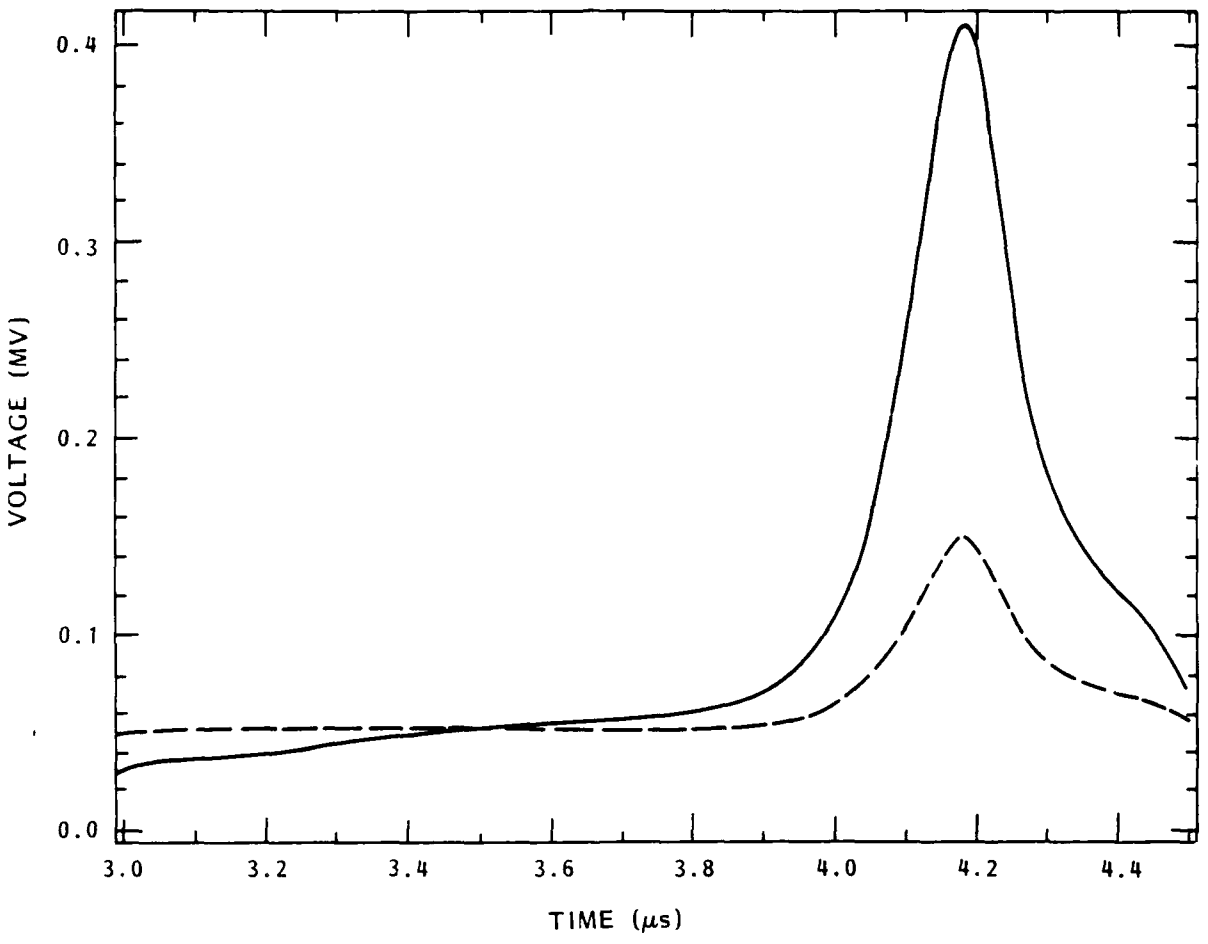

Figure 4. Voltage at the muzzle (solid curve) and at the location of the voltage monitor (dashed curve) in the MACH2 simulation of the high-voltage switch.

An incomplete draft of a paper that describes the physics, algorithms, and numerical methods used in MACH2 was produced under this subtask. The physical models in the code are largely those that were required to generate believable solutions to fast imploding liner and PFS problems for the WL. Since the design and implementation of MACH2 makes modification easy, the list of physical processes that are modeled has grown over the duration of this contract. The processes of ideal MHD, resistive diffusion of magnetic field and consequent joule heating, thermal diffusion, and radiation cooling comprise the core of MACH2, and will be described here. Packages for multimaterial transport and material interface tracking, elastic/plastic strength of materials, and Hall transport of the magnetic field are well into the validation stage at this time. The various new physical models will be discussed under the appropriate subtask heading.

PHYSICAL MODELS OF MACH2

The differential equations expressing the conservation laws relevant to these processes will be described in detail. In practice however, most of these equations are implemented in finite volume difference form. This means that the difference equations more closely represent the integral conservation laws from which these partial differential equations are usually derived than they do the partial differential equations themselves.

In what follows, d/dt represents the convective derivative. That is,

$$\frac{d\phi}{dt} = \frac{\partial \phi}{\partial t} = \vec{v} \cdot \nabla \phi \tag{3}$$

for any scalar function ϕ defined in terms of spatially fixed (Eulerian) coordinates and $\vec{v}$ is the velocity of the fluid relative to the grid.

THE ELECTROMAGNETIC FIELD EQUATIONS

As explained in Krall and Trivelpiece (Ref. 37), plasma phenomena with characteristic times much longer than the plasma oscillation period can be analyzed by neglecting the displacement current; this is the MHD approximation. In rationalization MKSA units then, the MHD fields are described by

$$\nabla \times \vec{E} + \frac{\partial \vec{B}}{\partial t} = 0 \tag{4}$$

$$\nabla \times \vec{B} = \mu_0 \vec{J}$$

supplemented by an equation relating $\vec{J}$ and $\vec{E}$ that depends on the properties of the medium, i.e., Ohm's law for the moving fluid

$$\vec{E} = \overleftrightarrow{\eta} \cdot \vec{J} - \vec{v} \times \vec{B} \tag{5}$$

Substituting 3 in 2 and expanding the iterated curl yields

$$\frac{d\vec{B}}{dt} = -\nabla \times \left(\frac{1}{\mu_0} \overleftrightarrow{\eta} \cdot \nabla \times \vec{B} \right) - \left(\vec{B} \nabla \cdot \vec{v} - \vec{B} \cdot \nabla \vec{v} \right) \tag{6}$$

Here the left-hand side represents the field transport, the first term of the right-hand side represents diffusion of field, and the second, both the modification of field intensity by the divergence of the velocity field transverse to $\vec{B}$ and the field line bending.

The resistivity used must model two physical effects: one is classical and due to particle-particle interactions, the other is nonclassical (anomalous) and intended to model particle interactions with the turbulent fields. The tensor nature of the resistivity is due to the differing resistivities for currents parallel or perpendicular to the magnetic field that points in a direction, $\hat{e}_B$. Thus

$$\overleftrightarrow{\eta} = \eta_n \overleftrightarrow{I} + \eta_{c\parallel} \hat{e}_B \hat{e}_B + \eta_{c\perp} \left(\overleftrightarrow{I} - \hat{e}_B \hat{e}_B \right) \tag{7}$$

where $\eta_{c\parallel}$ and $\eta_{c\perp}$ are the classical parallel and perpendicular resistivities and η_n is the nonclassical resistivity.

THE MOMENTUM EQUATION

The compressible Navier-Stokes equations supplemented by the addition of the electromagnetic force are

$$\rho \frac{d\vec{v}}{dt} = -\nabla p + \vec{J} \times \vec{B} + \nabla \cdot \overleftrightarrow{\sigma} \tag{8}$$

It is possible, and convenient, to write the entire right-hand side as the divergence of a tensor:

$$\left(-\nabla p + \vec{J} \times \vec{B} + \nabla \cdot \overleftrightarrow{\sigma} \right)_i = \frac{\partial}{\partial x_j} \left[\left(-p - \frac{1}{2} \mid \vec{B} \mid^2 \right) \delta_{ij} + B_i B_j + \sigma_{ij} \right] \tag{9}$$

$$= \left(\nabla \cdot \overleftrightarrow{S} \right)_i$$

An artificial compressive viscosity is implemented using σ_{ij}.

THE CONTINUITY EQUATION

Conservation of mass is represented by

$$\frac{d\rho}{dt} = -\rho \, \nabla \cdot \vec{v} \tag{10}$$

THE ENERGY EQUATION

If we let e be the internal energy per unit mass, then the energy equation in MACH2 is

$$\rho \frac{de}{dt} = -p \, \nabla \cdot \vec{v} + \left(\nabla \times \vec{B} \cdot \left(\overleftrightarrow{\eta} \cdot \nabla \times \vec{B} \right) \right) + \left(\overleftrightarrow{\sigma} \cdot \nabla \right) \cdot \vec{v} - \nabla \cdot \vec{F}_{diff} - \dot{q}_{rad} \tag{11}$$

and includes the flow work, joule heating due to diffusion of magnetic field, diffusive transport of energy and radiation cooling.

The diffusive flux

$$\vec{F}_{diff} = \vec{F}_{thm}^{lim} + \vec{F}_r \tag{12}$$

is the sum of a limited thermal conductive flux and the flux due to radiation in equilibrium with the plasma.

The thermal conductive flux is given by

$$\vec{F}_{thm} = - \overleftrightarrow{k}_p \cdot \nabla T \tag{13}$$

where the tensor conductivity

$$\overleftrightarrow{k}_p = k_{p\parallel} \hat{e}_B \hat{e}_B + k_{p\perp} \left(\overleftrightarrow{I} - \hat{e}_B \hat{e}_B \right) \tag{14}$$

accounts for the inhibition of thermal conduction by the magnetic field. This flux is limited to prevent it from exceeding the free-streaming, or saturated, flux

$$F_{sat} = C_1 \, n_e \, T^{3/2} \tag{15}$$

which would be achieved if the entire plasma moved in one direction at the local average thermal velocity. The limit is applied using

$$\vec{F}^{lim}_{thm} = \min \left(\mid \vec{F}_{thm} \mid, \gamma \, F_{sat} \right) \frac{\vec{F}^{thm}}{\mid \vec{F}_{thm} \mid} \tag{16}$$

where $0 \leq \gamma \leq 1$ is a control parameter.

The energy flux due to diffusion of a radiation field in equilibrium with the plasma is

$$\vec{F}_r = \frac{C_2 T^3}{\kappa \rho} \nabla T \tag{17}$$

where κ is the Planck mean opacity.

The radiation cooling rate is taken to be

$$\dot{q}_{rad} = C_3 \kappa T^4 \tag{18}$$

This is applicable when the plasma is thin, and the radiation spectrum may be assumed to be Planckian.

THE EQUATIONS OF STATE AND TRANSPORT PROPERTIES

All of the equation-of-state quantities and transport properties, may be determined from idea gas laws and similar simple analytic expressions, or by using EOSPAC (Ref. 38) to do table look-up in the Los Alamos SESAME Equation of State Library (Ref. 39).

Application of these tables allows users of MACH2 to incorporate the skill, knowledge, and experience of equation of state and transport property experts into their simulations. It does not relieve them of the responsibility to choose an equation of state judiciously. The models used to generate the SESAME library are among the best known; however, they should not be used outside their stated range of validity. Determination of the suitability of a particular table for a particular problem is important, since tables of small range and high resolution are available for some materials. In many of the tables, there are regions in density and temperature space where interpolation between models has been used. If the lack of a tractable numerical model was the cause, substitution of a simple analytic model is not likely to provide superior results. However, the interpolation may have been used for other reasons, so that simple analytic models may be more appropriate.

DETAILED NUMERICAL SIMULATIONS OF A PFS

In the QUICK-FIRE series of experiments at the WL, a fast capacitor bank, an inductive store, and a PFS were used together to produce multimegampere currents with submicrosecond rise times in cylindrical foil loads. The capacitance of the SHIVA STAR bank is 1.3 mF, and the total initial inductance including the PFS and inductive store is 16.5 nH. In this series, the bank was charged to 95 kV which results in 5.9 MJ of stored electrical energy. Details of the QUICK-FIRE series of experiments may be found in Baker, et al. (Refs. 29, 30). As a result of the simulations of the QUICK-FIRE shots, suggestions were made for geometry changes that predicted improved current delivery to the load. These ideas were tested in subsequent shots that are described in a paper by Degnan, et al. (Ref. 40). Below we discuss the numerical simulations that led to the improved current delivery.

A drawing of the PFS is shown as Figure 5; the configuration is coaxial with the axis of symmetry at the left. A chordal array of 120 2.0-mil aluminum wires is used to initiate the gun plasma. Below the wire array is a barrier foil of 0.12-mil Mylar film which serves to limit travel of a plasma precursor generated by the explosion of the wire array. The total mass of the wire array and barrier foil is approximately 120 mg. The load consists of a thin cylinder of copper- or aluminum-plated Formvar with a mass of 10–25 mg. The radial vanes provide diagnostic access to the load. The axial vanes at the bottom

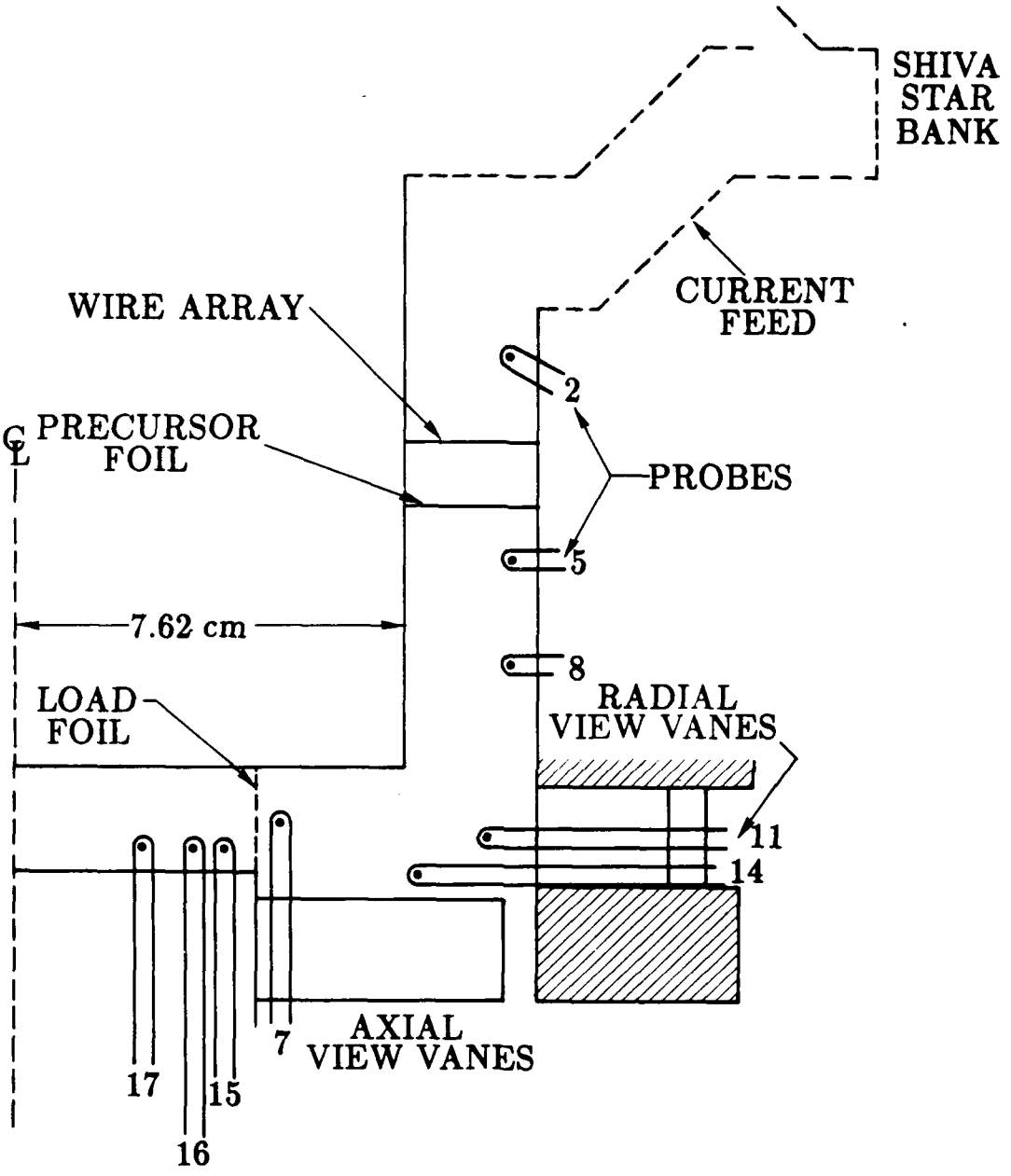

Figure 5. Sketch of PFS/imploding liner system.

provide diagnostic access and serve as a current path after switching. Typical positions of magnetic current probes are also shown.

At the beginning of a shot, energy from the SHIVA STAR capacitor bank is transferred to the vacuum inductor as the current carrying annular plasma is accelerated to 7–10 cm/μs down the gun. When the plasma runs off the corner of the gun, current is switched into the cylindrical foil load causing it to implode radially on axis. To produce a high quality efficient implosion, a large fraction of the total current must be delivered to the implosion foil during a short time interval.

The simulations are performed with the 2 1/2-dimensional MHD code, MACH2 which is described in detail above.

The best fractional current delivery in a low-mass implosion occurred in the fifth (QF5) of the QUICK-FIRE series of shots. For this reason, the parameters for this shot were used in simulations reported here. The initiation of the wire array and the interaction of the wire array with the barrier foil is a complex three-dimensional process which cannot be modeled in detail at the present time; thus, the first 1.9 μs of the experiment were modeled with a one-dimensional slug model. All MACH2 simulations discussed begin when the centers of mass of the wire array and the precursor foil overlap. The initial calculation mesh for simulations is shown in Figure 6. The switch plasma is located in the block at the upper right and is assumed to be 1.8 cm thick. The density of the switch plasma does not vary in a direction parallel to the axis of symmetry but is graded in the radial direction to approximate the actual density profile of the wire array and barrier foil. The actual density profile is approximately inversely proportional to the radius squared so that the magnetic force per unit area is proportional to the mass per unit area. The switch plasma is given an initial uniform velocity of 1.28 cm/μs as predicted by the slug model and a uniform temperature of 1.5 eV which is consistent with one-dimensional simulations of exploding wires under these experimental conditions. The switching plasma is taken to be pure aluminum. At the beginning of the simulations, the current is assumed to flow along the top edge of the switch plasma.

In the experiment the path of current flow and the location of the switch plasma and load plasma are inferred from current probes. Locations of the current probes are shown in Figure 5. Data from shot QF5 are shown in References 29 and 30.

In simulation 1, material was pulled in through the top of the coaxial gun at 10^{-6} g/cm^{-3} and allowed to freely flow through the vanes. The MACH2 simulation starts 1.9 μs after the bank is fired. This simulation gives good agreement with the experiment. Current traces at the experimental probe locations are shown in Figure 7. The curve labeled B is

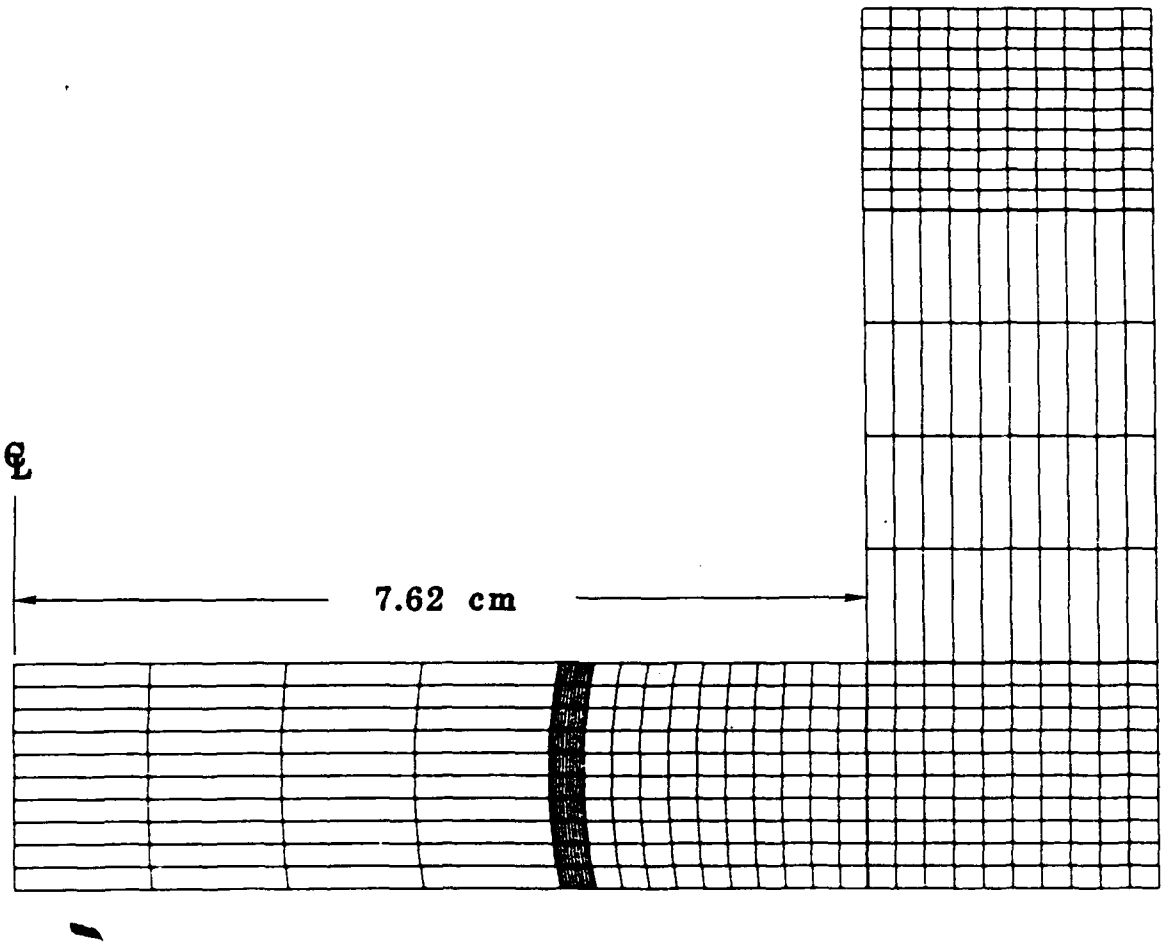

Figure 6. Initial calculation mesh for the MACH2 model of the PFS/Liner system.

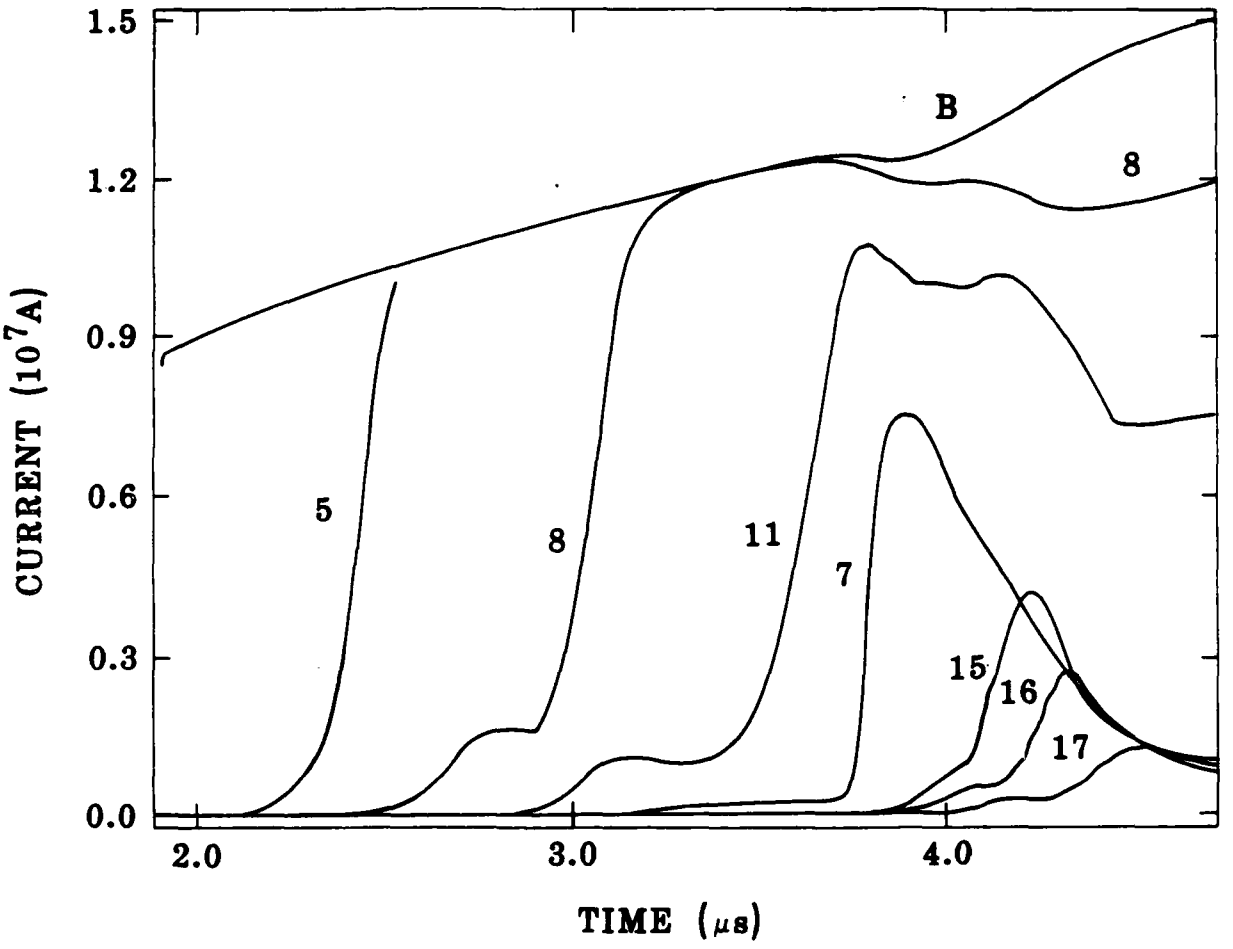

Figure 7. Current traces for simulation 1. Unlimited exit velocity and an injection density of 10^{-6} g/cm^3.

that determined by the circuit solver and should correspond to the current measured at probe 2. The other curves are labeled with the appropriate probe numbers as in Figure 5.

The total current is about 12 MA near the time when switching begins at 1.7 μs. Almost all the current arrives at the end of the gun as shown by probes 5 and 8. Some 20 percent of the current is lost at the probe 11 location. Probe 7 shows that only 60 percent of the current is initially delivered to the liner. As the liner starts to move, more current is lost. Probe 15 shows a maximum current of only 4.2 MA and probe 17 shows that only a little more than 1 MA is flowing through the liner as it passes that probe location.

In the current traces of probes 8, 11, and 7, one can clearly see a precursor. This results from gas being thrown ahead of the major portion of the current sheath, and a precursor is also observed in the experimental data. However, the size and shape of the precursor is determined by the assumptions made at the beginning of the simulation. So one should not attach too much significance to it other than to note that it is difficult to make it go away.

The current traces from the simulation are in good agreement with the experimental data from shot QF5. The experiment shows a little better current delivery than the simulation; this could be brought into closer agreement by lowering the density of the gas that is pulled in at the top of the gun.

Since the experiment and the simulation both show poor current delivery to the load, the next problem is to find a way to get more current to the load. One might expect that lowering the background plasma density would help. Also, in simulation 1, the low density gas is ejected out the end of the gun at high velocity (almost 80 cm/μs) by the current that flows there. One might expect that the velocity of this low density gas should be limited to the ejection velocity of switch mass (7 cm/μs) as it exits the vanes. The switch mass plugs the vanes, therefore, limiting the velocity of the low density flow.

In simulation 2, the density at which plasma is pulled in through the top of the gun is reduced to 10^{-7} gm/cm^3, and the outflow velocity through the vanes is limited to be no greater than 7 cm/μs. The current traces for this simulation are shown in Figure 8. Almost all the current is delivered to the load. This is the kind of performance that one would like to achieve experimentally.

The question of whether lowering the background density or limiting the outflow velocity is more important remains. In simulation 3, the density at which plasma is pulled in is 10^{-7} g/cm^3, but the outflow is unlimited as in simulation 1. The current traces are shown in Figure 9. While the current delivery to the load is improved over that of

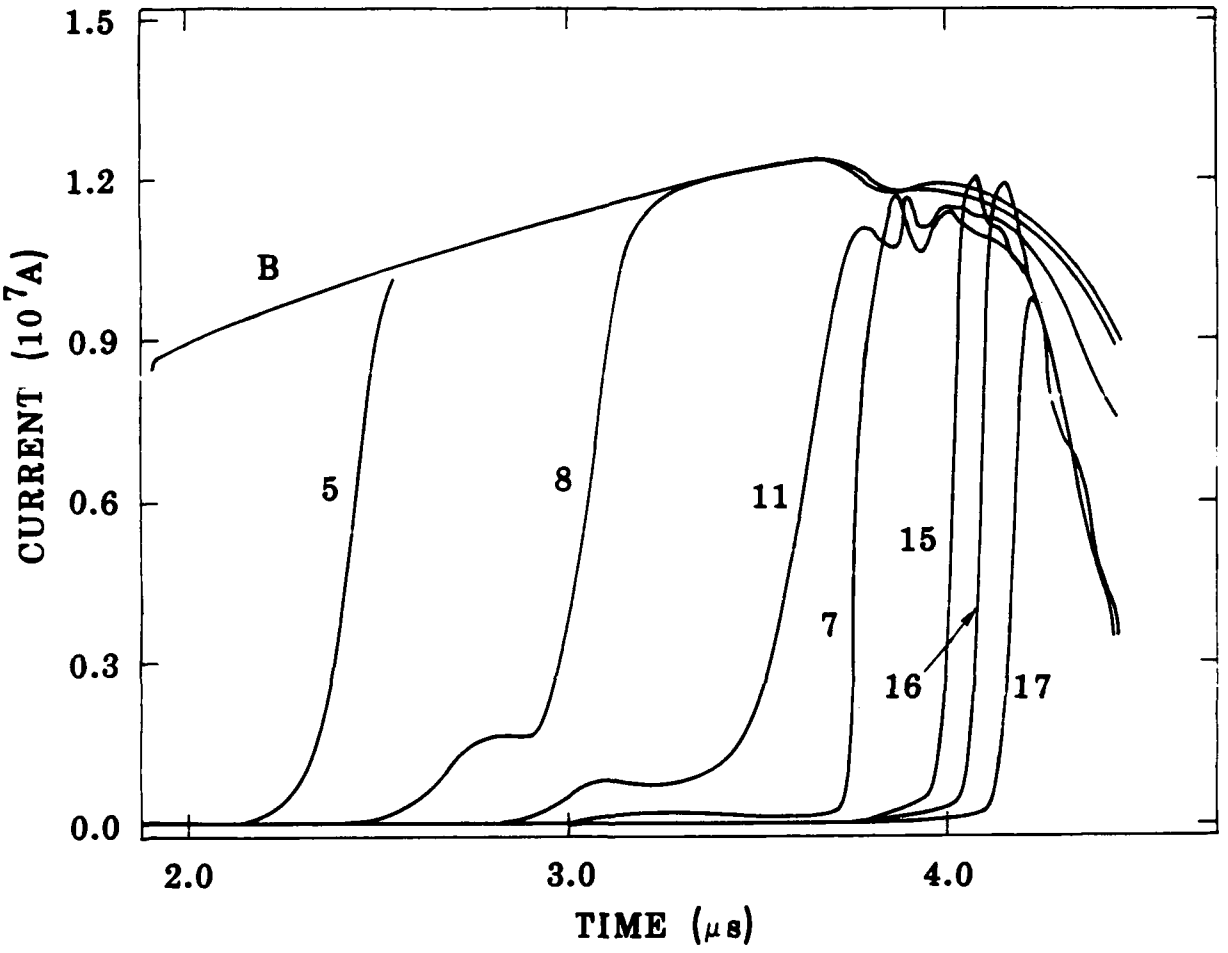

Figure 8. Current traces for simulation 2. Exit velocity limited to 7 cm/μs and injection density of 10^{-7} g/cm^3.

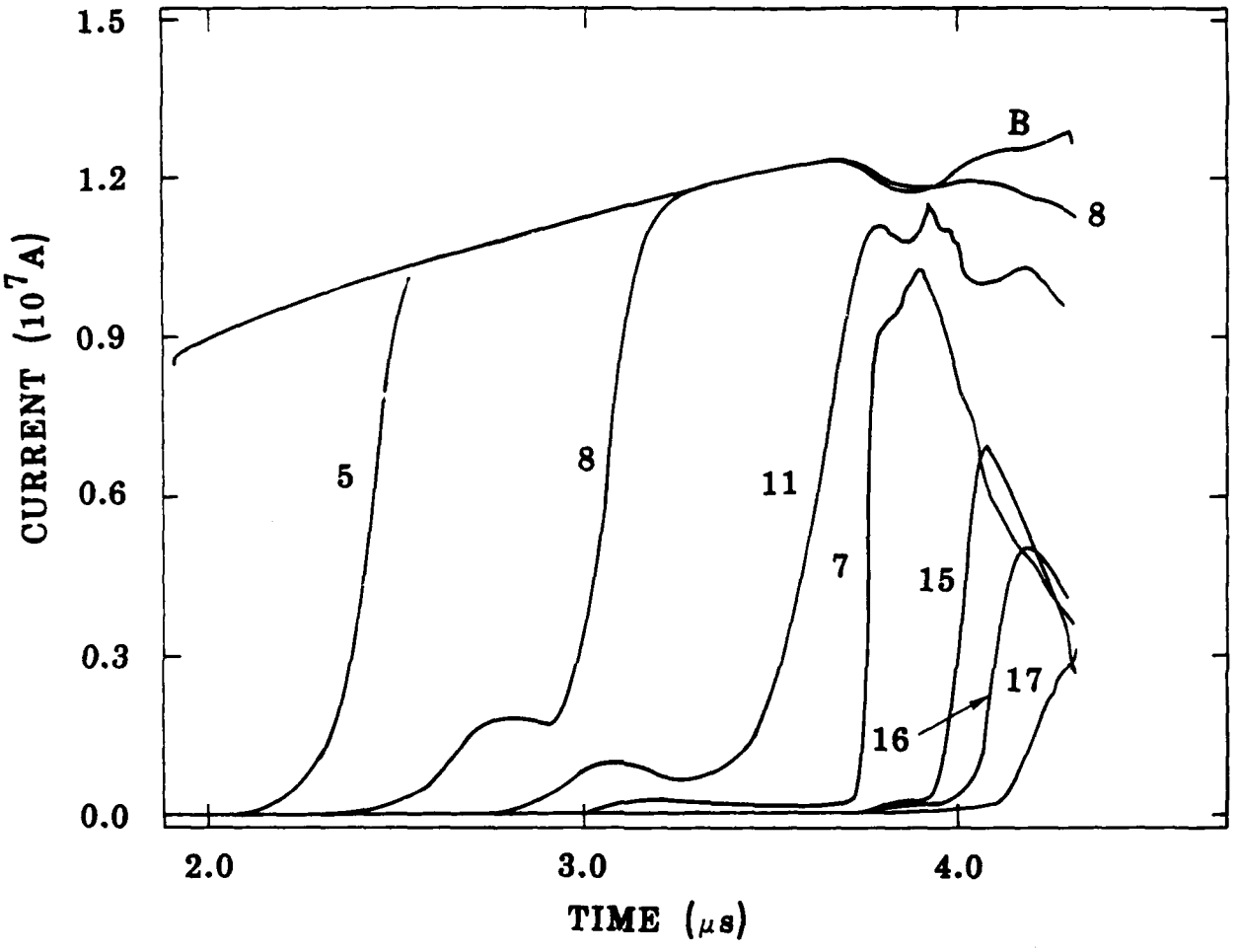

Figure 9. Current traces for simulation 3. Unlimited exit velocity and an injection density of 10^{-7} g/cm^3.

simulation 1, it is far from perfect. The maximum current delivery at probe 15 is only 57 percent, for example.

In simulation 4, the density at which plasma is pulled in is 10^{-6} g/cm^3 as in simulation 1, but the outflow velocity is limited to 7 cm/μs as in simulation 2. Note from Figure 10, that the current delivery to the load is quite good. About 90 percent of the current is delivered to the load as it passes the location of probe 15. The load is carrying 8 MA as it passes the location of probe 17.

Limiting the outflow velocity is more important because this is easier to achieve than reducing the background density. One can reduce the outflow velocity in the experiment by closing the radial view vanes completely and closing the axial vanes partially. Reducing the background plasma density, which is presumably created by ablation powered by the ultraviolet radiation from the switch plasma, is likely to be much more difficult.

IMPROVED GEOMETRY SPECIFICATION METHOD FOR MACH2

Under this subtask, MRC got MACH2 running on the Cray 1 and the Cray 2 at the WL Supercomputing Center. As part of this effort, MACH2 was upgraded to provide the ability to easily specify the geometry of the MACH2 computational problem domain.

Using the namelist, $EZGEOM, the user describes a grid by specifying the coordinates of the corners of each block only once. Two new methods of describing arcs have also been added. The MACH2 arrays KNBR, NBRBDY, BDYGEOM, and BGPARMS are all built from this information. If $EZGEOM is used, these variables will be written to file <s>om2 in the form of namelist $INMESH. It is still necessary to include $INMESH to give ICELLS, JCELLS and any nondefault boundary conditions. This new facility is optional; old input decks will work without modification.

If $EZGEOM is used, it may be placed before or after $INMESH, but there are two things to consider when deciding which to place first. First, note that although NBLK can be input via either namelist, it must be given in the first of $EZGEOM or $INMESH to appear in an input file. Second, it is important to remember that the namelist that occurs last will determine the value on any parameter which occurs in both.

To describe a geometry with $EZGEOM, three sets of parameters must be given. The first is a list of the coordinates of points in the plane. Each point is assigned a unique integer label. The next set connects the points into blocks by listing the integer labels of the four points that are the corners of each block. The corners should be listed in the

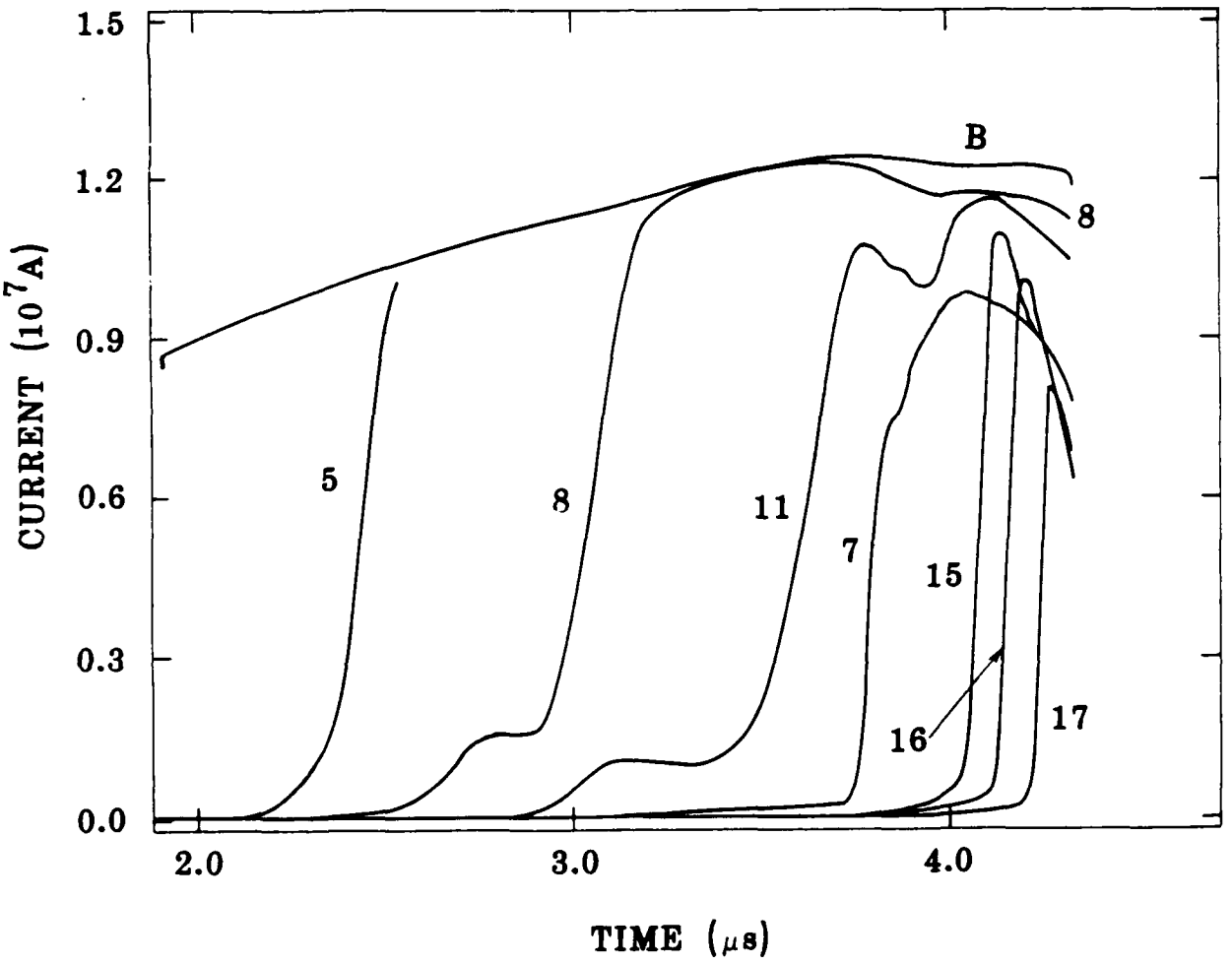

Figure 10. Current traces for simulation 4. Exit velocity limited to 7 cm/μs and an injection density of 10^{-6} g/cm^3.

standard MACH2 order (clockwise from the upper left). Lastly, any arcs in the problem are described by choosing two end-points (these two points must form an edge in at least one block) and either an angle of departure from the first point, or a third point (not a corner of a block) that lies on the arc between the two end-points. Figures 11 and 12 illustrate the arc specifications.

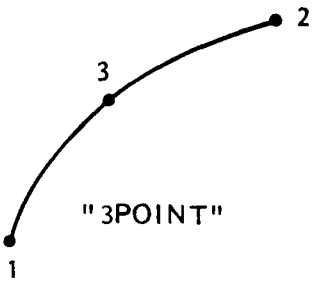

Figure 11. Data that are required to specify a block boundary in a MACH2 simulation in which the user chooses arctype (this arc) = "3point."

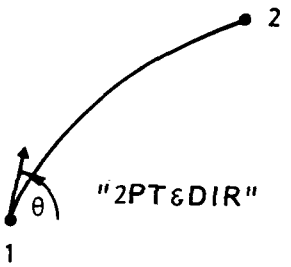

Figure 12. Data that are required to specify a block boundary in a MACH2 simulation in which the user chooses arctype(this arc) = "2pt&dir."

2.3.2.2 Reports. Documents prepared under this subtask are summarized here.

"Simulations of a Plasma Flow Switch"
J. Buff, M. H. Frese, A. J. Giancola, R. E. Peterkin, Jr. and N. F. Roderick
AMRC-R-928
April 1987

ABSTRACT: In a portion of the experimental program using the SHIVA STAR capacitor bank at the WL, a cylindrical foil load is imploded using an inductive store and a PFS. We have performed a number of two-dimensional simulations of the switch and load using the MHD code MACH2. In addition to explaining the data from the first series of

experiments, the simulations led to design modifications of the basic PFS that resulted in improved current delivery and in enhanced radiation yield. The experimental results are reported in a companion paper by Degnan et al. The key modification was closing portions of the vane structure. The switch must be sealed shut or else substantial current will flow in the diffuse gas that is ablated from the walls of the switch barrel.

"New MACH2 Grid Specification Method"
Anthony J. Giancola
AMRC-N-371
June 1987

ABSTRACT: The MACH2 code has been upgraded to provide the ability to easily specify the geometry of the MACH2 computational problem domain. This is done via namelist, a Cray Fortran extension, with the new namelist, $EZGEOM. The implementation is discussed in this technical note.

"MACH2: A Two-Dimensional Magnetohydrodynamic Simulation Code for Complex Experimental Configurations"
Michael H. Frese
AMRC-R-874
September 1987

ABSTRACT: The MACH2 code is a flexible and powerful two-dimensional MHD simulation code designed specifically to handle complex experimental configurations. The code's capabilities include a numerically generated solution-adaptive grid which permits it to be used for either Eulerian or Lagrangian flow problems, use of real equations-of-state and transport properties from the LANL SESAME package, and a multigrid implicit magnetic field diffusion solver which can be used to simulate problems with vacuum.

This report details the physical model, including boundary conditions; permissible problem geometries; time differencing; and spatial discretization, centering, and differencing of MACH2. The next revision of this report will also cover the iteration procedures for the implicitly differenced physical processes, as well as the boundary conditions and block coupling implementation techniques.

"Task Report: SHIVA STAR Computational Physics Studies I"
James Buff, Michael H. Frese, Anthony J. Giancola, Robert E. Peterkin, Jr. and Norman F. Roderick
MRC/ABQ-R-1036
February 1988

ABSTRACT: This report documents the work performed by MRC under the SHIVA STAR Computational Physics Studies subtask of the Beam and Plasma Physics contract with the WL. This report consists of three topical reports which are (1) a paper describing our simulations of the PFS experiments, (2) a paper describing the physics, algorithms, and numerical methods used in the two-dimensional MHD simulation code MACH2, and (3) a description of the new and much simpler grid specification for MACH2.

2.3.3 Subtask 03-03, Coaxial Plasma Gun Physics Studies

2.3.3.1 Research Summary. The objective of the Coaxial Plasma Gun Physics Studies subtask was to provide theoretical support for the plasma projectile R&D program at the High Energy Plasma Division. This program includes investigation of phenomenology and techniques applicable to the creation and acceleration of low-temperature plasmas to high velocities for use as plasma projectile weapons.

Initially, the scope of the subtask was limited to the design of diagnostic techniques relevant to the measurement of plasma characteristics in the plasma gun experiments, analysis of results from the diagnostics, and comparison with theoretical predictions. Mission Research Corporation chose, with the concurrence of WL scientists, to focus on the development of a time-resolved optical spectroscopy diagnostic and analysis methodology. The results of this work are described below.

During this subtask, the scope of the work was expanded to address pulsed power issues related to plasma acceleration schemes. Within the expanded scope, MRC participated in the design and analysis of air-core transformer circuits and the assessment of techniques to improve the performance of radially-imploded liners. The air-core transformer work and the liner implosion topic are discussed below.

AIR-CORE TRANSFORMER PULSED POWER DEVELOPMENT

One of the tasks, in conjunction with Maxwell Laboratories personnel, was to design an air-core, air-insulated pulse transformer circuit. The purpose was to develop a convenient and dielectric-oil-free method of converting the output of a moderate voltage (120 kV) SHIVA module capacitor bank so that it would be suitable for driving electron beams at voltages of 250 kV or more. Given that the capacitor bank could not be altered, a voltage step-up transformer was chosen to match the driver to the load. Much of the groundwork for this effort was laid by Colclaser, et al., at the WL previously (Ref. 41).

The transformer technology described below will also satisfy requirements for light weight air- and space-borne platforms. The weight of transformers is greatly reduced by eliminating ferrite core material and dielectric oil insulation. The resulting problems of transformer coupling and high voltage insulation are solved by placing the largest possible diameter, spiral-wound secondary coil within the primary coil and the use of voltage grading techniques.

The transformer circuit is shown in Figure 13. The driver is a single SHIVA capacitor module with a maximum output voltage of 120 kV, a capacitance of 36 μF, an inductance of 20 nH, and a maximum stored energy of about 250 kJ. The module consists of two 72-μF capacitor banks, one charged positively and one charged negatively, which are discharged in series. The output pulse is of negative polarity. A 61.0-cm (24-in) wide parallel plate transmission line in series with a fuse connects the capacitor bank to the primary coil of the pulse transformer. The transmission line/fuse assembly is 203 cm (80 in) long. A fuse is necessary to protect the capacitor module from voltage ring-over when the initial charging voltage is 50 percent of maximum or greater. Thirty-three sheets of 0.013-cm-thick Mylar provided insulation between the upper and lower halves on the transmission line. This circuit possessed a nominal inductance of 40 nH and a resistance of 10 mΩ.

TIME-RESOLVED OPTICAL SPECTROSCOPY

As mentioned above, we were tasked with developing diagnostics suitable for coaxial gun plasmas. Fundamental to the understanding of complex plasma processes, such as formation and acceleration, is a knowledge of the evolution of plasma species, temperature, and density. Spectroscopic techniques (that is, methods based on the spectral features of the plasma radiation) are potentially the most effective means of obtaining this information (Ref. 42). Therefore, one of the main goals of the Coaxial Plasma Gun Physics Studies subtask was to develop a capability for time-resolved optical spectroscopy using an optical multichannel analyzer (OMA). This required setting up the equipment to acquire spectra, as well as developing a methodology for analyzing the spectral data.

EQUIPMENT

The basic instrumentation used for this work was an EG&G Princeton Applied Research OMA III optical multichannel analyzer system, comprising a Model 1460 System Processor, a Model 1211 High Voltage Pulse Generator, a Model 1216 Multichannel Detector Controller, a Model 1254E Silicon Intensified Target (SIT) Vidicon Detector, a Model 1233 Spectrograph, and a Model 1301 Optical Trigger Unit. A block diagram of the

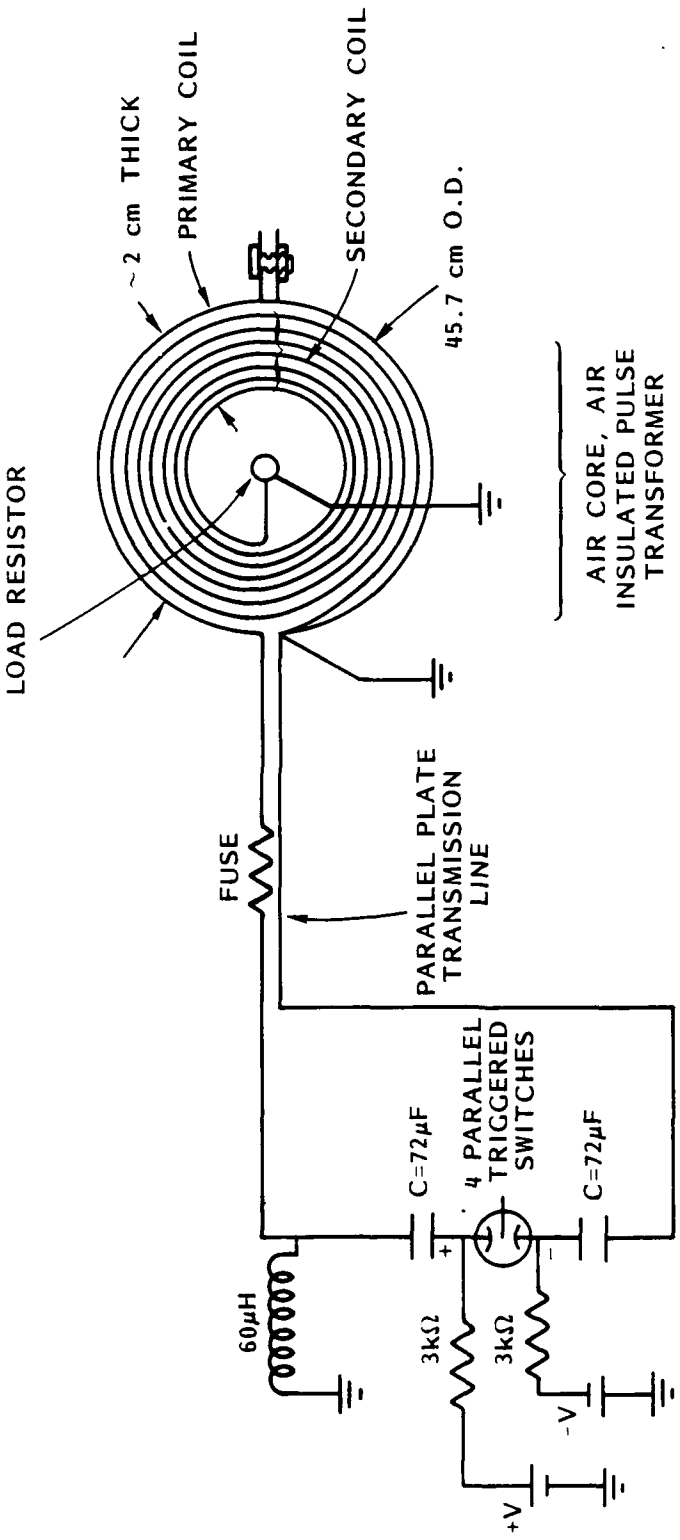

Figure 13. Air-core transformer circuit.

system is shown in Figure 14. Also indicated in the figure is an RF shield designed to protect the instrumentation from the extreme ambient noise levels encountered.

The spectrograph was actually a Jarrell-Ash Monospec 27 Monochromator/Spectrograph, Model 82-499, equipped with a triple grating turret with rulings of 150 l/mm, 600 l/mm, and 1800 l/mm, in a crossed Czerny-Turner configuration. The characteristics of the spectrograph are summarized in Table 5 for each of the gratings. The spectrograph focal length was 275 mm, and the focal ratio was f/3.8. A variety of entrance slits were available, but a 25-μm fixed width slit was routinely used for maximum resolution.

TABLE 5. Spectrograph and grating specifications.

Ruling (l/mm)	Blaze (Å)	Range (Å)	Dispersion (Å/mm)	Resolution* (Å)
150	holo	2000-8000	240	24
600	5000	4800-12000	60	6
1800	holo	1900-7000	20	2

*Instrument resolution with 25 μm $\times$ 5 mm (w $\times$ h) fixed slit

The detector used at the exit port of the spectrograph was a SIT-tube vidicon. A typical vidicon detector target consists of a disk of silicon 16 mm in diameter, with a microscopic array of several million photodiodes on it. The diodes have a common cathode and isolated anodes, which are selectively addressed by a scanning electron beam. The beam serves both to read out signals from the target, and to recharge it. When light falls upon the target, electron-hole pairs are generated, which recombine to deplete the surface charge. As the beam scans the depleted area, a recharging current flows, which is sensed, amplified, and integrated. The scanning beam, when properly focused, is approximately 25 μm in diameter, resulting in a pixel array of 512 $\times$ 512. A channel is defined as any number (from 1 to 512) of vertically aligned pixels one pixel wide. A track is any number (from 1 to 512) of adjacent channels.

IMPLOSION FOIL STABILIZATION

Mission Research Corporation investigated possible experimental approaches to improve the symmetry of the QUICK-FIRE implosion (Refs. 29, 30) without significantly

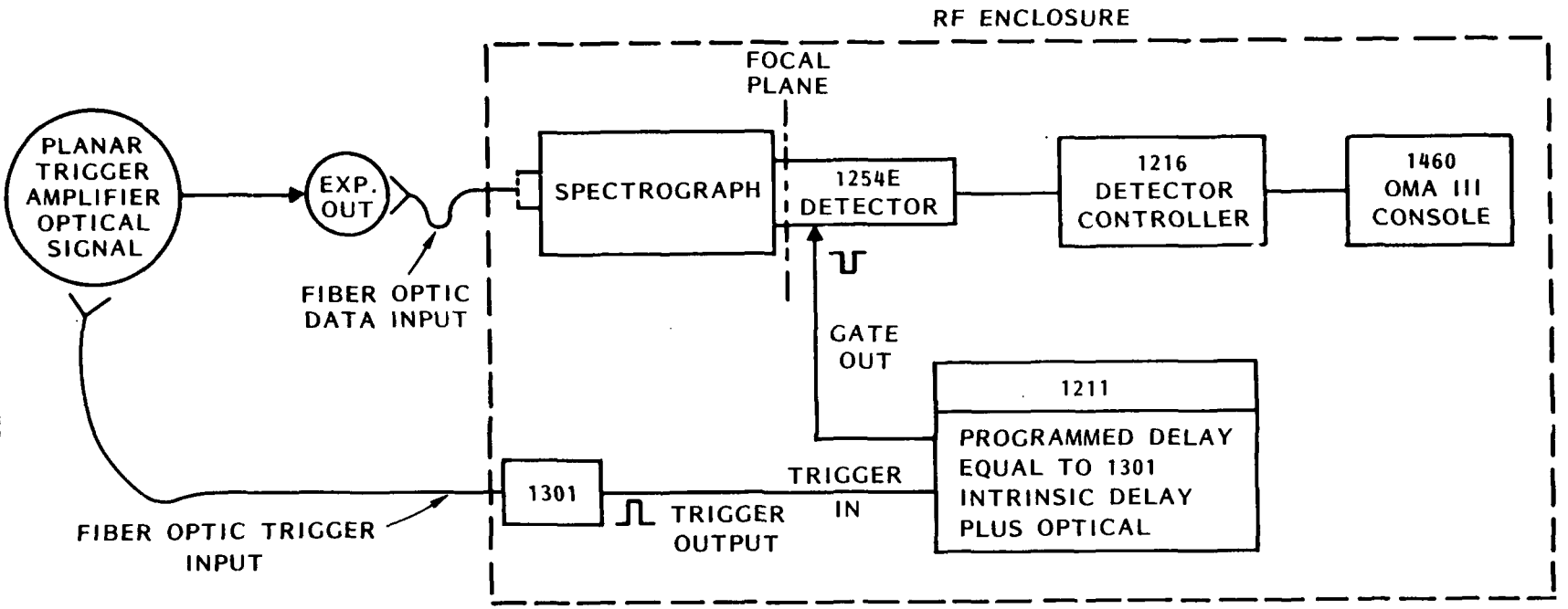

Figure 14. Instrumentation block diagram.

complicating the preparation of SHIVA for each shot. The three most important tasks that will improve the foil implosion are as follows, in their order of importance:

1. straightening the bowed foil,
2. preventing plasma streamers, and
3. reducing switch effects.

To understand why the above tasks need to be done, the basic concepts of SHIVA's operation need to be reviewed. The QUICK-FIRE (foil implosion) setup is shown above in Figure 5. The purpose of this device is to multiply the power output of SHIVA STAR by means of an intermediate storage inductor and a foil implosion to produce a 10 TW, short burst (tens to hundreds of nanoseconds) X-ray source. The SHIVA has a maximum output voltage of 120 kV, a capacitance of 1313 μF, an inductance of 3 nH, a maximum stored energy of 9.45 MJ, and a nominal output current of 12 MA, depending upon the load. A negative pulse from the capacitor bank is directed through a convoluted power feed into the inner conductor of the assembly. The outer conductor is grounded. The power feed is anodized, evacuated, and shaped so that the intense ultraviolet radiation from the plasmas formed in QUICK-FIRE is absorbed and does not lead to a high voltage breakdown of the power feed.

As current is injected into the inner conductor, it is initially conducted to ground by a wire grid located just below the power feed. The wire grid becomes ionized and is accelerated downward by the Lorentz force. In the process, the inductance caused by the power feed and the short coaxial section between the wire grid and the foil becomes charged in about 4 μs. At the end of the inner conductor (coaxial gun muzzle) where the foil is located, the plasma due to the wire grid is moving downward at a speed of 7 cm/μs and begins to travel across the gap. Current is no longer conducted from the inner to outer conductors and the once shorted inductance (which is due to the power feed and the short coaxial section) becomes open circuited. A 500-kV voltage spike across the foil results, and it conducts about 10 MA of current and is imploded radially inward for 0.5–0.8 μs. Kinetic energy is imparted to the foil until the implosion stagnates near the center. Then the foil thermalizes and a 0.1–0.5 μs burst of soft X rays results. The maximum X-ray power achieved thus far is 2–3 TW, with a total energy of about 0.5 MJ.

STRAIGHTENING THE BOW

Straightening the bow in the foil is the most important task. The longest wavelength corresponds to that of the foil bow, and thus any macroscopic displacement due to the

bow grows rapidly as the foil implodes. Since there is no effective method to control this growth once it begins, the bow must be straightened so that the initial displacement from which the instability grows is minimized. The displacement will still grow, but its amplitude at the end of the implosion cycle will be less. Seven approaches to straightening the foil were considered. They are:

1. heat treatment of the foil during sputtering so that the surface tension and thus the bow are reduced,
2. a cast foam instead of a foil,
3. injection of a gas puff to push out the bow,
4. commercially available seamed foils,
5. static gas fill to push out the bow,
6. mechanical fingers to push at the sides of the foil to reduce the bow, and
7. a wire mesh.

While sputtering a metallic coating onto the surface of a Formvar foil, the operator can increase the power of electron beam impinging a metallic target which is providing the sputtered atoms, thereby heating the foil. The heating has tended to reduce the bow to less than 1-mm displacement by relaxing the surface tension of the foil. A typical foil in past experiments has about 3 mm of bow. The heating induces wrinkles which may serve as initial displacements from which shorter wavelength instabilities may grow. We expect that an additional two man-months of trial and error experimentation will reduce the extent of the wrinkles. To date, the best foil ever produced at the WL has been prepared using this method. Therefore, this method is the first choice.

Microcellular ultralow-density foams (Ref. 43) are a recent development of the SNL and LANL. Programs such as the X-ray laser effort have stimulated the research into foams. Foam densities ranging from 3–20 mg/cm^3 have been achieved by quick-freezing a polyacrylic acid solution to form a cellular structure and freeze-drying to remove the water. The intercellular spacing is 20 μm or less. The advantages of foam are that it can be molded into the desired shape and, with some minor changes of existing hardware, can be quickly mounted into the QUICK-FIRE assembly. To produce a 300-$\mu g/cm^2$ surface density liner, a 0.6-mm thick foam is required (assuming a 5-mg/cm^3 density; 3 mg/cm^3 is difficult to achieve). Typical foils now in use are 200–300 μm thick and thus the 0.6-mm thick foams will be much easier to handle (Fig. 15).

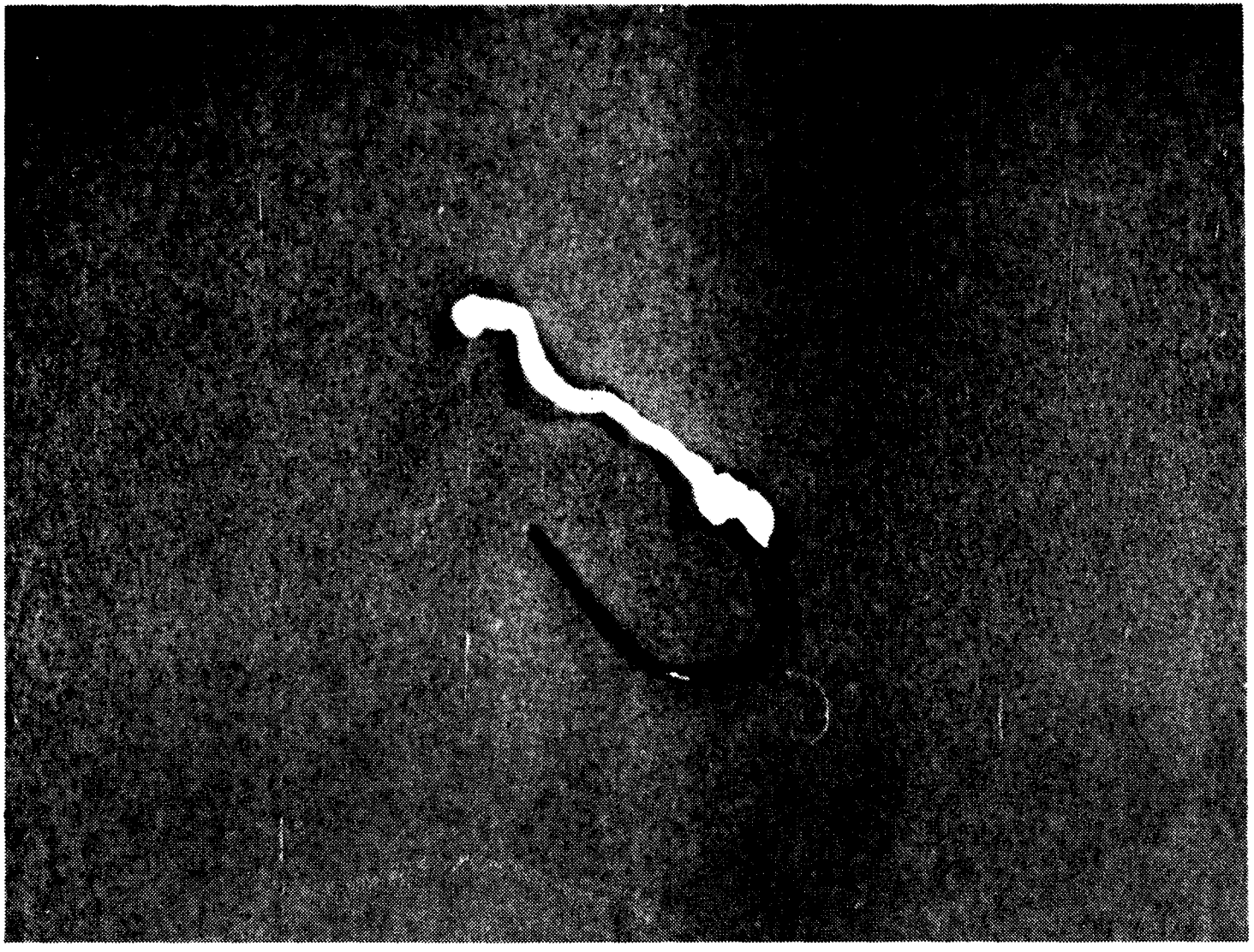

Figure 15. Microcellular foam sample from which a fast liner may be constructed.

The foam dimensions that is required lie well outside the experience of SNL and therefore annular foam shells of 10-cm diameter require some development. In addition, these foam shells may be bowed. For near-term experiments, foams should not be used.

The injection of a gas puff is another contender. The WL possesses a fast gas puff valve of a design developed by Wong and coworkers (Ref. 44). To push out the bow in the foil, a gas pressure as low as a few millitorr to a few torr would be sufficient. The advantages of this approach are that the gas puff valve hardware exists and, with some development, this technology can be applied to Raleigh-Taylor stabilization (discussed below) or to compact toroid (CT) research. The largest disadvantage is that the valve is not a passive element like a foil and the timing between when the puff valve is fired and when the foil is straightened may be critical to within a few tens of microseconds. The timing may differ from foil to foil. A test setup is being assembled to determine the viability of gas puffing. To adapt this system to the SHIVA hardware, some modifications will be necessary to rigidly mount the bottom of the foil so that it will not be displaced by the gas puff pressure. Presently, only the top of the foil is attached to the inner conductor and the bottom hangs free.

Another alternative is the use of commercially available sheet foils. They come in thicknesses as small as 2 μm with or without conductive coatings. When wrapped to form an annulus, there will be a seam; but the foil material can be ordered thin enough such that three or more wraps are required to obtain the required foil mass and the effect of the seam can be minimized. The SHIVA technicians have tried this approach before and consider it more difficult than making a continuous annular foil. Therefore, the seamed foil approach is rejected.

The fifth alternative of a static gas fill has been rejected. We considered the possibility of sealing the volume inside the foil and filling with a static gas to push out the bow. The major disadvantage is that the foil will be porous because it is so thin (about 200–300 μm) If any gas leaks into the power feed region, it will arc and disrupt QUICK-FIRE.

The next alternative of mechanical fingers has also been rejected. The reason is that the heating techniques discussed above will achieve the same basic result (straightening the foil while causing some wrinkles) with less mechanical complexity.

The last alternative considered is the use of a wire mesh instead of a foil. Wire meshes are straightforward, but time consuming, to fabricate. Their disadvantage is that the mass density will vary either in the azimuthal or axial direction or both. For now, this approach is not considered a high priority.

In summary, we recommend that the heat treating of a continuous Formvar foil to relieve surface stress and reduce the bow be the primary approach for the next series of QUICK-FIRE shots. Gas puffing should be the backup. Ultralow-density foams are the most exciting new development, but they require a 6-mo development period because the dimensions of the foams required for QUICK-FIRE are much larger than any foam targets made to date. Seamed foils, static gas fills, mechanical fingers, and wire meshes should be ruled out for now.

2.3.3.2 Report. Document prepared under this subtask is summarized here.

"Subtask Report: Coaxial Plasma Gun Physics Studies"
Gerald F. Kiuttu and Kenneth O. Busby
MRC/ABQ-R-957
December 1987

ABSTRACT: This report reviews and summarizes the work performed by MRC under the Coaxial Plasma Gun Physics Studies subtask of the Beam and Plasma Physics contract with the WL. The three areas that were addressed in this work are (a) development of an air-core transformer circuit to couple low-impedance capacitor/transmission line drivers to moderate-impedance resistive loads, (b) development of time-resolved optical spectroscopy techniques and analysis methodology for diagnosing coaxial gun plasmas, and (c) evaluation of methods for improving the performance of alternate final loads for coaxial gun systems.

2.3.4 Subtask 03-04, Compact Toroid Computational Physics Studies

2.3.4.1 Research Summary. This subtask was one in which MRC and the WL began to develop the ability to study compact torus (CT) plasmas with the aid of 2 1/2-dimensional numerical simulations. The code of choice was MACH2 because its design included all three components of vector fields such as the velocity and the magnetic induction. However, in previous computational subtasks under task area 3, magnetic fields with only a toroidal component were employed, and the resulting velocities had components only in the plane of the computation.

This study demonstrates that the poloidal field capability of MACH2 is ready to be used in a coordinated theoretical and experimental program to investigate the generation, acceleration, and focusing of compact toroids. In addition, it demonstrates a capability to model those effects in the full scope of complex geometries for which MACH2 was designed. Further, the addition of poloidal fields to MACH2 makes possible many problems which could not have been done before. Among these is the study of effects of two-dimensional

perturbations during liner initiation, which can now be carried out in the plane transverse to the liner. This would provide an understanding of the observed nonuniform initiation seen for low current rise rates.

Prior to this study, no extensive use had ever been made of the capability of MACH2 to model poloidal magnetic field effects. Hence, the governing equations and their implementation had to be validated as the first step in the study of compact toroids using MACH2. Remarkably, few mistakes were found in this process; all of those were corrected.

As part of this validation, numerous simple one-dimensional problems were run to test the models of the diffusion, transport, and MHD processes included in the code (Ref. 45). These included a symmetric θ-pinch, and z-pinch compressing B_z in the center. In all cases, problems which should have remained one-dimensional did so to the level of accuracy of the geometric coefficients (approximately 12 significant figures out of the available 14). None of those calculations will be discussed here.

PROBLEM SETUP

The experimental geometry used to generate a compact toroid is essentially a stepped expansion in a coaxial plasma gun, as shown in Figure 16. This particular geometry is almost the same as that of the generation simulated by J. L. Eddleman and coworkers using HAM (Ref. 46). The MACH2 version consists of 4 blocks. The simulation described here was run using Version v8702 of MACH2, the first version to run on the Cray 1 at the WL.

An initial field of 0.73 T is imposed through the bottom half of the smaller cross-section coaxial region at the top. This corresponds to a poloidal flux of 0.046 Wb, or approximately twice that of Eddleman's simulation. All other parameters are the same as those of Eddleman's. The initial density of the plasma in the gun is 3.3×10^{-5} kg/m^3 which corresponds to a particle density of 2.0×10^{16} cm^{-3}.

The plasma in the upper blocks is expelled through the poloidal field by the action of a poloidal current injected into the top of the simulation region from an attached single loop resistor-conductor-capacitor (RLC) circuit. The circuit parameters (also the same as used by Eddleman) are

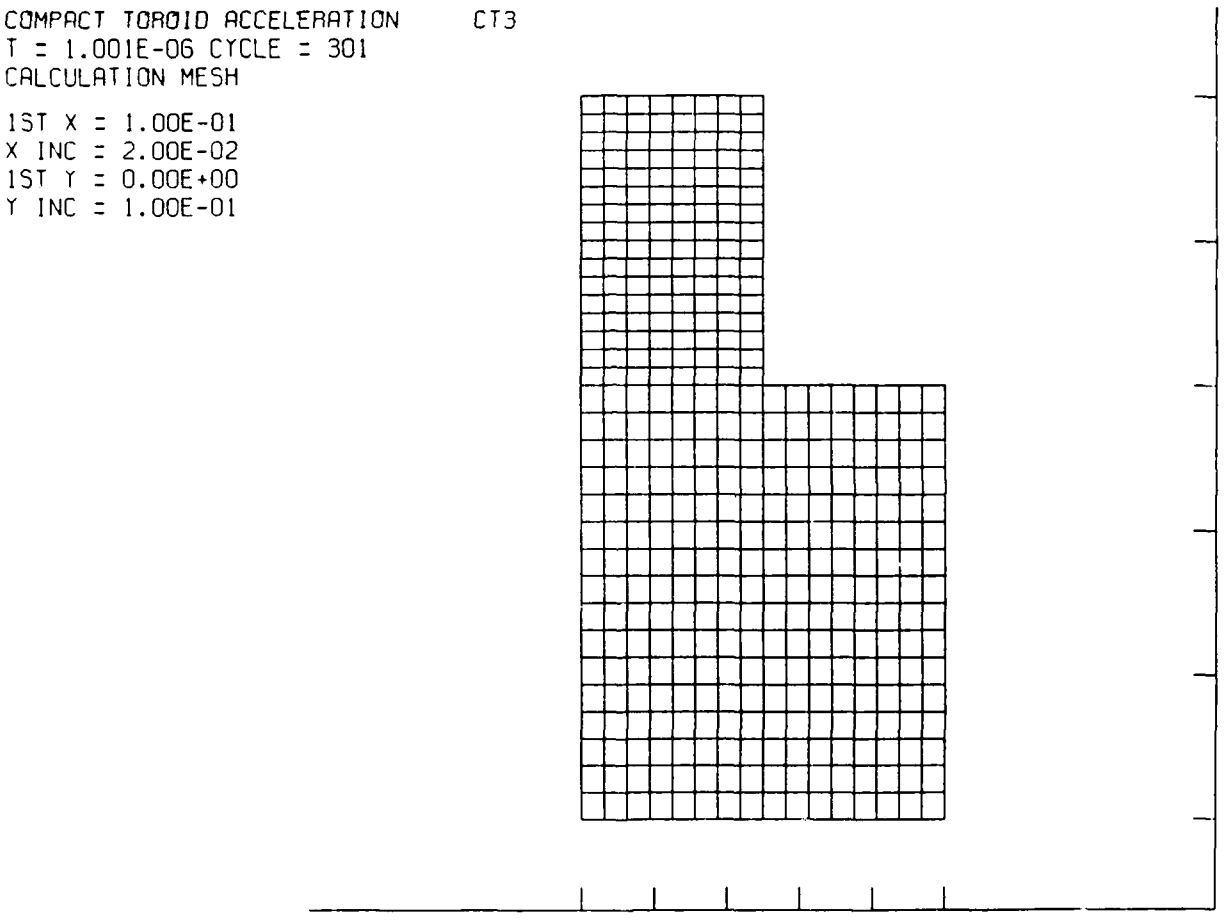

Figure 16. Toroid generation simulation geometry.

external inductance = 10 nH

bank capacitance = 37 μF

bank voltage = 50 kV

with a resulting bank energy of 46 kJ. The short circuit RLC time of this bank is 0.95 μs, but due to the sudden increase in the inductance of the coaxial gun when the ring pops out into the expansion region, the peak current in the simulation occurs somewhat earlier at 0.75 μs. The peak current is also reduced from the short circuit value, and peaks at approximately 1.5 MA.

SIMULATION RESULTS

It was found, as discovered previously by Eddleman (Ref. 47), that the velocity boundary condition in the field injection region was critical to the formation of the toroid. The condition imposed there must be a no-slip condition or the field lines will be swept along the boundary, and toroid formation through reconnection of the field lines will be very weak. The suppression of slip at these boundaries is a reasonable assumption because the field lines that enter through the conducting walls there will be trapped in the conductor and in the plasma, and will resist formation of a thin shear layer at the interface.

Figures 17 through 19 show the state of the plasma and fields at 2.0 μs after the current begins to rise from zero. The three figures show the plasma electron number density, the toroidal field, and the poloidal magnetic field. While considering these figures, it is important to remember that the quantities in the upper two blocks are scaled separately from those in the lower two blocks.

At 1.0 μs the plasma initially in the upper two blocks is just beginning to be pushed out into the expansion region by the poloidal current sheath. The poloidal field lines are being bent along the toroidal field contours, and the resultant toroidal current is causing a circulation in the poloidal field there. The formation of the magnetic torus is just beginning. At 1.5 μs the ejected plasma is just starting to impact the outer wall of the expansion region, as evidenced by the slight peak in the number density. The poloidal magnetic field shows the existence of a ring-like structure near the same location. At 2.0 μs, as seen in Figures 17–19, the ring is fully formed and shows clearly in both the magnetic field plots and the density plot.

MACH2 is clearly capable of simulating experiments with poloidal field and its effects.

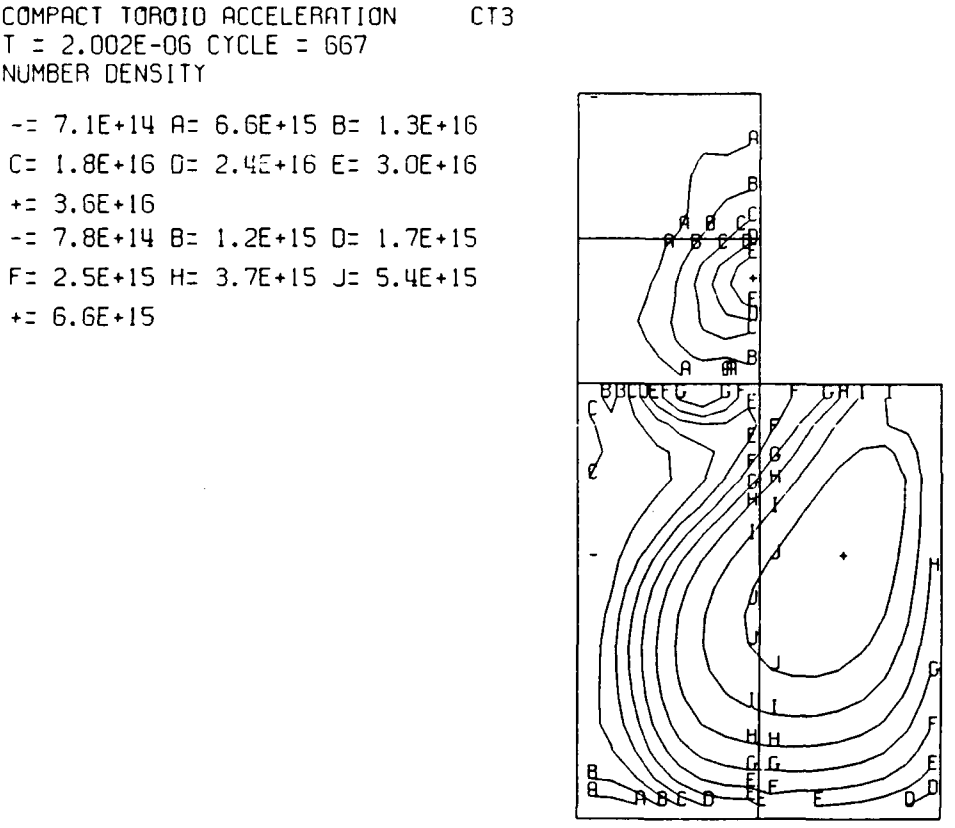

Figure 17. Toroid generation at 2.0 μs: number density.

COMPACT TOROID ACCELERATION CT3
T = 2.002E-06 CYCLE = 667
TOROIDAL FIELD

-= 1.9E+02 A= 4.9E+02 B= 8.0E+02
C= 1.1E+03 D= 1.4E+03 E= 1.7E+03
+= 2.0E+03
-= 3.8E-01 B= 3.4E+02 D= 6.8E+02
F= 1.0E+03 H= 1.4E+03 J= 1.7E+03
+= 1.9E+03

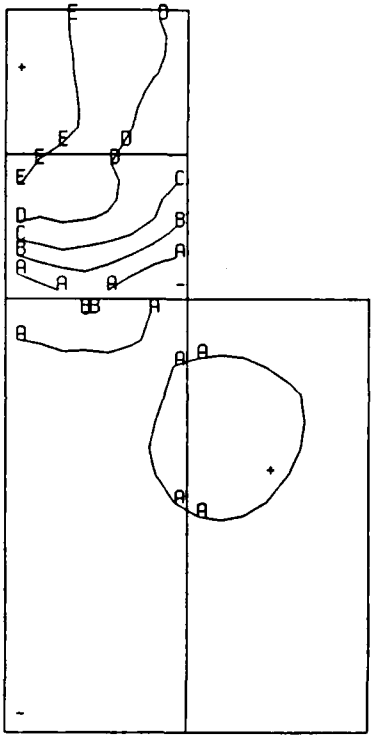

Figure 18. Toroid generation at 2.0 μs: toroidal field.

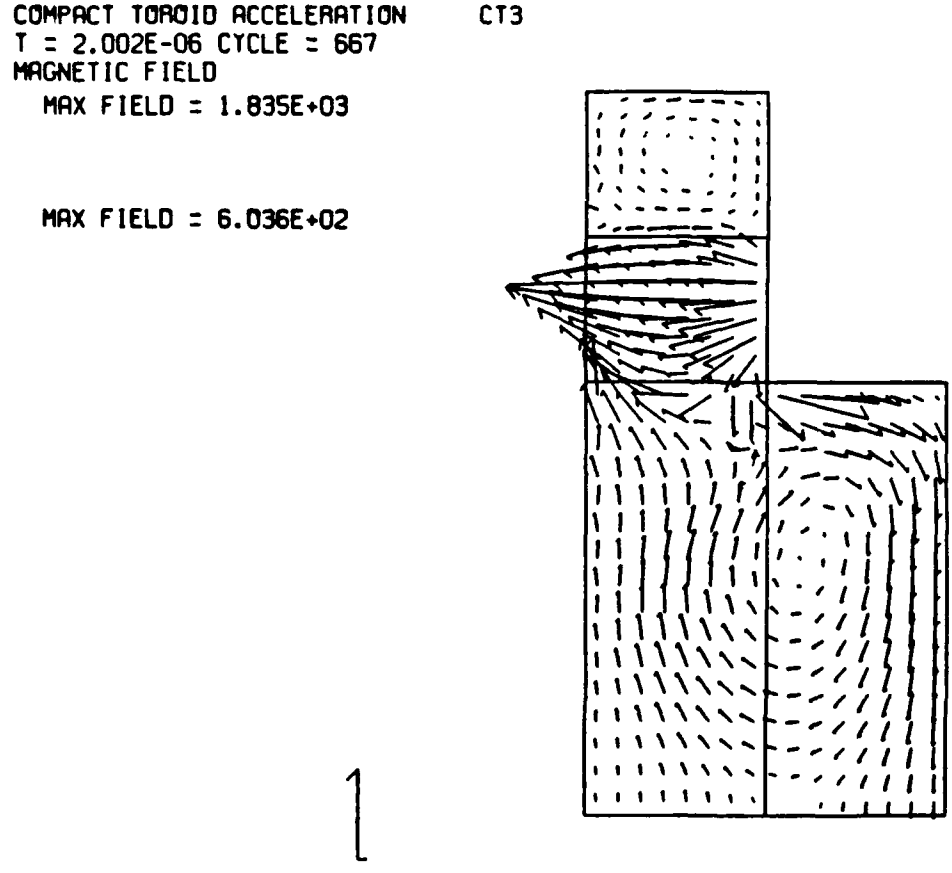

Figure 19. Toroid generation at 2.0 μs: poloidal field.

Further work will center on better initiation of the toroid for acceleration and focusing. In addition, all of the simulations reported here need to be done with better resolution. Actual predictions of the experimental B traces for both toroidal and poloidal fields in the Livermore RACE experiments will also be made soon.

A simulation of the generation phase continued through the compression process is discussed under subtask 03-05. Finally, it should be noted that a full simulation of all the component processes, formation, compression, acceleration, and focusing are within the scope of MACH2 using the detailed adaptive grid control.

2.3.4.2 Report. Document prepared under this subtask is summarized here.

"Demonstration of the Poloidal Field Capability of MACH2: Compact Toroid Simulations"
Michael H. Frese and Thomas A. Bida
AMRC-R-973
September 1987

ABSTRACT: This study demonstrates that the poloidal field capability of MACH2 is ready to be used in a coordinated theoretical and experimental program to investigate the generation, acceleration, and focusing of compact toroids. In addition, it demonstrates a capability to model those effects in the full scope of complex geometries for which MACH2 was designed. Further, the addition of poloidal fields to MACH2 makes possible many problems which could not have been done before. Among these is the study of effects of two-dimensional perturbations during liner initiation, which can now be carried out in the plane transverse to the liner. This would provide an understanding of the observed nonuniform initiation seen for low current rise rates.

2.3.5 Subtask 03-05, SHIVA STAR Computational Physics Studies II

2.3.5.1 Research Summary. Under this subtask, MRC intensified its efforts to provide theoretical and computational guidance to the advanced weapons program at the WL. The program focused on investigations of CT production and the use of the PFS to produce X rays by driving fast liners to implosion. Mission Research Corporation performed computational optimization studies that used the PFS and an imploding plasma liner in an attempt to guide the experimental program to a goal of producing 10 TW of X-radiation as the liner stagnates on axis.

INVESTIGATIONS TO INCREASE X-RAY POWER FROM LINER IMPLOSIONS

In a series of experiments at the WL, a fast capacitor bank, an inductive store, and a PFS have been used together to produce multimegampere currents with submicrosecond rise times in cylindrical foil loads. The capacitance of the SHIVA STAR bank is 1.3 mF, and the total initial inductance including the PFS and inductive store is 16.5–19 nH. In recent experiments, the bank was charged to 84–95 kV which results in 4.6–5.9 MJ of stored electrical energy. As a result of the simulations of the QUICK-FIRE shots, suggestions were made for geometry changes that predicted improved current delivery to the load (Ref. 48). These ideas were tested in subsequent shots that are described by Degnan et al., (Ref. 40) and by Price et al., (Ref. 49). This paper presents the results of a series of simulations in which the goal was to improve the radiation yield above the 2.5 TW reported by Degnan et al.

At the beginning of a shot, energy from the SHIVA STAR capacitor bank is transferred to the vacuum inductor as the current carrying annular plasma is accelerated to 7–10 cm/μs down the gun. When the plasma runs off the corner of the gun, current is switched into the cylindrical foil load causing it to implode radially on axis. To produce a high quality efficient implosion, a large fraction of the total current must be delivered to the implosion foil during a short time interval.

In Reference 48. the goal was to demonstrate a method of improving the current delivery. This was accomplished theoretically and experimentally by closing portions of the vane structure. The switch must be sealed shut or else substantial current will flow in the diffuse gas that is ablated from the walls of the switch barrel. Once this was accomplished, almost full current delivery to the load is achieved. In order to enhance the radiation yield further, the quality of the implosion must be improved. Recommendations to accomplish this goal are:

1. remove the bow in the load foil,
2. use a heavier load foil—300 μg/cm^2, and
3. remove the corner section that is immediately to the right and below the liner in Figure 5.

The MACH2 simulation of this configuration yielded a peak radiated power of 6 TW when the capacitor bank is charged to store 5.9 MJ of energy. Nine terawatts is obtained in the simulation when the capacitor bank is charged to 9 MJ.

Other ideas that seemed promising were tested, but found that neither shaping the electrodes, lengthening the load foil, using loads of different mass per unit area, nor using a higher Z liner substantially increased the peak radiated power.

COMPACT TORUS MODELS

The production of CT plasmas by means of a magnetized coaxial plasma gun was discussed as early as 1958 by Alfvén. The CT configuration has received much attention from, among others, researchers at LLNL. Early experiments at the LLNL Beta II facility, and subsequent experiments on the RACE (Ring Acceleration Experiment) facility, have successfully demonstrated the stability and resiliency of the CT, at least at moderate energies.

The experimental and theoretical program at LLNL has been well documented (Refs. 50 and 51) and is well known in the scientific community. However, the WL has also, in collaboration with LLNL, begun a theoretical and experimental program in CT research. Mission Research Corporation has been active in this program during the past few years.

Experiments to form, accelerate, and focus CT plasmas will be performed on the 9.4 MJ SHIVA STAR fast capacitor bank at the WL during the next few years. The MARAUDER (Magnetically Accelerated Rings to Achieve Ultrahigh Directed Energy and Radiation) program is a research effort to accelerate magnetized plasma rings with masses between 0.1 and 1.0 mg to velocities above 10^8 cm/s and energies above 1 MJ. Research on these high-velocity CTs may lead to development of very fast opening switches and HPM sources, an alternative path to inertial confinement fusion, and sources of intense X rays.

OVERVIEW OF COMPACT TOROIDS

A CT is a minimum energy state of a magnetized plasma (Taylor, Ref. 52) with a nontrivial magnetic helicity. The magnetic helicity is defined:

$$k = \int \vec{A} \cdot \vec{B} \, dv \tag{19}$$

where $\vec{B}$ is the magnetic induction that can be written as the curl of a vector potential, $\vec{A}$. The integral is over the volume of the torus—the boundary of which, for MARAUDER experiments, is defined by a coaxial metallic flux conserver having both an inner and an outer conductor. The CT is an ionized plasma, hence an electrical conductor that can be accelerated within a coaxial railgun. If the plasma beta is low, the CT is essentially force

free with the internal currents parallel to the magnetic fields that are generated by those currents.

Design of a CT accelerator experiment on the SHIVA STAR capacitor bank is underway, and computer simulations with the 2 1/2-dimensional MHD code, MACH2 have been performed to guide this endeavor.

In previous research efforts, MACH2 has been successfully used to model PFSs as well as to explain experimental current-probe signals and to predict radiation output from fast z-pinch experiments that used the SHIVA STAR BANK, an inductive store, and a PFS to drive a cylindrical foil liner to implosion (Refs. 40 and 48). In the early phase of CT simulation effort, we successfully duplicated with MACH2 the early simulation results of the RACE experiment produced by J. L. Eddleman, C. W. Hartman, and J. H. Hammer with the two-dimensional resistive MHD HAM code.

Calculations of formation and equilibration of a low beta magnetic force-free configuration (curl $\vec{B} = k\vec{B}$) have been performed with MACH2. The focusing and acceleration of the toroid has been simulated with the inclusion of resistive diffusion. The resiliency of the accelerated CTs against resistive decay is sensitive to the model that is used for the plasma resistivity. Simulations of the experimental configuration which include a magnetized coaxial plasma gun, an expansion region, and a compression cone have been performed. Further computations that use the adaptive grid capability of MACH2 will allow the formation, focusing, and acceleration of the CT to be modeled with good resolution and modest computer time.

The models discussed below include a precompression cone that adiabatically compresses the CT in a self-similar fashion, in the process performing work on the torus by converting kinetic into magnetic energy. At the top of this cone in the MARAUDER experiment (but not yet included in our model) is a long (few meters) coaxial acceleration tube, followed by a final compression cone the purpose of which is to dramatically increase the energy density of the CT immediately before it stagnates against a target. The resulting hydrodynamic shock will induce bound-bound transitions and electron bremsstrahlung that generate radiation in the form of X rays.

The X-ray spectrum may be determined by a mixture of ion-species within the CT. The RACE at LLNL has successfully accelerated 1 μg rings to 3.0×10^8 cm/s imparting to them 4.5 kJ in kinetic energy. The MARAUDER program at WL envisions creating 2.5-mg, 5-MJ rings. If a 5-MJ Xe plasma CT stagnates against a solid plate, one may expect copious X-ray production in the 5-keV range from L-edge transitions: L_{II} at 5.1 keV and L_{III} at 4.8 keV. Xenon K-shell transitions could produce X rays at 34.6 keV.

CT FORMATION, EXPANSION AND COMPRESSION WITH MACH2

Some models of formation, expansion, and compression of a CT in the MARAUDER geometry with SHIVA STAR formation parameters are discussed. These simulations were performed with Version 8801 of MACH2. The simulations are cylindrically symmetric with the center line to the left of computer-generated pictures. The simulations discussed are Eulerian. We emphasize that the CTs are not accelerated by a driving current in these models.

CT FORMATION, EXPANSION AND COMPRESSION WITH MACH2: INITIAL CONDITIONS

A cross-section of the formation and preexpansion section of the MARAUDER experiment is illustrated in Figure 20. The coils that produce poloidal magnetic flux are shown near the bottom of the figure. The coaxial acceleration region is not included, but in reality is attached at the top of the figure. The radius of the inner electrode (cathode) is 12 cm at the top and 44 cm at the bottom. The radius of the outer electrode is 20 cm at the top and 62.5 cm at its widest towards the bottom.

Initially, somewhat less than 1 μg of fully-ionized hydrogen plasma exists in the computational region. The density of the injected plasma that resides in the bottom region of the computational mesh is 1.376×10^{-5} kg/m^3. This plasma is initially at a temperature of 10 eV. A radiation cooling model, appropriate for a low density hydrogen gas with 10 percent oxygen impurity, is used. The present models include thermal diffusion with an isotropic Spitzer thermal conductivity and a classical thermal flux limiter with a multiplier of 0.4, and resistive diffusion without an anomalous diffusivity term. The electric resistivity is obtained from the Spitzer model with a minimum diffusivity of 25 m^2/s. We have not included a model of the Hall effect in the present set of simulations. An ideal gas equation of state is used with $\gamma = 5/3$. The initial configuration for the best model of a CT, model cptfec7, is shown in Figure 21. The fixed computational mesh is shown on the left, and the initial poloidal magnetic induction is shown along on the right. Plasma of constant density and temperature is continuously injected through the flow-through bottom boundary.

The magnetic induction is initiated at the bottom of the computation region as a pure radial field that varies as 1/r and is therefore divergenceless. The magnitude of the initial field is on the order of 1 kG at the inner electrode (the cathode). In the MARAUDER experiment, this field is initiated by inner and outer solenoids that are energized by a pulsed 750 kJ, 15 mF capacitor bank. Hydrogen along with a fraction (10 percent in these models) of oxygen impurity is puffed into the region that initially contains the poloidal

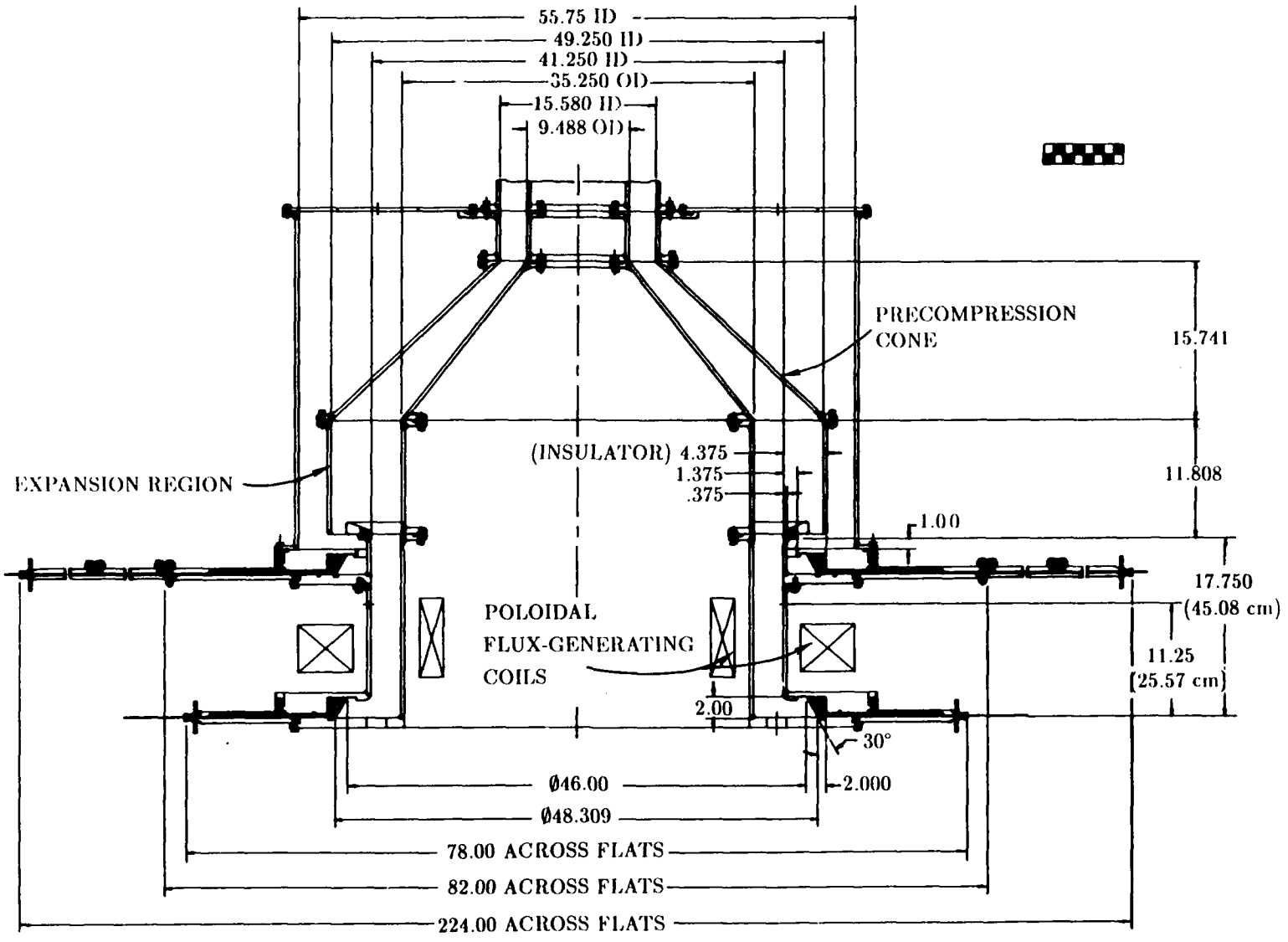

Figure 20. The 1988 Schematic for the formation, expansion, and precompression section of the MARAUDER experiment. The vertical dashed line on the centerline. Dimensions are given in inches.

INITIAL CONDITIONS FOR MODEL CPTFEC7

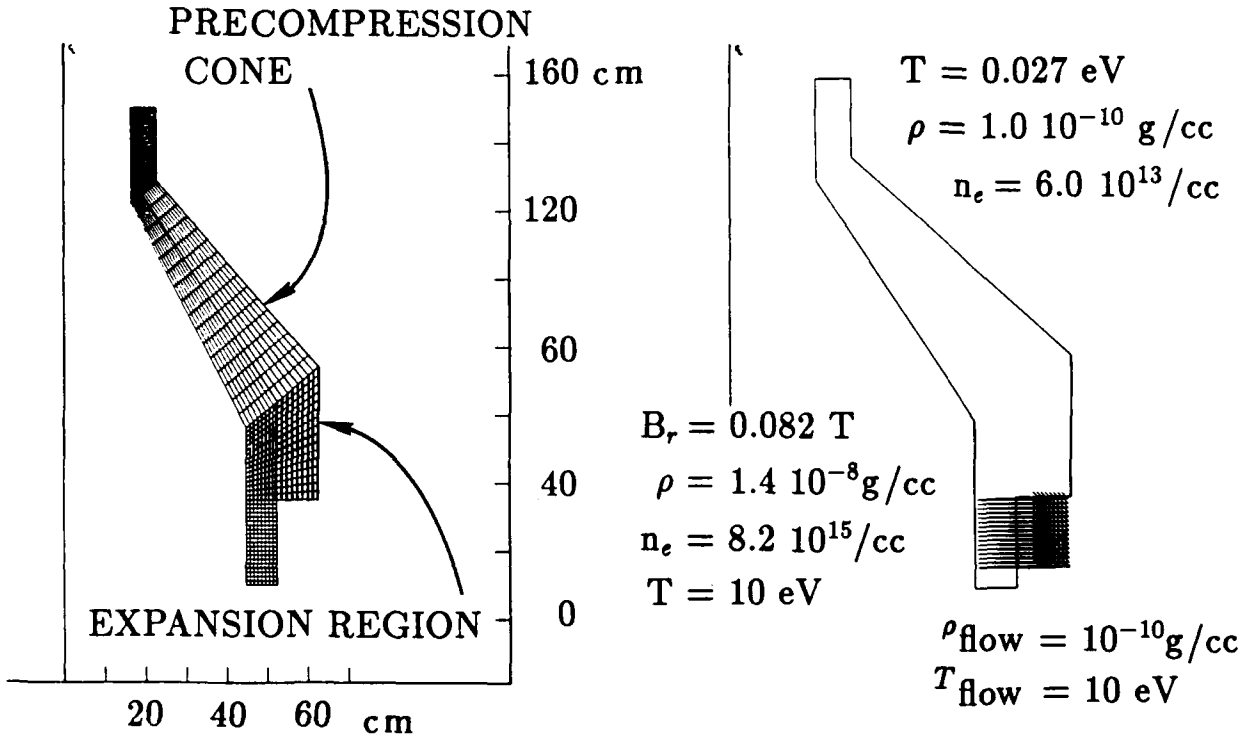

Figure 21. Initial conditions for MACH2 model cptfec7 of CT formation.

field. The low density gas is subsequently ionized and becomes a conducting plasma. We have not modeled the ionization process, but assume a 10 eV initial electron temperature and the associated Saha ionization state.

The CT is formed by a discharge from a 750 kJ, 108 μF pulsed capacitor bank that produces a poloidal current, and hence a theta induction, and is connected to the bottom boundary of the computation region. The driving current is computed in MACH2 from a single-loop RLC circuit with an external inductance of 21.1 nH. The associated magnetic pressure pushes up on the poloidal field files while they remain tied to the conducting side walls. After the poloidal lines enter the expansion region, reconnection takes place, confining the injected plasma (approximately 1 μg in these simulations) within the CT. The velocity boundary condition in the field injection region is critical to the formation of the CT (Ref. 53). The necessary condition is to impose zero velocity to vertices on the boundaries through which poloidal flux emerges. This condition is reasonable because the field lines that emerge through highly conductive walls tend to be trapped in the conductor as well as in the plasma—in effect tying the plasma to the walls.

The current pulse from the formation bank peaks at a value of 5.4 MA at the quarter-cycle time, $\pi/2\ \sqrt{LC}$, 2.4 μs. Reconnection generally takes place at between 2 and 2.6 μs.

CT FORMATION, EXPANSION AND COMPRESSION WITH MACH2: RESULTS

In this section, the best CT model is discussed: cptfec7. The initial fill density is 10^{-7} kg/m^3 at room temperature (0.027 eV). The inflow plasma is of the same density, but is hot: 10 eV. A torus forms when the field lines reconnect after the magnetic structure begins moving radially into the expansion cavity. This process is illustrated in Figure 22 where all three components of the magnetic induction are plotted at 0.2-μs intervals between 1.8 and 3.2 μs. Reconnection takes place sometime between 2.4 and 2.6 μs.

Figure 23 shows the magnetic induction, at 0.5-μs intervals between 3.5 and 7.0 μs—during the compression and equilibration phase. The current pulse from the formation bank is essentially completed after 5 μs, so the CT is no longer forced, but attempts to come to equilibrium in the precompression cone. At 5 μs the center of the torus has moved two-thirds of the way up the compression cone. At this time, the CT bounces off of the end of the cone and rebounds into the expansion region. The CT is warm (between 5 and 20 eV), but the plasma beta is between 0.01 and 0.04. The torus is moving through the cone at a speed of approximately 5×10^7 cm/s. The total angular momentum of the torus is zero, but the magnitude of the rotational velocity of some regions approaches the magnitude of the in-plane velocity. The torus is composed of two counter-rotating

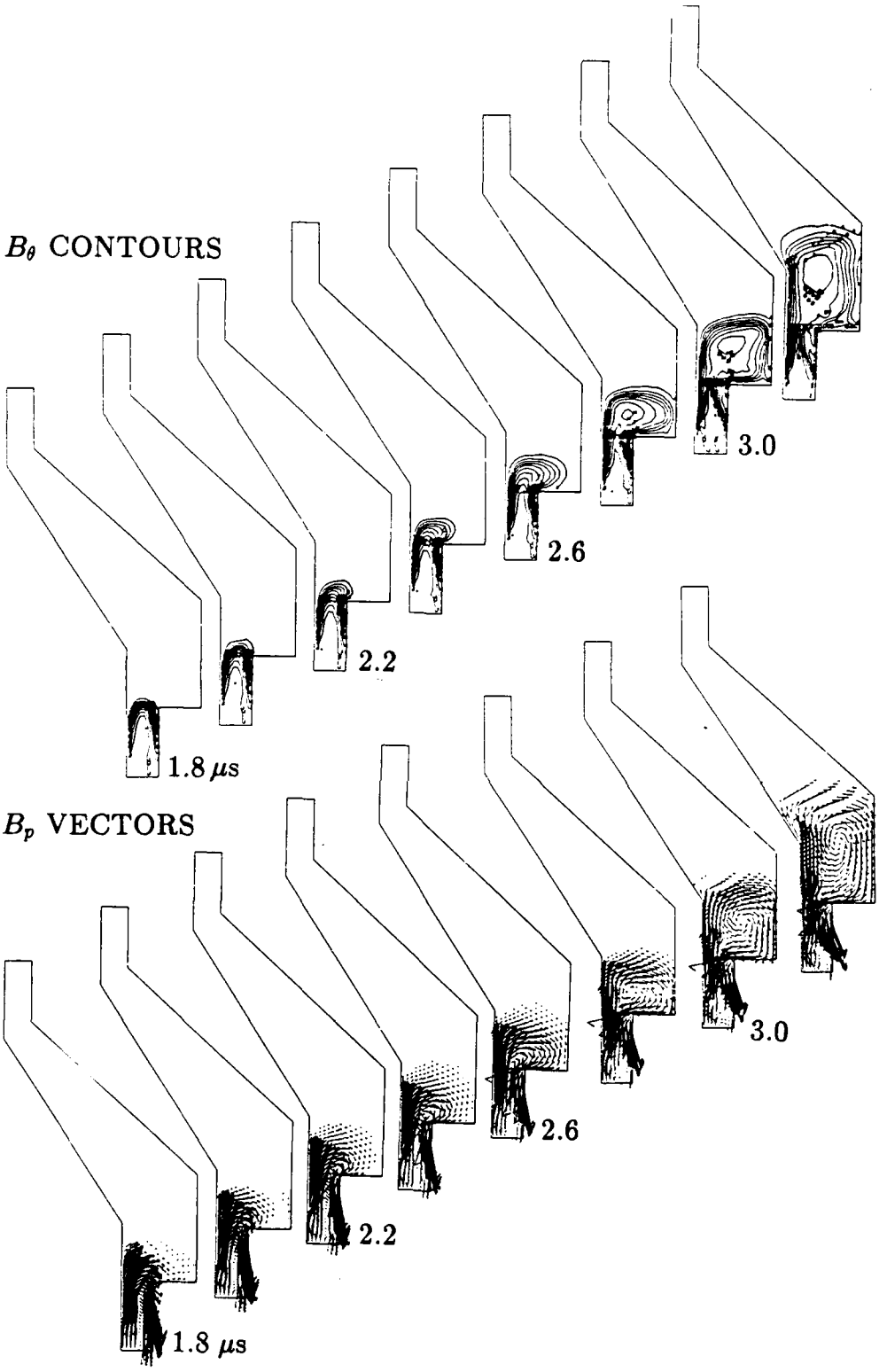

Figure 22. Toroidal magnetic induction contours and poloidal magnetic induction vectors at 8 times between 1.8 μs and 3.2 μs, at 0.2 μs intervals, that show reconnection and formation of a CT in model cptfec7.

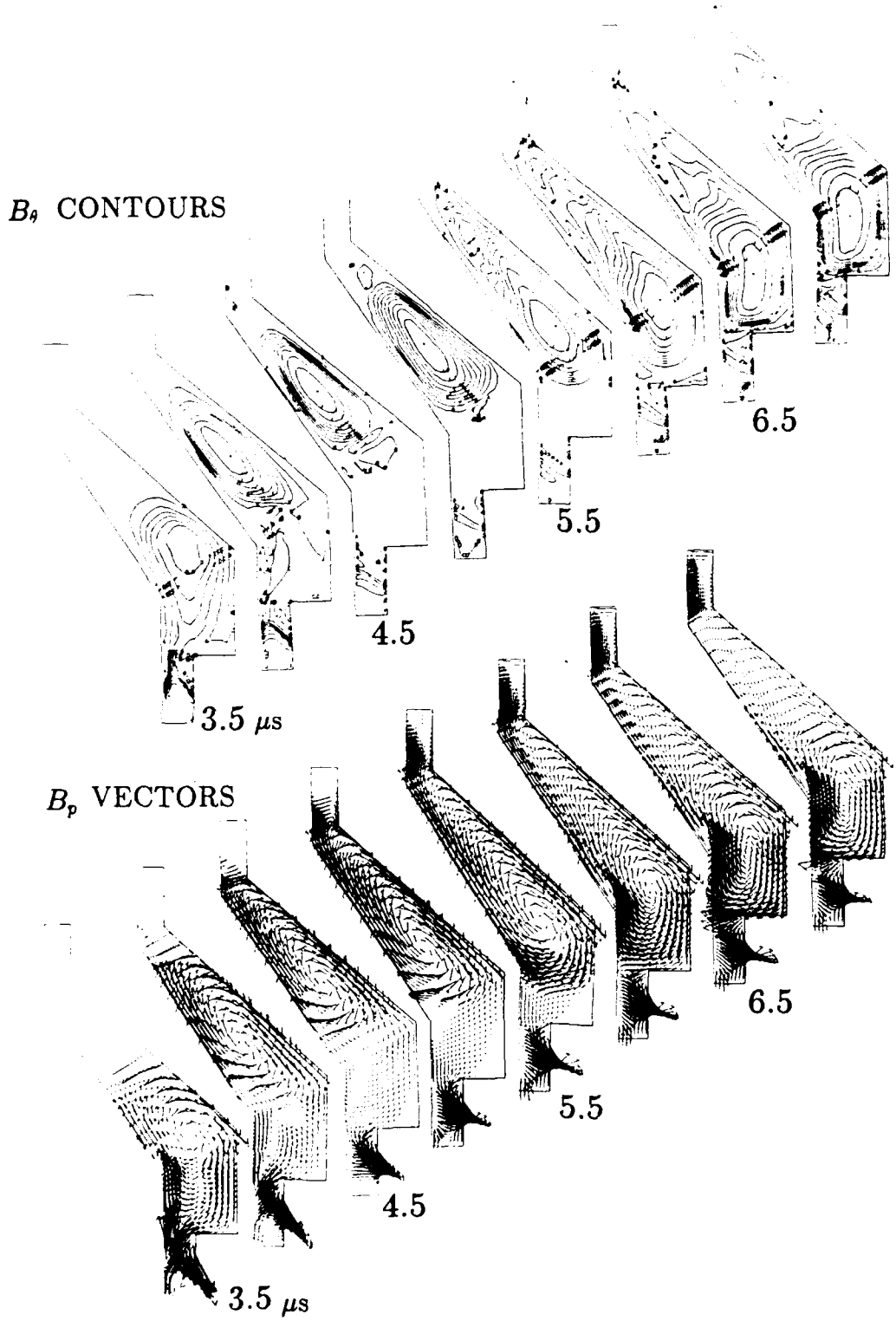

Figure 23. Toroidal magnetic induction contours and poloidal magnetic induction vectors at 8 times between 3.5 μs and 7.0 μs, at 0.5 μs intervals, that show equilibration of a CT in model cptfec7 in the compression cone.

sections. The density of the center of the torus is approximately 2–6 $\times 10^{-6}$ km/m^3, or 1–4 $\times 10^{15}$ electrons/cc.

CT RESISTIVE DECAY

The magnetic helicity, k, is a conserved entity in ideal MHD. However, k decays in a resistive MHD model linearly in time with the resistivity, η. The implication of this is a finite lifetime for the CT. Various resistivity models and the effect of each on the CT lifetime have been considered. In this section, some preliminary conclusions are reported; the details are given in Reference 54 in detail and are reviewed under subtask 03-07.

Recall that the resistivity is related to a collision frequency as:

$$\eta = \frac{m_e}{n_e^2}\,\nu \tag{20}$$

The classical electrical resistivity, proportional to the electron-ion collision frequency, is independent of mass density and inversely proportional to the 3/2 power of the electron temperature. This Spitzer resistivity allows a CT lifetime much larger than the 5–10-μs formation and equilibration time scales of our simulation, and indeed longer than the anticipated acceleration time down a coax. However, in the presence of strong electric fields when the electron drift speed greatly exceeds the ion thermal speed, electron collisions with essentially random field fluctuations dominate the collisions with ions giving rise to the so-called anomalous resistivity. As suggested by Milroy and Brackbill (Ref. 55), our anomalous resistivity is 2-phased. A Chodura model was used, i.e., an anomalous collision frequency that is proportional to the ion plasma frequency:

$$\nu_{Chodura} = \omega_{pi}\left[1 - \exp\left(-\mid v_{de} \mid / f v_s\right)\right] \tag{21}$$

before reconnection, then abruptly switch to an anomalous collision frequency based on the saturation of the lower-hybrid-drift instability:

$$\nu_{an-LHD} = \omega_{LHD}\left(v_{de}/v_i\right)^2 \tag{22}$$

that is somewhat smaller in magnitude than the Chodura case for the parameters of interest. In the above formulae, ω_{pi} is the ion plasma frequency, ω_{lhd} is the lower-hybrid-drift frequency ($\sqrt{(\omega_{ci}\omega_{ce})}$, where ω_{cs} is the cyclotron frequency for a species, s), v_{de} is the

electron drift speed, v_s the ion sound speed, v_i the ion thermal speed, and f an adjustable parameter of order unity.

Compact torus formation and equilibration has been simulated with a Spitzer plus 2-phased anomalous resistivity model. In the former case, the CT connects approximately 2 μs into the simulation and has a lifetime much longer than the 7-μs equilibration time. In the later case, the time of reconnection is 1.5 μs, but of greater importance is the CT lifetime that is reduced to less than 2 μs. If we forego the lower-hybrid-drift instability and use only a Chodura model, the CT lifetime is reduced further to 1 μs. These times are short compared to the equilibration time. The important implication is that, if something like the Chodura model for anomalous resistivity is correct, high-energy CT may not survive sufficiently long to be accelerated to large velocity. However, these numerical calculations employed relatively coarse zoning and first-order accurate donor-cell advection. It is possible that improved numerical accuracy would be less diffusive and would allow longer CT lifetimes.

An anomalous collision frequency that is proportional the ion plasma frequency, as is the Chodura model, is reported by Milroy and Brackbill to be necessary for their Hall-resistive-MHD numerical computations to predict reconnection times that agree with those measured in the FRX-C/T field-reverse configuration experiment at LANL.

THREE-DIMENSIONAL MHD

Also under this subtask, MRC conducted a preliminary assessment of the feasibility of a three-dimensional radiation MHD code which would exploit the computational capability of the Cray-2 supercomputer at the WL. Two codes were considered: (1) an update of the MACH2 MHD code, and (2) an improved version of a smooth particle hydrodynamics (SPH) code. Updating MACH2 to three dimensions while preserving the ability to model complex geometry would require considerable manpower—probably in excess of ten man-years and hence the effort would probably be beyond the anticipated resource level at the present time. However, a single block version is doable in a few man-years or less. A better path is to add magnetic fields and a radiation treatment to the existing three-dimensional SPH code. Smooth particle hydrodynamics codes can be run in much shorter times than codes with grids for most three-dimensional problems.

2.3.5.2 Reports. Documents prepared under this subtask are summarized here.

"MACH2: A Reference Manual—Third Edition"
Robert E. Peterkin, Jr., James Buff, Michael H. Frese and Anthony J. Giancola
MRC/ABQ-R-1066
May 1988

ABSTRACT: This is the third edition of the MACH2 user's guide. Since we published the second edition, many improvements have been made to the code. The purpose of this document is to bring a description of these changes under a single cover.

"Compact Toroid Simulations with MACH2"
Robert E. Peterkin, Jr.
MRC/ABQ-R-1130
December 1988

ABSTRACT: A brief overview of CT physics is given. Some models of formation, expansion, and compression of a CT in the MARAUDER geometry with SHIVA STAR formation parameters are discussed. A potential "show stopper" in the proposed experiments is anomalous resistivity. At the high current densities required in larger experiments, anomalous resistivity may decrease the magnetic decay times to unacceptable levels. A number of test simulations of magnetic force-free configurations are presented.

"Enhancement of the Radiation Yield in Plasma Flow Switch Experiments"
James Buff, Robert E. Peterkin, Jr., Norman F. Roderick, James H. Degnan (Weapons Laboratory), Michael H. Frese (Numerex) and Peter J. Turchi (R&D Associates)
MRC/ABQ-R-1171
April 1989

ABSTRACT: In a series of experiments at the WL, the SHIVA STAR fast capacitor bank, an inductive store, and a PFS have been used together to produce multimegampere currents with submicrosecond rise times in cylindrical foil loads. Based on a two-dimensional MHD simulations with the MACH2 code, we have previously suggested design modifications to the basic PFS experiment that resulted in improved current delivery to the load. This paper presents the results of a new series of simulations in which the goal was to improve the radiation yield. Changes considered include: shaped electrodes, dimensions and mass of the load foil, vane structure, shape and mass of the plasma gun, liner material, removing the bow in the load foil, and energy in the capacitor

bank. Radiation yields in the range 6–9 TW are predicted for experiments on SHIVA STAR.

"SHIVA STAR Computational Physics Studies II"
James Buff, Michael H. Frese, Anthony J. Giancola, Robert E. Peterkin, Jr. and Norman F. Roderick
MRC/ABQ-R-1173
April 1989

ABSTRACT: This work is the final report for subtask 03-05, SHIVA STAR Computational Physics Studies II. The bulk of the report consists of the three reports which are entitled (1) "Enhancement of the Radiation Yield in Plasma Flow Switch Experiments," (2) "Compact Toroid Simulations with MACH2," and (3) "MACH2: A Reference Manual—Third Edition." Work performed under this subtask is summarized.

2.3.6 Subtask 03-06, Compact Toroid Accelerator Physics Studies

2.3.6.1 Research Summary. The work performed under this subtask was in support of the WL's MARAUDER program: a large-scale theoretical and experimental research program whose goals are the creation of CT plasmas, their acceleration to high velocities, and their focusing to high energy density. There are numerous conceivable applications for such plasmas, including inertial confinement fusion drivers, fast opening switches, high field pinches, and RF cavity field compression (Ref. 46).

Compact toroids are essentially donut-shaped plasmas entrained in, and surrounded by, self-toroidal (azimuthal) and poloidal (perpendicular to the toroidal direction) magnetic fields (Fig. 24 and Refs. 56 and 57). In appropriate geometries, CTs are in minimum magnetic field energy (per unit of magnetic helicity) states, resulting in robust configurations capable of withstanding tremendous forces while maintaining topological integrity (Refs. 52 and 58).

For the MARAUDER experiments, typical CT plasma parameters expected are temperatures of a few to tens of electronvolts and densities of about 10^{12} to 10^{15} cm^{-3}. To understand the physics of the experiments and validate theoretical and simulation results one needs to diagnose the plasmas (that is, to make measurements of these plasma parameters).

The activities of MRC for this project were concentrated primarily in the area of theory-experiment interfacing. Specifically, we were tasked with analysis of data from

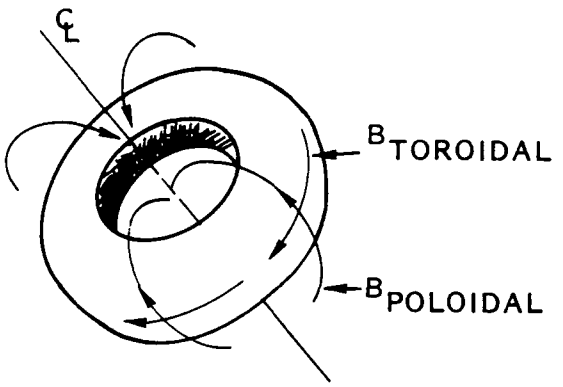

Figure 24. Compact toroid schematic showing toroidal and poloidal magnetic field directions.

MARAUDER experiments, analysis of plasma and pulsed power diagnostics, and design and analysis of CT focusing experiments.

DATA ANALYSIS

Experimental data for MARAUDER experiments is usually produced in the form of oscilloscope waveforms recorded on photographic film. Because of the plethora of data generated in these experiments, analysis by reference to pictures is inconvenient.

To facilitate the data analysis and allow the direct comparison of different scope traces as well as different sets of data, the data were digitized using the PC program "BONES," (Ref. 59) and preprocessed it using the PC computer codes "TURTLE," "BASCOR," and "FIDU," (Ref. 60) for use by the commercial integrated data analysis software "ASYSTANT©" (Ref. 61). The details of these procedures are described in MRC Note MRC/ABQ-N-383 (June 1988).

PLASMA DIAGNOSTIC ANALYSIS

For plasma temperatures on the order of 10 eV, much of the emitted radiation falls in the ultrasoft X-ray region of the spectrum (10–200 eV, 50–1,000 Å). The radiation emitted by moderate density plasmas at this temperature consists of line (bound-bound) and continuum (primarily free-bound, or recombination) radiation that is characteristic of the relative plasma specie abundancies, their ionization states, densities, and temperatures. It is therefore appropriate to consider ultrasoft X-ray emission spectroscopy as an important

diagnostic for CT plasmas. Emission spectroscopy has the added advantage of being nonintrusive.

The WL/AWX has two Spectral Precision 1-m grazing incidence spectrographs which have been used previously for spectroscopic measurements (Refs. 62 and 63). Under this subtask, MRC personnel checked out the two instruments (one of which had been damaged), realigned them, and fielded them on three plasma implosion experiments.

The spectrographs employ a Rowland circle mount (Ref. 64), a variety of gratings, a 35-mm film cassette, optional grazing incidence mirrors (for multiple-order, short wavelength cutoff), and a built-in HeNe laser alignment system. Note that upon examination, both instruments were found to be configured incorrectly. That is, all components mounted on the Rowland circle have a correct orientation—with the numeric engraving upright as viewed from the entrance end. For both instruments, the components were mounted "upside-down," making alignment and focusing impossible. Furthermore, one of the spectrographs had the entrance mask and entrance slit in reverse position. The correct positioning and orientation of the instruments is shown in Figure 25. Once the components were positioned properly, the laser alignment systems were checked. The alignment for the undamaged instrument was satisfactory, but the beam-spreading cylindrical lens of the damaged instrument was out of position, due to loose mounting and probable mechanical shock. When the lens was repositioned, laser alignment was satisfactory.

Inventory of available film was taken. Although there was a considerable amount of relatively new RAR-type film, we decided to use older 101-01 film, since its low-energy X-ray sensitivity and response are fairly well known, while that of the newer films are not. To test the overhauled spectrograph system, one of the spectrographs was configured with a gold-coated 2-m radius grazing incidence entrance mirror for enhanced reflectance, 80-μm entrance slit, full mask, 1200 l/mm grating, and Kodak 101-01 film for QUICK-FIRE Shot #6119. The entrance mirror was used to transmit multiple-order high-energy radiation, simplify alignment, increase the solid angle collection area, and offer some protection to the grating from debris. The 80-μm entrance slit provided poor resolution in exchange for high sensitivity. The 1200 l/mm grating was selected to provide survey coverage from roughly 8 to 300 Å. The spectrograph was mounted on the top side of the plasma load region with an intervening pneumatically actuated fast shutter. Precise alignment of the entrance mirror was accomplished with the built-in laser and a cardboard alignment target mounted in the center of the load region. The setting of the mirror micrometer from the *in situ* alignment agreed almost exactly with the setting calculated from the geometry and well-known optics relations. After all other diagnostics were in place and the load inserted, the light-tight film cassette was loaded to minimize the possible exposure due to long-time low-level light leakage.

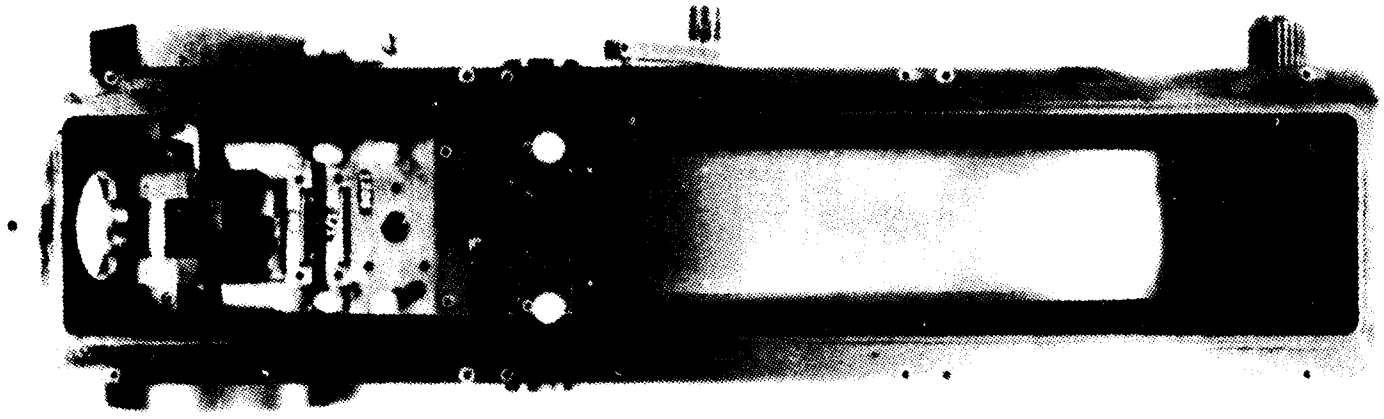

Figure 25. Spectral Precision 1-m grazing incidence spectrograph showing correct placement of components along the Rowland circle.

Shot #6119 was not particularly good in terms of radiation production. Furthermore, the integrity of the spectrograph's pneumatic valve was compromised by a bolt which ruptured the valve blade, allowing considerable debris and light to penetrate the instrument. The debris was enough to damage the grating and impinge on the film. With the additional overexposure due to light leakage, the film was virtually unreadable and unsuitable for reproduction. Nevertheless, we could still detect several relatively diffuse emission lines, especially in the low energy (~200 A) region, and what appeared to be diffuse bands in the range of 30–1000 Å, where one would expect many emission lines from intermediate ionization states of aluminum—the load material. This would indicate a characteristic plasma temperature on the order of tens of electronvolts. Based on the results of Shot #6119, we decided to field the other spectrograph for the next experiment, with a narrower entrance slit and half mask.

Analysis of the grazing incidence spectral data from Shot #6120 was performed. Emission lines in the 250–300 Å range only were observed. One would expect, from the elements present in the pinch region, emission from the following, in order of concentration: aluminum (liner), oxygen (chemi- and physisorption on the liner surface), gold (electrodes), tungsten (plasma flow switch), other minor contaminants. Only a few possible line identifications were made, consisting of Al VI, VII, and VIII, and Oxygen III and IV. Information on gold and tungsten transitions in the ultrasoft X-ray region of the spectrum could not be located. On the basis of the range of lines observed, however, the aluminum charge states to be expected and the approximate temperature of the plasma can be estimated.

To obtain the charge state, assume that the dominant line(s) arise from the transition between the two lowest major energy levels, corresponding to the two lowest principal quantum numbers. Then the energy of the transition is approximately given by

$$E = Z^2 E_H / \left(n_0^{-2} - n_1^{-2} \right) \tag{23}$$

where Z is the effective ionic charge, $E_H = 13.58$ eV is the hydrogenic ionization potential, and n is the principal quantum number. For aluminum with three electrons in the outer shell, $n_0 = 3$ and $n_1 = 4$ for Al I-III, and $n_0 = 2$ and $n_1 = 3$ for Al IV-XII. Insertion of the energies associated with the observed lines into the above equation yields an effective Z of between 4.7 and 5.1, so we should expect Al V, VI, and possibly VII. A preponderance of Al VI implies a temperature of between 20 and 30 eV, based on a coronal equilibrium balance between collisional ionization and radiative recombination.

CT DIAGNOSTIC EVALUATION

Two additional diagnostics considered for implementation on the MARAUDER experiments were a microwave interferometer and vacuum ultraviolet spectrometer. The resources available for these two diagnostics were evaluated.

Discussions were made with Pulse Sciences Inc., San Leandro, California, since they were in the process of fielding a similar diagnostic. These discussions led us to conclude that a realistic upper bound on frequency is in the range of 50–75 GHz. Cutoff plasma densities for this range (above which microwaves do not propagate) are 3×10^{13} cm^{-3} to 7×10^{13} cm^{-3}. Higher frequencies cost substantially more for amplifiers and associated hardware. In addition, the power available is somewhat lower. We estimate that a system at the upper range will cost approximately 15–20K. This assumes using a klystron tube at power levels of a few hundred milliwatts, which should be adequate for the high noise environment during operation.

Dr. Charles Wharton of Cornell University suggested the possibility of performing the microwave interferometry with a portable system he has. We believe that, if Dr. Wharton can perform the measurements, it will probably be the most cost-effective and time-effective approach. The obvious trade-off is the lack of in-house hardware. However, valuable time and resources could be saved by observing the expert firsthand, and, if desired, acquiring a system afterwards based on the observations.

Although the WL neutral particle laboratory has a vacuum ultraviolet (VUV) monochromator and several detectors, we concluded that for single-shot high-flux events characteristic of CT plasmas, a monochromator is of questionable value (as opposed to a spectrograph or spectrometer), and the available detectors are far too sensitive. Therefore, unless WL/AWX is willing to purchase a VUV spectrographic system, this diagnostic should not be considered at this time.

2.3.6.2 Report. Document prepared under this subtask is summarized here.

"Compact Toroid Accelerator Physics Studies"
Gerald F. Kiuttu and Dawn D. Vigil
MRC/ABQ-R-1162
April 1989

ABSTRACT: The work described in this report was performed by MRC in support of the WL's MARAUDER program. The MARAUDER is a large-scale theoretical

and experimental research program whose goals are the creation of CT plasmas, their acceleration to high velocities, and their focusing to high energy density. There are numerous conceivable applications for such plasmas, including inertial confinement fusion drivers, fast-opening switches, high field pinches, and RF cavity field compression. The activities of MRC for this project were concentrated primarily in the area of theory-experiment interfacing. Specifically, we were tasked with analysis of data from MARAUDER experiments, analysis of plasma and pulsed power diagnostics, and design and analysis of CT focusing experiments.

2.3.7 Subtask 03-07, SHIVA STAR Computational Physics Studies III

2.3.7.1 Research Summary. The objective of this subtask was to provide guidance and direction to the advanced weapons research program at the High Energy Plasma Division of the WL by providing theoretical and computational support of existing and proposed experiments.

The experimental effort to which major contributions were made is the MARAUDER concept. This is a 3-phase R&D program to generate, accelerate, and focus CT plasmas to multimegajoule kinetic energies. Research on these high-mass (0.1 to 1.0 mg), high velocity ($>10^8$ cm/s) toroids may lead to development of very fast opening switches, HPM sources, an alternative path to inertial confinement fusion, and sources of intense X rays. Phase 1-a is a research effort to design a robust gas-injection and pulsed poloidal-field generation device; this experimental phase is complete. In Phase 1-b, currently in progress, an expansion region is added to the Phase 1-a device. These experiments use some of the modules from the SHIVA STAR fast capacitor bank to produce a CT formation discharge. Phase 2 experiments will include a compression cone that is mounted on the Phase 1-b hardware; the cone will be designed to compress the torus in a self-similar fashion. After the torus is compressed, it will be accelerated along a linear coax by an electric discharge from the remaining modules of SHIVA STAR.

The most important computational tool that has been, and shall continue to be, applied to guide and direct the MARAUDER program is MACH2. The MACH2 code is a continuously developing computational tool. Proper documentation of a physics simulation code encourages good research, and the frequency at which substantial computational advancements are made to MACH2 has compelled MRC to update the MACH2 Reference Manual at a frequency approaching once per year. The purpose of the fourth edition of the MACH2 Reference Manual, produced under this subtask, is to bring under a single cover all the information contained in the third edition as well as a description of the many changes made to the code in the intervening 18 months.

Some of the most important MACH2 code developments are discussed in detail in separate reports which are summarized below. Many other important additions and improvements to the MACH2 code are mentioned in the document entitled: "MACH2: A Reference Manual—Fourth Edition." These include: (1) namelist-generated custom color movies at LANL and at the WL, (2) region-dependent equation-of-state models, (3) region-dependent ionization models, (4) region-dependent anomalous resistivity models, (5) region-dependent radiation models, (6) independent material fluxed through a problem boundary, (7) equilibrium radiation diffusion, (8) wall ablation, and (9) periodic boundary conditions.

The physical model, including boundary conditions, permissible problem geometries, time differencing, and spatial discretization and centering of MACH2 was published in 1987 as the technical report AMRC-R-874. A new draft of this report was created by M. H. Frese. This report expands on the earlier version to include the iteration processes for the implicitly differenced physical processes, as well as the boundary conditions and block coupling implementation techniques.

ELASTIC-PLASTIC MODEL

An explicit elastic-plastic package (or strength of material package) has been added to MACH2, and is documented in the report entitled: "A Material Strength Capability for MACH2" by R. E. Peterkin, Jr. and M. H. Frese. Many substances, if deformed by external forces, have the ability to recover their initial size and shape when those forces are removed. This is elasticity. If the deforming stresses exceed some material-dependent critical value, many materials will yield and exhibit plastic behavior. The ability to include elastic-plastic effects in physics models is important for a class of problems of interest to WL researchers. This class includes initiation problems (exploding wires, fuses, etc.) and impact problems. A particularly interesting problem is the impact of either a solid or a magnetically-confined plasma projectile on a target. If the details of the subsequent deformation of the target are important, elastic-plastic effects are important. Consistent with the modular nature of MACH2, the elastic-plastic code does not interfere with the existing implicit magneto-fluid code.

In the elastic-plastic model, MACH2 assumes an isotropic, homogeneous elastic medium that is characterized by two elastic constants: the shear modulus and the bulk modulus. The implementation demands that the user specify Poisson's ratio in lieu of the shear modulus. The bulk modulus is assumed to be included in an independent model for the isotropic component of the stress-tensor—that is the pressure.

A number of test problems were run to exercise the elastic-plastic code. In general, numerical models of materials that support transverse (shear) waves as well as longitudinal (compressional) waves were satisfactory.

TWO-TEMPERATURE MODEL

In the paper entitled "A Two-Temperature Model for MACH2" by R. E. Peterkin, Jr., we present the details of a new two-temperature model for MACH2. For our purposes, a two-temperature model means that the electrons and ions are not a-priori assumed to be in mutual equilibrium—i.e., that the ions and electrons are not characterized by the same Maxwellian velocity distributions. From an operational point of view, separate electron and ion temperatures implies that the single energy equation in a one-temperature code such as Version 8901 of MACH2 must be split into two energy equations in a two-temperature code. This was done to create Version 9001 of MACH2.

The assumption of complete electron-ion equilibration is justified under certain conditions and is not justified under others. The electron-ion equilibration time is proportional to the electron temperature to the 3/2 power, and inversely proportional to the mass density. Therefore, equilibration is quickly reached at low temperatures in high-density fluids, whereas the electrons and ions will tend to be out of equilibrium in hot, rare plasmas.

When tabular equation-of-state data are desired, MACH2 takes advantage of the temperature-splitting capability of the driver to the SESAME libraries, EOSPAC. The EOSPAC, a code written by Charles W. Cranfill of LANL, allows MACH2 to use split tables if they exist, or creates split tables by using built-in analytic models if the tables do not exist. In general, EOSPAC does a good job of creating split tables, and the algorithms are robust. In our experience, the lone exception occurs in simulations with low-temperature regions—for example, solid aluminum at or below room temperature using SESAME table 3717. In that case, the split tables yield nonphysical derivatives that yield an unreasonable sound speed in cold, dense regions. Ideally, the user should to be able to use a two-temperature model in hot regions and a single-temperature model in cold, dense regions where the large collision frequencies produce ion-electron equilibrium anyway. However, such is not possible in the present MACH2 implementation.

MAKING MACH2 FASTER

The Hall effect is important in rare plasmas that support large current densities. That portion of the differential equation that governs the time evolution of the magnetic induction which depends on the Hall electric field is quadratic in the magnetic induction. This is unlike all other differential operators in MHD codes. We informally polled other

research groups and found that all who modeled the Hall effect used an explicit treatment. Furthermore, we have been unable to think of a reasonable implicit model.

Experience has shown that models in which the Hall effect is important often run 2 to 10 times slower when this effect is included than when it is not. A factor of 10 decrease in performance is often deemed intolerable. In an attempt to increase the speed at which MACH2 executes, the possibility of replacing the current double-loop structure with an equivalent single-loop structure was investigated. Results of this investigation are found in the document entitled "Can MACH2 Run Faster if We Replace Double Vector Loops with Single Vector Loops" by M. L. Haley. The answer appears to be no.

The physical domain for a particular MACH2 simulation is obtained via an invertible mapping from a logical domain that is called a block complex. Because MACH2 is an ALE code, simulations can be performed on a time-dependent physical domain. The capability of the code has been expanded to allow the logical domain, or block complex, to also be time-dependent. This is done by modifying Version 9001 of MACH2, and the implementation of this code is discussed in the technical note entitled "Dynamically Changing the Logical Computational Domain of a MACH2 Physics Simulation" by A. J. Giancola, R. E. Peterkin, Jr., and M. H. Frese.

Researchers who use MACH2 historically have been able to run relatively fast simulations, thus providing the opportunity to perform parameter studies with modest use of computer resources. The need to dynamically adjust the logical structure of a problem arises when one conceives of global problem domains that are both large and modular. One class of such problems that is of particular interest is illustrated by the MARAUDER CT program. The ability to numerically simulate the CT through its various stages of life—which include in chronological order: formation, acceleration, focusing, and impact stages—shall be of immense benefit to the research program.

Under this subtask, much progress was made in the ability to postprocess data from numerical simulations on Sun SPARC workstations. Mission Research Corporation has modified the IMAGETOOL software from the National Supercomputing Center at the University of Illinois to allow it to handle the complex shapes that are typical for MACH2 simulations. The MACH2 can create files that can be processed and read by IMAGETOOL to create continuous-color images. A sequence of images from a single simulation can then be displayed sequentially to create a movie.

ANOMALOUS RESISTIVITY CONSIDERATIONS FOR CT PHYSICS

During this subtask, we reported on the investigations concerning the effect of microturbulence-induced anomalous resistivity at high energy densities that are characteristic of the MARAUDER CT program. We learned much concerning the implications of high anomalous resistivities that are caused by microturbulence or edge plasma-neutral interactions on CT lifetimes. Earlier experiments at the LLNL Beta II facility, and subsequent experiments on the RACE facility, have successfully demonstrated the stability and resiliency of the CT, at least at moderate energies. The purpose of the effort was to investigate the effects of microturbulence-induced anomalous resistivity at the high energy density characteristic of the MARAUDER program.

Following the initial set of CT formation-extraction-compression (F-E-C) experiments in a Phase 2 configuration (Refs. 65 and 66), a short series of calculations was performed in the Phase 1-b configuration. These simulations used the same mass and magnetic field distribution as the F-E-C calculations. The only difference in the initial calculation was the geometry.

The configuration and initial field and density distribution are shown in Figure 26. This calculation produced the formation and extraction of a toroid into the expansion region as shown in Figure 27. Reconnection occurred at 2.9 μs. The toroid moved to the end of the expansion region and rebounded back toward the gun muzzle. As can be seen in Figure 28, the magnetic field structure of the toroid is still well formed at 5.0 μs. The toroid has not decayed significantly by 10 μs.

The first models of CT formation and extraction were run with the microturbulent (anomalous) resistivity turned off. Resistivity and magnetic diffusivity were determined by classical Spitzer resistivity with an effective ionization of 1, characteristic of fully ionized hydrogen.

The second Phase 1-b extraction calculation turned on the standard MACH2 microturbulent resistivity from Version 8801 (Ref. 67). This model is global in nature with the microturbulent collision frequency, ν^*, given by

$$\nu^* = \alpha \, \omega_{pe} \tag{24}$$

where α is an adjustable parameter.

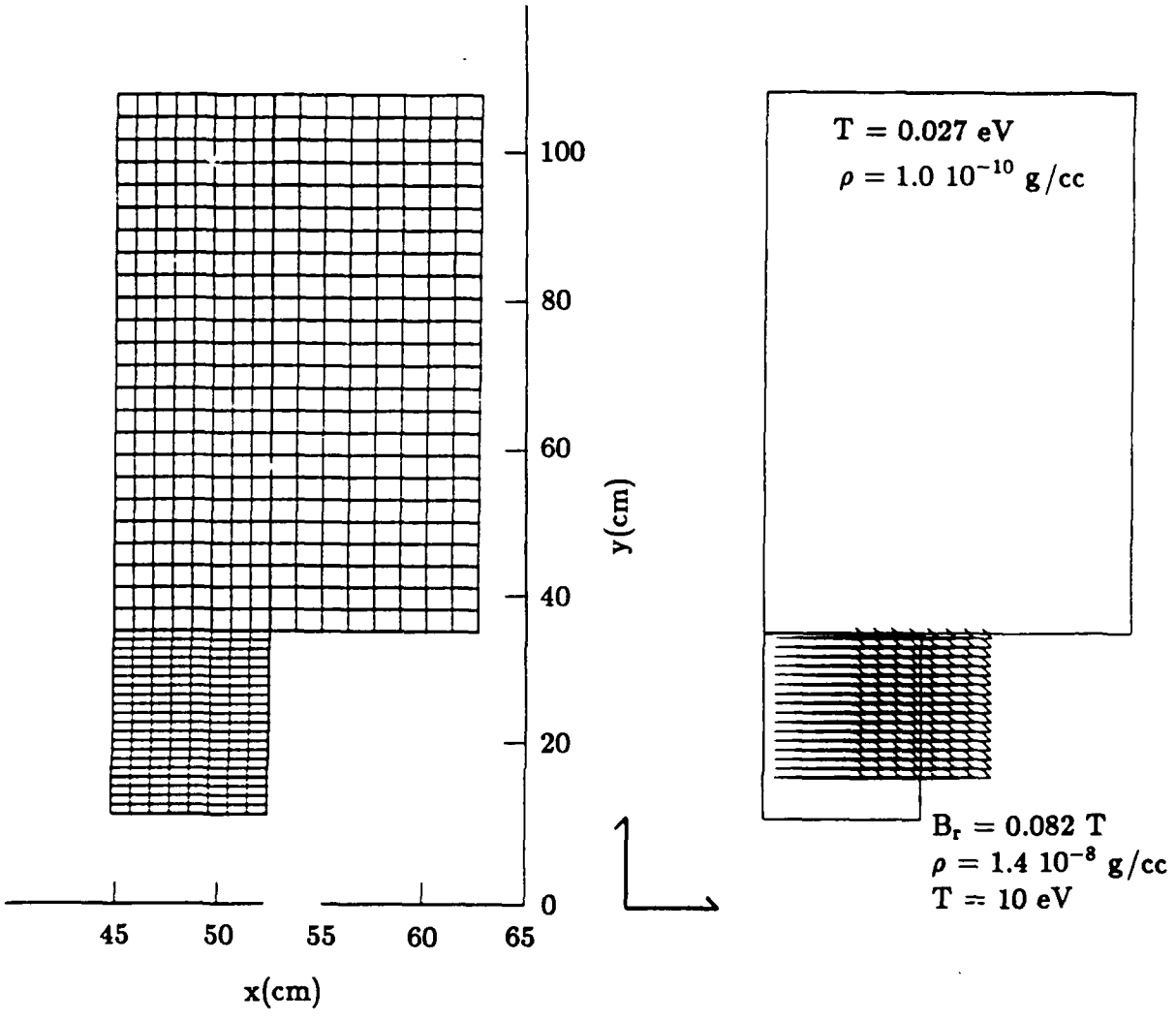

Figure 26. Initial grid and physical conditions for the MACH2 calculations.

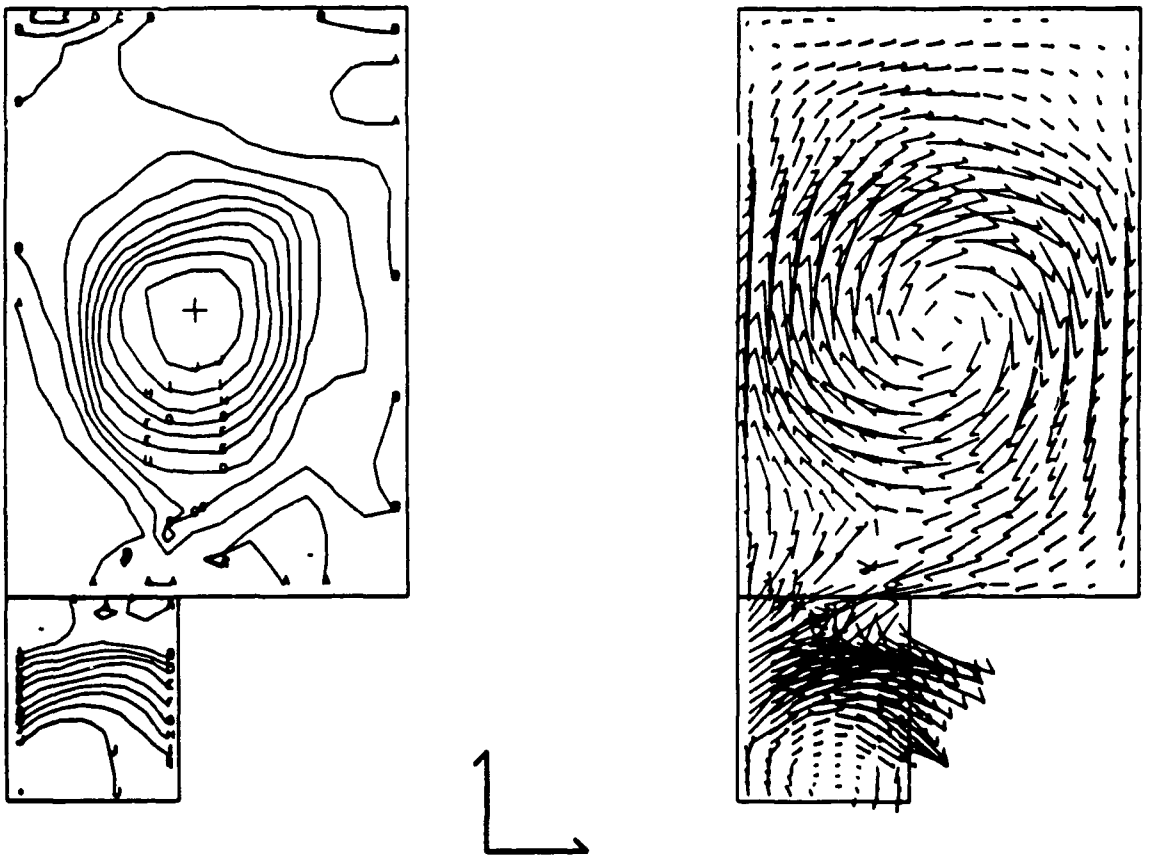

Figure 27. B_θ and B_p at 3 μs for Spitzer resistivity calculation. B_θ peaks at 1.7 T in the center of the torus, and the magnitude of the largest B_p is 1.1 T near the containing walls.

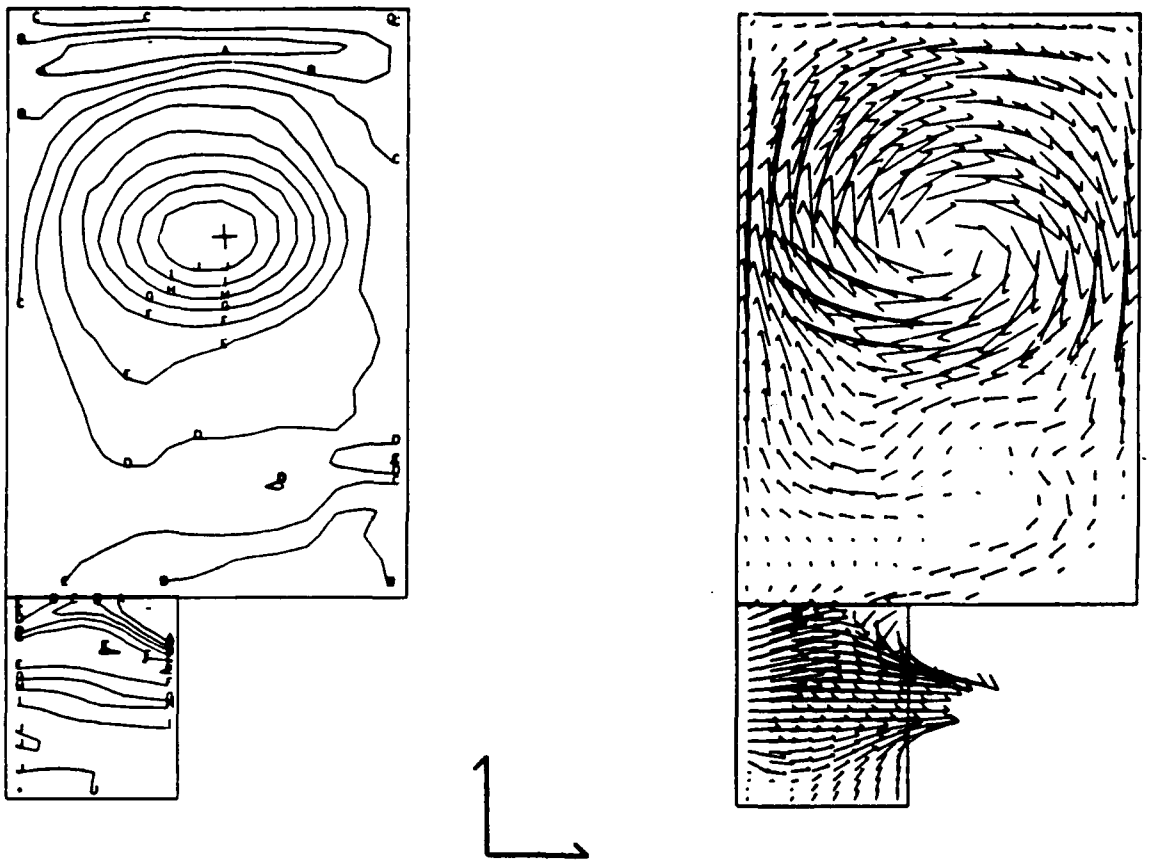

Figure 28. B_θ and B_p at 5 μs for Spitzer resistivity calculation. B_θ peaks at 0.67 T in the center of the torus, and the magnitude of the largest B_p is 0.73 T near the containing walls.

When the anomalous resistivity is turned on in MACH2, this model increases the resistivity everywhere in the problem region. This model has been successfully used in PFS imploding liner calculations (Ref. 48).

This model, with $\alpha = 0.01$, produced significantly different results in the CT formation-extraction simulation. The plasma was again moved from its initial position into the expansion region as in the previous calculation. Reconnection occurred earlier with this higher resistivity value, at 1.9 μs for this case versus the 2.9 μs for the Spitzer resistivity case. More significant, however, was the decrease in magnetic field lifetime resulting from the globally higher resistivity. The magnetic field structure decays significantly, as can be seen in Figure 29. The toroidal structure in the toroidal magnetic field has essentially disappeared by 2.6 μs.

While providing the gross effects of plasma microturbulence, this global model does not properly represent the physics associated with microinstabilities and microturbulence. In the global model, the microturbulence is present everywhere. In a physical situation, however, the microturbulence exists only where there is free energy available that can lead to plasma microinstabilities. The microturbulence is thus a local phenomena. It exists only when threshold conditions for instabilities, which can tap the available free energy, are exceeded. The microturbulence has a threshold for initiation and extinction.

One of the most used local models for plasma microturbulence is the Chodura model (Refs. 68 and 69). This model was originally developed to model ion acoustic turbulence, but has been used as a phenomenological model to represent a wide range of microturbulent processes. In this model the saturated value of the microturbulent collision frequency is given by

$$\nu^* = A\,\omega_{p_i}\,\left(1 - \exp\,\left(-v_{d_e}/B v_{i_s}\right)\right) \tag{25}$$

Here v_{d_e} is the electron drift velocity, v_{i_s} is the ion acoustic velocity and A and B are phenomenological parameters. The term in parenthesis represents the threshold conditions on the instability producing the microturbulence. Typical values for the constants are A = 1 and B = 3.

To investigate the effects of a local model of microturbulent resistivity on CT formation-extraction, a Chodura model was implemented in MACH2. A third formation-extraction calculation was performed that used this local model. While the decay was not as significant, there were clearly regions in the plasma where the threshold conditions were met, and microturbulence again significantly increased the resistivity. This increased resistivity again resulted in early decay of the toroid, as illustrated in Figure 30.

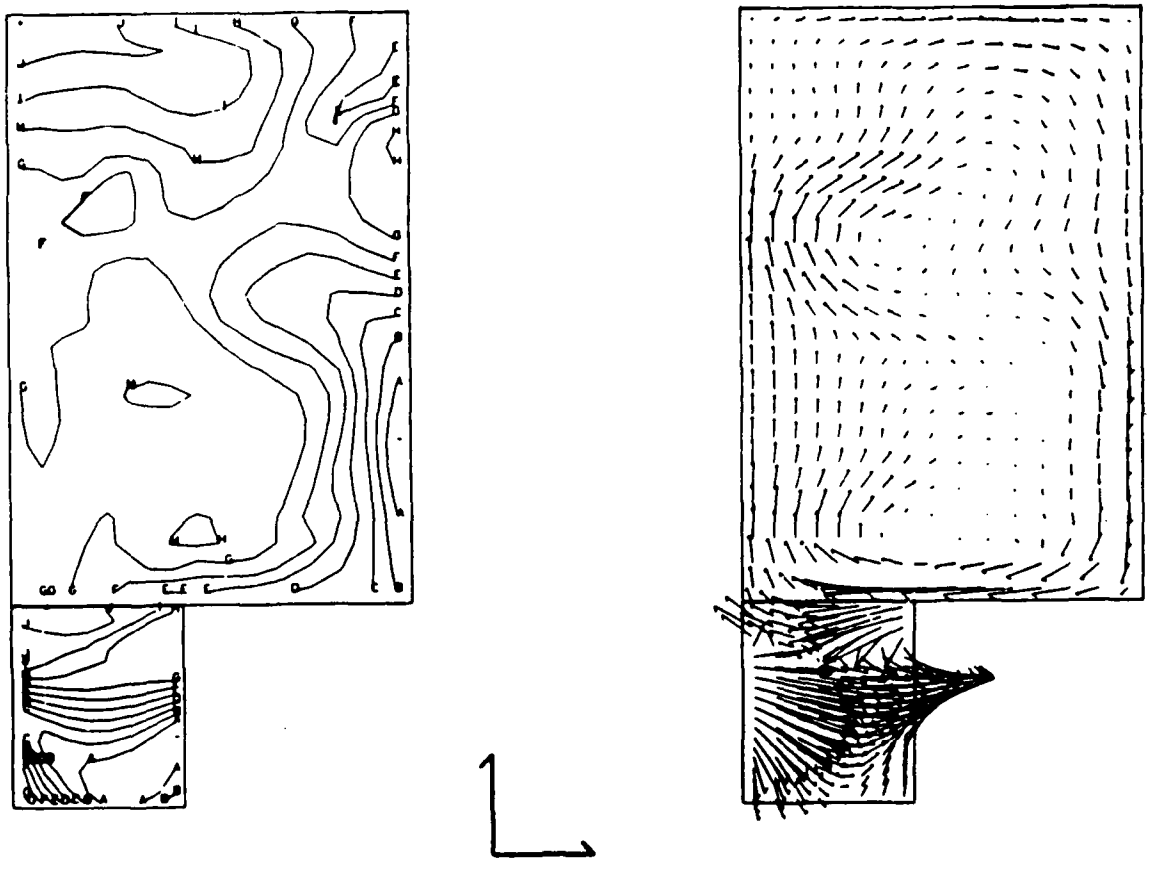

Figure 29. B_θ and B_p at 5 μs for the $\nu^* = 0.01\ \omega_{pe}$ calculation. Ten B_θ contours are displayed at equal intervals between A (0.355 T) and J (0.67 T). The largest $\vec{B}_p$ occurs near the breach of the formation region and has magnitude 0.68 T.

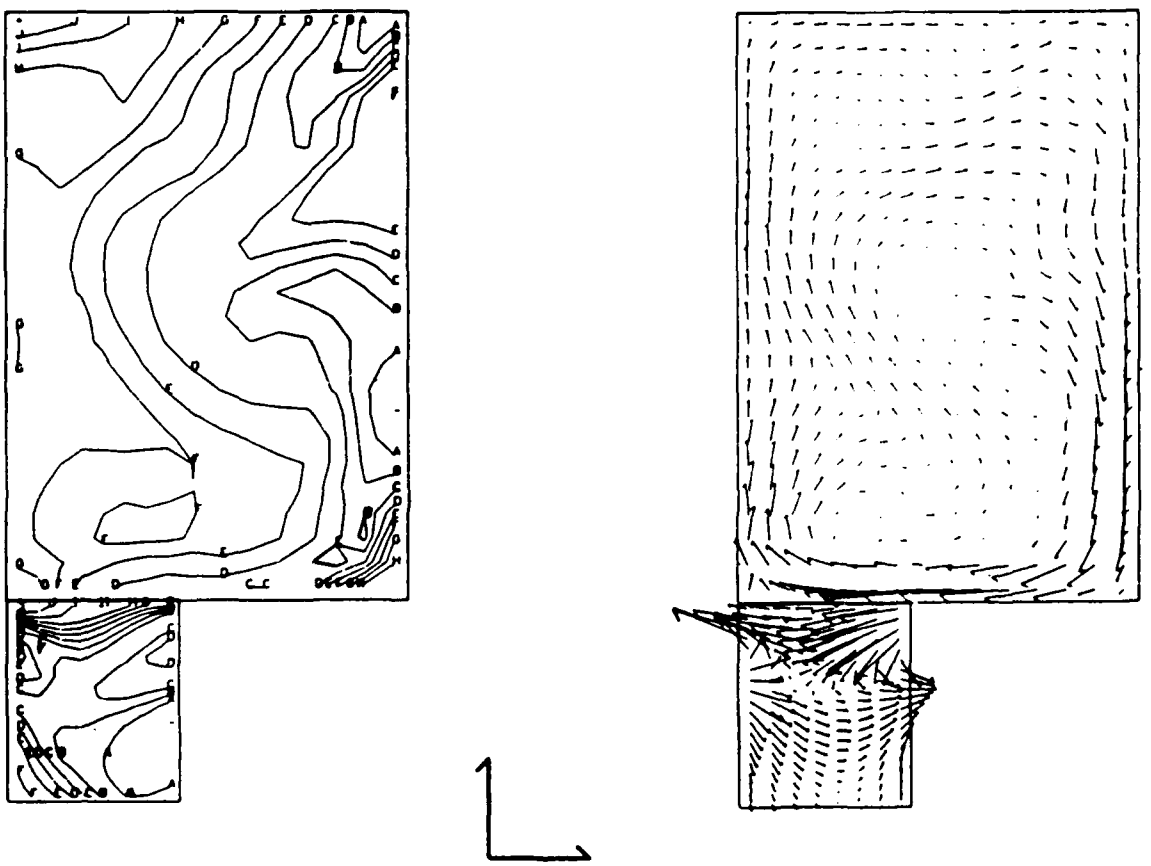

Figure 30. B_θ and B_p at 5 μs for the microturbulence calculation. Ten B_θ contours are displayed at equal intervals between A (0.505 T) and J (0.82 T). The largest $\vec{B}_p$ occurs near the breach of the formation region and has magnitude 0.56 T.

Reconnection for this case occurred at 1.9 μs, and again the toroidal field has essentially decayed by 2.6 μs.

Note that the threshold conditions do indeed affect the resistivity. As the discharge developed, the electron drift velocity increased as the current density increased. This created large regions of higher resistivity where the threshold was exceeded. The higher local resistivity gave rise to increased joule heating. This in turn increased the temperature, and in some regions this increase was sufficient to extinguish the microturbulence.

The results of these calculations with microturbulent are disconcerting with respect to toroid lifetime. There are several issues, however, which could mitigate these results. The first is the existence of microturbulence in the CT RACE and MARAUDER configurations. Nonclassical resistivities have been inferred in other CT configurations. The most notable of these is the Field Reversed Configuration (FRC). Here both the timing of reconnection and the toroid lifetime occur with time scales shorter than those associated with classical Spitzer resistivity. Early attempts to explain these discrepancies used models with a multiplier to the classical Spitzer resistivity. The presence of impurities was postulated to physically explain the higher effective ionization state. Milroy and Brackbill (Ref. 55) use a Chodura model of microturbulent resistivity for the first microsecond before magnetic reconnection, and then a modified lower-hybrid-drift model after reconnection occurred. (A model similar to this was tried in MACH2 for the CT formation-extraction problem. Results again were an early decay of the magnetic field structure similar to the simple Chodura model.) Krall (Ref. 70) has proposed regional models based on lower-hybrid-drift and drift wave turbulence to try to explain the experimental data. The best results to date have been those of Krall's regional model, but this model is incomplete in explaining FRC scaling.

With respect to the RACE/MARAUDER CT configurations, the FRC results have a major drawback. This is because the RACE/MARAUDER CTs have high magnetic shear (Refs. 71 and 72). Many of the instabilities that occur in the FRC configuration, which has only poloidal fields, are stabilized in the presence of shear. The RACE/MARAUDER configurations are directly related to the high shear Spheromak configurations. There are few plasma microinstability and microturbulence studies in the presence of shear. The canonical opinion is that shear stabilizes the plasma, and that one need not worry about resistivities much above Spitzer.

This is not necessarily the case however. Reversed Field Pinch (RFP) configurations, which are highly sheared, show decay times shorter than Spitzer. While theoretical calculations of stability in sheared systems are few, Gladd and Krall (Ref. 73) have

reported the existence of current driven drift modes, which exist in the presence of shear, to explain flux and energy losses in the RFP.

Additionally, prior to the last few years, it was postulated that Spheromak lifetimes were based on classical Spitzer resistivity. Spheromak flux decay was within a factor of a few of classical Spitzer. The difference was attributed to impurities giving an effective ionization state of 2 or 3. Experiments conducted at LANL in 1987 showed effective to classical resistivity ratios could be as high as 15 to 20 (Ref. 74). More typical values were near 10. These variations occurred at high ratios of drift speed to thermal speed (factors of 0.05 to 0.20). These results could not be explained by impurity effects.

Following these experiments a detailed study was made of the experimental parameters, diagnostic techniques, and magnetic field structure. Based on this study the field structure was improved. The previously used cage flux conserver structure was replaced by a solid flux conserver, and the experiments were repeated (Refs. 74 and 75). In addition to the change in the flux conserver structure, diagnostics were incorporated to make local measurements of parameters affecting the resistivity. The results of these experiments again showed a high average effective resistivity compared to classical. The detailed measurements of local parameters indicated that this was not a problem with the bulk plasma contained inside the toroidal magnetic surfaces, but the effects of electron-neutral collisions at the plasma edges. Similar results on edge plasma/neutral interactions, and the impact on energy confinement and resistive decay, have been found for the S-1 Spheromak at Princeton (Ref. 76). While not anomalous in the microturbulent sense, the high resistivity due to electron neutral effects represents a significant departure from classical Spitzer.

What the short series of calculations indicates is that non-Spitzer resistivity can significantly affect toroid lifetime. The work done since the original calculations has been to establish the theoretical and experimental data base for microturbulent instabilities and transport in CT configurations. The literature on these subjects for highly sheared configurations is not as fully developed as we would like. The canonical view that toroid lifetime will be classical still has some questions, especially at high energy density.

On the other hand, even if high resistivities exist, due either to microturbulence or edge plasma-neutral interactions, CT lifetime may not be reduced as significantly as shown in these microturbulent resistivity calculations. The Hall effect or the possible replenishing of magnetic flux by an acceleration discharge may increase CT lifetimes above that expected from consideration only of resistive decay.

In order to better model CT formation, a second-order accurate van Leer advection scheme was added to MACH2. The algorithm was implemented in MACH2 by Capt Carl Sovinec of the High Energy Plasma Division. Mission Research Corporation installed this algorithm in the code and ran a number of test problems to validate the new treatment of advection.

RECONNECTION GUN STUDIES

Mission Research Corporation computationally studied the reconnection gun experiments performed at the WL (Ref. 77). The reconnection gun experiments consisted of two phases. The first phase was conducted at low bank energy to characterize plasma gun performance with a single gun and three gun sectors. The second phase used a complete circular arc of 24 guns on the SHIVA STAR capacitor bank to investigate neutron production at the 2.3-MJ stored energy level. The 24 medium-energy coaxial plasma gun discharges combined to form a single high energy hypocycloidal pinch discharge via magnetic reconnection. This effort represented an increase in energy of an order of magnitude over that conducted by Cowan and coworkers (Ref. 78).

The single gun experiments were modeled with MACH2 initiating the plasma discharge with a region of high temperature plasma next to the insulator. In this configuration the computational center-line is the axis of the gun barrel and the barrel is 34.56 cm in length. The flange at the end of the gun barrel was simulated with a disk in the computational model. The return conductor was a plane at the breach end of the gun and the insulator extended 12.7 cm from the return conductor plane onto the barrel. Calculations were performed at the 50-kV level at pressures from 2 to 10 T. The R-L-C driver was used for the circuit. An ideal gas equation of state for deuterium was used. For these single gun experiments there was good qualitative and quantitative agreement between the experimental results and the MACH2 simulations. For the 4-T experiment, pinch occurred at 2.8 μs in the experiment and 2.85 μs in the calculations. Peak experimental current was between 350 and 400 kA and peak computational current was 368 kA.

After successful completion of the single gun simulations, an attempt was made to model the full arc experiment. This was a three-dimensional problem with reconnecting plasma sheaths forming as the plasma from the individual guns formed two current paths from the initial 24-gun paths. In this model, the 24 guns become one disk. The center line of the computation is at the center of the gas region with the disk beginning 15.4 cm from the center. The insulator lies on the outside of the disk. The return conductor is now a cylinder at the outer disk edge. The flange at the end of the gun barrels now is a cylindrical flange as in the experiment.

The usefulness of a two-dimensional simulation was in doubt from the beginning. Nevertheless, two calculations were attempted to investigate the feasibility of approximating the three-dimensional behavior in a quasi-two-dimensional manner.

The first model used the results of the single gun calculations to form a quasi-two-dimensional representation of the collapsing plasma. To form the approximate two-dimensional model, a link was made from a single gun calculation at the time when the current sheaths would begin to reconnect to an equivalent disk calculation. In the disk model, the 24-gun reconnection plasma sheaths are modeled as a single disk center conductor with an axisymmetric current sheath running on the disk under the action of the $\vec{J} \times \vec{B}$ forces of the current flowing in the sheath. The second model initiated a disk discharge from the initiation of current flow in the plasma. In this case, no attempt was made to follow the individual plasma gun sheath.

For both models, quantitative agreement with the experiment was poor. Qualitatively, both showed a plasma sheath run down and pinch. In both cases, however, the pinch occurred late. This is attributed to the difference in inductance between the three-dimensional reconnecting plasma sheath configuration and the two-dimensional disk problem.

From these simulations two immediate conclusions can be drawn. The first is that MACH2 is a good tool for simulating single gun behavior. The second is that a quasi-two-dimensional model of the disk type used does not provide an adequate model for the three-dimensional multiple gun reconnection process.

2.3.7.2 Reports. Documents prepared under this subtask are summarized here.

"A Material Strength Capability for MACH2"
Robert E. Peterkin, Jr. and Michael H. Frese
MRC/ABQ-R-1191
November 1989

ABSTRACT: An explicit elastic-plastic package has been added to MACH2 and is documented in this paper. The MACH2 code is a 2 1/2-dimensional MHD simulation code that is ideally suited for problems with complex shapes. It is an arbitrary Lagrangian Eulerian (ALE) code designed to run on Cray supercomputers. The elastic-plastic code that has been added to MACH2 is discussed in detail, and the results of some simple test simulations that exercise this code are presented.

"MACH2: A Reference Manual—Fourth Edition"
Robert E. Peterkin, Jr., Anthony J. Giancola, Michael H. Frese and James Buff
MRC/ABQ-R-1207
November 1989

ABSTRACT: This report is the fourth edition of the MACH2 Reference Manual. The MACH2 code is a 2 1/2-dimensional MHD simulation code that is ideally suited for problems with complex shapes. It is an ALE code written in CFT-77 FORTRAN and designed to run on Cray supercomputers. This report documents the state of MACH2 in its most recent manifestation, Version 8901. Discussed in detail is everything a sophisticated code user requires to run the MACH2 code including: the equations that MACH2 solves and the FORTRAN subroutines that perform the computations, how to create an executable version of MACH2, how to construct (in the form of an input file) the necessary initial data for a physics simulation, how to control the MACH2 simulation mesh, and how to create and interpret the various output files.

"A Two-Temperature Model for MACH2"
Robert E. Peterkin, Jr.
MRC/ABQ-R-1260
February 1990

ABSTRACT: This paper presents the details of a new two-temperature model for the MHD simulation code, MACH2. A two-temperature model means that an ensemble of electrons and ensemble of ions are not a-priori assumed to be in mutual thermodynamic equilibrium. Separate electron and ion temperatures implies that the single energy equation in a one-temperature code must be split into two energy equations in a two-temperature code. The MACH2 code is a 2 1/2-dimensional MHD simulation code that is ideally suited for problems with complex shapes. It is an ALE code designed to run on Cray supercomputers. All previous versions of MACH2 assumed that electrons were in equilibrium with the ions, and hence a single energy equation was solved. Version 9001 of MACH2, however, has the flexibility to model a magnetofluid that is characterized by a single temperature or by separate electron and ion temperatures.

"Can MACH2 Run Faster If We Replace Double Vector Loops with Single Vector Loops?"
Mary L. Haley
MRC/ABQ-N-458
February 1990

ABSTRACT: It has often been suggested that it might be possible to obtain a substantial speedup of the 2 1/2-dimensional MHD code, MACH2, by rewriting all double vector loops as single vector loops. The idea is that a single large vector loop might execute faster than a series of smaller vector loops. This is not the case when implemented in MACH2. The results of the investigation are documented in this report.

"Dynamically Changing the Logical Computational Domain of a MACH2 Physics Simulation"
Anthony J. Giancola, Robert E. Peterkin, Jr. and Michael H. Frese (Numerex)
MRC/ABQ-N-462
February 1990

ABSTRACT: The MACH2 code is a 2 1/2-dimensional MHD simulation code that is ideally suited for problems with complex shapes. It is an ALE code designed to run on Cray supercomputers. The physical domain for a particular MACH2 simulation is obtained via a mapping from a logical domain that is called a block complex. Because MACH2 is an ALE code, simulations can be performed on a time-dependent physical domain. The capability of the code has been expanded to allow the logical domain, or block complex, to also be time-dependent. This is done by modifying Version 9001 of MACH2, and the implementation of this code is discussed in this note.

"Anomalous Resistivity Considerations for Compact TORUS Formation and Decay"
Norman F. Roderick
MRC/ABQ-N-463
March 1990

ABSTRACT: Experiments to form, accelerate, and focus CT plasmas are presently being performed on the 9.4 MJ SHIVA STAR fast capacitor bank at the WL. The MARAUDER program is a research effort to accelerate magnetized plasma rings with masses between 0.1 and 1.0 mg to velocities above 10^8 cm/s and energies above 1 MJ. The effects of microturbulence-induced anomalous resistivity at high energy densities were investigated. The implications of high anomalous resistivities from microturbulence or edge plasma-neutral interactions for CT lifetimes is discussed.

"MACH2: A Two-Dimensional Magnetohydrodynamic Simulation Code for Complex Experimental Configurations"
Michael H. Frese (Numerex)
March 1990

ABSTRACT: This report details the physical model presented in AMRC-R-874, including boundary conditions; permissible problem geometries; time differencing; and spatial discretization, centering, and differencing of MACH2. This report also covers the iteration procedures for the implicitly differenced physical processes, as well as the boundary conditions and block coupling implementation techniques.

"SHIVA STAR Computational Physics Studies III"
Robert E. Peterkin, Jr., Norman F. Roderick, Anthony J. Giancola, Mary L. Haley, James Buff and Michael H. Frese
MRC/ABQ-R-1278
March 1990

ABSTRACT: This manuscript is the final report for Subtask 03-07, SHIVA STAR Computational Physics Studies III. The bulk of this report consists of six technical reports. These are entitled (1) "MACH2: A Reference Manual—Fourth Edition," (2) "A Material Strength Capability for MACH2," (3) "A Two-Temperature Model for MACH2," (4) "Can MACH2 Run Faster If We Replace Double Vector Loops with Single Vector Loops," (5) "Dynamically Changing the Logical Computational Domain of a MACH2 Physics Simulation," and (6) "Anomalous Resistivity Considerations for Compact Torus Formation and Decay." Work performed under this subtask is summarized.

2.3.8 Subtask 03-08, Smooth Particle Hydrodynamics

2.3.8.1 Research Summary. This subtask outlines a procedure for extending the codes available to WL personnel to include an SPH code for use in modeling solid liner implosions, plasma jets, and other hydrodynamic processes requiring an efficient approach and three-dimensional modeling capability.

The MRC smooth particle hydrodynamics code, named SPHC, has been developed to meet these requirements. The present capabilities include:

1. One-, two-, and three-dimensional run modes.
2. Spherical and cylindrical geometry options.
3. Conservative error-control Runge Kutta integration.
4. Analytic equation of state including Gruniesen terms for solid density models.
5. Complete input/output package, including restart dumps, parameter dumps, and history files. Appended data option allows plotting of time dependent effects.

6. Flux-limited electron thermal conduction option.

7. Variable smoothing length.

8. "Grid" generator routine to assist in setup of multimaterial and multiregion problems.

9. A full set of boundary condition options, including WALL, REFLECT, FIXED, INFLOW, OUTFLOW, PERIODIC, AXIS, and FLOW-THROUGH.

10. Laser deposition option, could be used to test the effects of a variety of energy deposition problems.

11. A full set of program guides, including: User's Guide, Programmer's Guide, Technical Guide, and Function Directory.

The SPHC code has been applied to simple models of plasma accelerated projectiles using the technique of shockless acceleration.

Although resources do not permit a detailed study, the tests performed are sufficient to demonstrate the applicability of this technique. To achieve positive results, a new rezoning technique using particle division to maintain resolution in rarefaction regions was developed and proven effective. This is the first application of such a technique.

The following is a summary of the tests undertaken:

1. Several cases were run with a cylindrical gun barrel in which a strong shock accelerates a low density plasma into a light bullet 5–10 cm down the barrel. Both constant density and graded density pusher plasma were tried. In all cases a high density shell (blast wave) formed at the leading edge of the accelerated plasma, defeating the "shockless" feature of the experiment, and instabilities rapidly fragmented the projectile.

2. Two additional cases were run with a straight rarefaction expansion of the initially hot plasma. These cases did produce nicely exponential density profiles and relatively smooth acceleration of the projectile. Two temperatures were chosen for the pusher, 10 eV resulting in a final velocity of 30 km/s, and 1 eV resulting in a final velocity of about 10 km/s for the standard setup. Figure 31 shows the density distribution for the hot case. Although neither case showed optimum behavior, these tests could form the starting point for a detailed study of this mechanism.

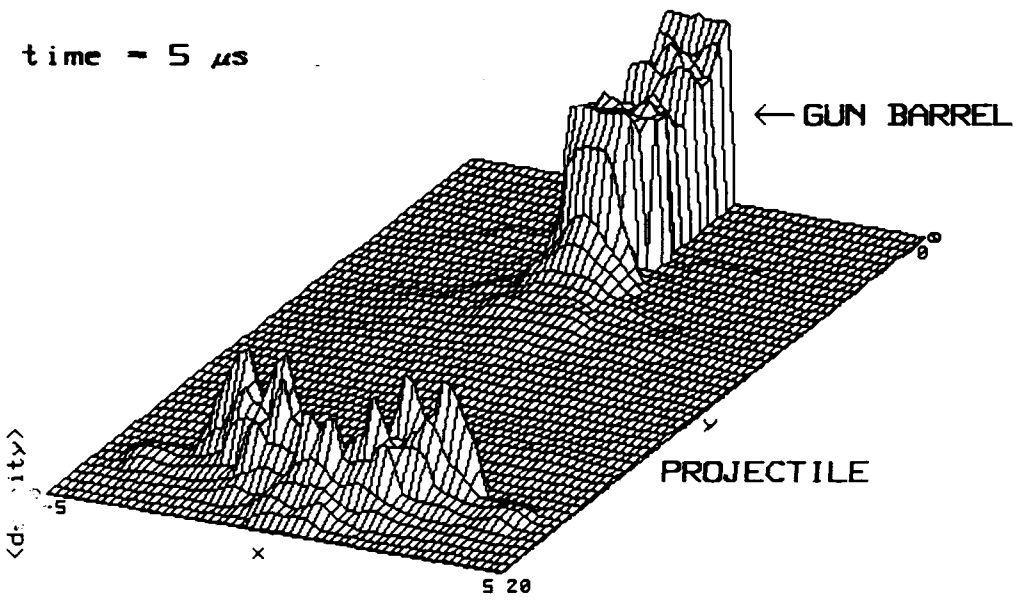

Figure 31. Model of a shockless-accelerated projectile with SPHC. Dimensions are in centimeters and grams per cubic centimeter. Projectile velocity is 30 km/s in this model.

2.3.8.2 Report. Document prepared under this subtask is summarized here.

"SPHC Manual"
Robert F. Stellingwerf
MRC/ABQ-R-1237
January 1990

ABSTRACT: This is a manual for use of the SPHC. It consists of four sections: User Guide, Programmer's Guide, Technical Guide, and Function Directory. All aspects of the code are discussed in sufficient detail to allow operation and local modification if necessary.

2.3.9 Subtask 03-09, Plasma Jet Diagnostics

2.3.9.1 Research Summary. Under this subtask, the following diagnostics that are relevant to plasma jets are discussed:

(1) Fast ion gauges for neutral gas density measurements prior to electrical discharge, (2) optical spectroscopy using an OMA for specie identification, relative abundances, plasma temperatures and densities, and directed velocity, (3) electric probes for electron temperature and densities, (4) "pepper pot" divergence measurements of plasma temperature distributions, (5) fast photography with a turbine/mirror camera, (6) the use of scintillators and phosphors, (7) piezoelectric and piezoresistive pressure transducers, (8) ballistic momentum transfer diagnostics, (9) biased Faraday cup beam current density monitors, and (10) calorimeters.

Based on diagnostic evaluations, several diagnostic apparatus, including a pepper pot divergence mask with scintillator detector, a biased Faraday cup array, and a pyrolytic graphite calorimeter were designed and fabricated. These devices were transported to the experiment site for deployment. A miniature Thomson parabola particle spectrometer was used for particle energy, momentum, and charge state measurements. Of these diagnostics, the calorimeter was never deployed, the Thomson parabola spectrometer yielded questionable results, and the pepper pot was fielded, but not used for quantitative measurements.

The Faraday cup array was installed late in the experiments for one series, but the electron stripper grid did not work effectively due to higher than expected plasma density (electron screening effects dominated). Thus, the recorded signals were primarily negative, due to the preferential collection of plasma electrons. Still, the Faraday cups yielded some radial density profile information (assuming no radial plasma temperature dependence), and timing/velocity information.

During these experiments at General Research Corporation (GRC), the main thrust of the work was in the area of time-resolved optical spectroscopy. The OMA at AWX was set up on site and careful optical and electrical alignments of the system were performed. Because of the harsh electrical noise environment near the beam range, the OMA was operated inside a metal RF enclosure, with data acquisition and triggering accomplished with fiber optic links. Three optical fibers were set up for data recording—taking advantage of the Jarrell-Ash Monospec 27 spectrograph's stigmatism to simultaneously record spectra from three separate locations. Three different diffraction gratings (150 l/mm, 1200 l/mm, and 1800 l/mm) were used for a variety of spectral ranges and resolutions. Although the OMA has 40-ns time resolution capability, it was routinely operated with gate widths of 1 μs to 1 ms.

The results of the spectroscopic measurements are summarized in the following paragraphs.

1. For all experimental parameters, locations, and times, the optical spectra were dominated by line emission from silicon. Silicon II (singly ionized) lines at 6355 Å, 4130 Å, 5051 Å, and 5972 Å were consistently strongest. Silicon III lines were also evident, but generally at lower intensities. Next in prevalence was the neutral hydrogen H_α line at 6563 Å. Hydrogen was identified whether it was the working gas or not. Next in strength were neutral oxygen lines, especially at 7773 Å. In some high-resolution spectra, low-intensity C II lines were seen. Although argon was the working gas for most of the experiments, no argon lines could be unambiguously identified.

2. The silicon seen in the spectra was found to originate from the gun insulator, which was made from quartz (SiO_2). To eliminate the beam range walls (glass) as a source of silicon contamination, the following tests were performed. First, the three optical sensors were set up at the 5-m pumping station. One fiber was positioned similarly to previous positionings—that is, at the range wall (radius approximately 5 in from axis) oriented perpendicular to the range axis. The second fiber was positioned to look perpendicular to the axis through one of the interferometer ports, where it could not "see" any of the glass wall. The third fiber was positioned to look almost tangential to the glass wall. The relative intensities of the silicon lines were not appreciably different among the three optical probes, indicating that the source of the lines was probably from the interior of the range tube. As an independent test, upon our recommendation, GRC personnel replaced the quartz insulator with an alumina (Al_2O_3) insulator for several shots. The optical spectra from these shots exhibited intense aluminum line emission and no silicon emission.

3. The intensity of optical emissions at a given downstream position peaked in time somewhat after gun current rise. In general, the time-position relationship indicated the highest intensity source travelling at an axial speed of roughly 50–80 km/s. The fastest inferred speed of detectable emitting plasma was between 100 and 150 km/s. The optical intensity variations seen by the OMA were consistent with those seen by photodiode detectors, although in some cases, the photodiodes also saw low-intensity "precursors" corresponding to somewhat higher speeds.

4. Local Thermodynamic Equilibrium (LTE) was assumed and applied to Si II line ratios, to estimate electron temperature as a function of axial position and time after current rise. These analyses indicated a monotonically decreasing temperature with time at any position, and with increasing downstream position at a corresponding time. The range of inferred temperatures was between 0.7 and 4 eV, with the highest temperatures occurring just in front of the gun muzzle, early in time (within 10 μs of current rise). At the 5-m position, the inferred temperature dropped from about

2 eV early in time to about 0.7 eV at the end of detectable emission. The LTE assumption, although simplifying analysis, is generally invalid. Both interferometry data and independent spectral data suggest peak electron densities, downrange, of less than about 10^{15} cm^{-3}. At electron temperatures of approximately 1 eV, LTE criteria for most optical transitions are not satisfied. To check the general validity of LTE, we plotted the relative intensities of several Si II lines, unweighted by their respective photon energies, upper state statistical weights and transition probabilities (Einstein A coefficients) against upper state excitation energy. Although the data followed a semilogarithmic trend, there were noticeable departures (in LTE, the unweighted intensities are proportional to $\exp(-E_{upper}/kT_e)$, so that on a semilog plot, the temperature is inversely proportional to the slope of the best straight line through the data). A collisional-radiative equilibrium model for Si II has begun to be built to improve the analysis. Still, the temperature ranges and trends reported should not be too inaccurate.

5. For a select number of shots, the hydrogen H_β line, at 4861 Å, was recorded. Over the range of temperatures inferred, the full width half maximum of the line in Angstroms is known to scale as electron density to the 2/3 power, so that for densities greater than about 10^{14} cm^{-3} to 10^{15} cm^{-3}, the effect is measurable. For the shots where H_β was recorded, significant line broadening was not observed, placing an upper bound on electron density of 10^{15} cm^{-3}.

Based on the above results, and corroborative independent diagnostic measurements, we conclude that for the experiments we observed, the gun discharge plasma was formed primarily from the insulator, and not the injected working gas, as intended. The bulk of this plasma appeared to travel at speeds typically less than 100 km/s. Although the electron temperatures were in the range from 1 to 4 eV, we can not infer a corresponding ion temperature, and therefore, a beam divergence based on the ratio of thermal to directed velocities. The equilibration times between electrons and ions can be relatively long compared to the experiment time scales to make inferences about ion temperatures from "excitation" temperature measurements. Similarly, the equilibration times between successive ionization states of a species, and between different ionic species, can be long, making relative abundancy estimates rather precarious. (Note that the presence of hydrogen could substantially reduce the equilibrium time, however, so an estimate of a few electronvolt ion temperature may, in fact, be reasonable.)

2.3.9.2 Report. Document prepared under this subtask is summarized here.

"Diagnostic White Paper Contributions"
Gerald F. Kiuttu, Robert J. Richter-Sand and Kenneth W. Struve
MRC/ABQ-N-451
June 1989

ABSTRACT: Several diagnostics are discussed which may be suitable for plasma jet experiments. The diagnostics include fast ion gauges, OMA, electric (Langmuir) probes, pepper pot (divergence) techniques, fast (turbine-driven) photography, scintillator targets, pressure transducers, ballistic targets, Faraday cups, and calorimeters.

REFERENCES

1. Friedman, M., Serlin, V., Lau, Y. Y., and Kroll, J., *Microwave and Particle Beam Sources and Directed Energy Concepts*, SPIE 1061, p. 34, 1989.

2. Lau, Y. Y., private communication.

3. Friedman, M. and Serlin, V., private communication.

4. Cabayan, H., Lawrence Livermore National Laboratory, private communication, April 1987.

5. Morgan, C. Grey, "Irradiation and Time Lags," Chapter 7 in J. M. Meek and J. D. Craggs, *Electrical Breakdown of Gases*, Wiley, 1978.

6. Yee, C. L. and Johnston, R. R., "Theoretical Support of Sparse Air Breakdown Experiment," SAIC-U-136-PA, Science Applications International Corporation, Los Altos, CA, 17 November 1988.

7. Birdsall, C. K. and W. B. Bridges, "Space-Charge Instabilities in Electron Diodes and Plasma Convertors," *J. Appl. Phys.*, Vol. 32, No. 12, p. 2611, December 1961.

8. Sullivan, D. J., Kiuttu, G. F., Adler, R., Voss, D., and Walsh, J. E., "Phase I Report: Resonant Vircator Study," AMRC-R-654, Mission Research Corporation, Albuquerque, NM, November 1984.

9. Sullivan, D. J., Walsh, J. E., and Coutsias, E. A., "Virtual Cathode Oscillator (Vircator) Theory," *High-Power Microwave Sources*, (V. L. Granatstein and I. Alexeff, editors), Artech House, p. 441, 1987.

10. Kwan, T. J. T., "High-Power Coherent Microwave Generation from Oscillating Virtual Cathodes," *Phys. Fluids*, Vol. 27, No. 1, p. 228, January 1984.

11. Kwan, T. J. T. and Thode, L. E., "Formation of Virtual Cathodes and Microwave Generation in Relativistic Electron Beams," *Phys. Fluids*, Vol. 27, No. 7, p. 1570, July 1984.

12. Sullivan, D. J., "Final Report of the Millimeter Wave Vircator," AMRC-R-692, Mission Research Corporation, Albuquerque, NM, June 1985.

13. Mahaffey, R. A., et al., "High-Power Microwaves from a Nonisochronic Reflecting Electron System," *Phys. Rev. Lett.*, Vol. 39, No. 13, p. 843, September 26, 1977.

14. Sze, H., Benford, J., Young, T., Bromley, D., and Harteneck, B., "A Radically and Axially Extracted Virtual-Cathode Oscillator (Vircator)," *IEEE Trans. Plasma Sci.*, Vol. PS-13, No. 6, p. 492, December 1985.

15. Thode, L. E., "Virtual-Cathode Microwave Device Research Experiment and Simulation," *High-Power Microwave Sources*, Op. Sit., p. 507, 1987.

16. Van Der Pol, B., "Forced Oscillations in a Circuit with Nonlinear Resistance," *Phil. Mag.*, 3 (13), 1927.

17. Van Der Pol, B., "The Nonlinear Theory of Electrical Oscillations," *Proc. Inst. Radio Eng.*, 22 (9), 1934.

18. Gisler, G., Jones, M. E., and Snell, C. M., "ISIS: A New Code for PIC Plasma Simulations," *Bul. Am. Phys. Soc.* 29, 1208, 1984.

19. Snell, C. M., Sheppard, M. G., and Peratt, A., "CONDO, Conductor Zoning Code for ISIS," memo X-10 (6/86)16, Group X-10, Los Alamos National Laboratory, Los Alamos, NM, 25 June 1986.

20. Snell, C. M., Kwan, T. J. T., Jones, M. E., and Gisler, G., "PEGASUS, Particle-in-Cell Editing, Graphics, and Analysis System for Electromagnetic Particle Codes," Group X-10, Los Alamos National Laboratory, Los Alamos, NM.

21. Arman, M. J., Sullivan, D. J., Godfrey, B. B., Clark, R. E., and Walsh, J., "Analytical Study and Numerical Study of High Power Vircator and Transvertron Microwave Sources," MRC/ABQ-R-1029, Mission Research Corporation, Albuquerque, NM, February 1988.

22. Godfrey, B. B., Sullivan, D. J., and Arman, M. J., "Linear Theory of Transvertron Microwave Sources," SPIE's *Microwave and Particle Beam Sources and Directed Energy Concepts*, Vol. 1061, p. 84, Los Angeles, CA, 16–20 January 1989.

23. Sullivan, D. J., Walsh, J. E., Arman, M. J., and Godfrey, B. B., "Simulation of Transvertron High Power Microwave Sources," SPIE's *Microwave and Particle Beam Sources and Directed Energy Concepts*, Vol. 1061, p. 92, Los Angeles, CA, 16–20 January 1989.

24. Clark, M. C., Marder, B. M., and Bacon, L. D., "Magnetically Insulated Transmission Line oscillator," *Appl. Phys. Lett.* 52, 78, 1988.

25. Rowhein, G., personal communication concerning high power repetitive switching, Sandia National Laboratories, Albuquerque, NM, March 1989.

26. Alme, M. L, Bird, G., Boyer, C., Coffey, S. K., Conte, D., Davis, J. F., Seiler, S. W., Turchi, P. J., Baker, W. L., Degnan, J. H., Hall, D. J., Holmes, J. L., Kriebel, J. B., McCullough, W. F., Price, D. W., Buff, J., Frese, M. H., Peterkin, R. E., Jr., Roderick, N. F., Graham, J. D., and Lopez, E. A., *IEEE Conference Record—Abstracts, Fifteenth IEEE International Conference on Plasma Science*, 6–8 June 1988, Seattle, WA, p. 74, IEEE, New York, NY, 1988.

27. Alme, M. L., Bird, G., Boyer, C., Coffey, S. K., Conte, D., Davis, J. F., Seiler, S. W., Turchi, P. J., Baker, W. L., Degnan, J. H., Hall, D. J., Holmes, J. L., Kriebel, J. B., McCullough, W. F., Price, D. W., Buff, J., Frese, M. H., Peterkin, R. E., Jr., Roderick, N. F., Graham, J. D., and Lopez, E. A., *Proceedings of the Sixth IEEE Pulsed Power Conference*, P. J. Turchi and B. H. Bernstein, eds., 29 June–1 July 1987, Washington, DC, IEEE, New York, NY, 1987.

28. Peterkin, R. E., Jr., Buff, J., Frese, M. H., and Giancola, A. J., "MACH2: A Reference Manual," AMRC-R-851, Mission Research Corporation, Albuquerque, NM, January 1986.

29. Baker, W. L., Bird, G., Buff, J., Boyer, C., Clouse, C. J., Coffey, S. K., Conte, D., Conley, D. W., Davis, J. F., Degnan, J. H., Dietz, D., Frese, M. H., Graham, J. D., Gonzalez, S. L., Hackett, K. E., Hall, D. J., Holmes, J. L., Lopez, E. A., McCullough, W. F., Peterkin, R. E., Jr., Price, D. W., Reinovsky, R. E., Roderick, N. F., Seiler, S., Turchi, P. J., Warren, S. W. R., and Welby, J. M., "QUICK-FIRE Plasma Flow Driven Implosion Experiments," *Digest of Technical Papers: Fifth IEEE Pulsed Power Conference*, M. F. Rose and P. J. Turchi, eds., 10–12 June 1985, Arlington, VA, IEEE, New York, NY, 1985.

30. Baker, W. L., Bird, G., Buff, J., Boyer, C., Clouse, C. J., Coffey, S. K., Conte, D., Conley, D. W., Davis, J. F., Degnan, J. H., Dietz, D., Frese, M. H., Graham, J. D., Gonzalez, S. L., Hackett, K. E., Hall, D. J., Holmes, J. L., Lopez, E. A., McCullough, W. F., Peterkin, R. E., Price, D. W., Reinovsky, R. E., Roderick, N. F., Seiler, S., Turchi, P. J., Warren, S. W. R., and Welby, J. M., "Multi-Megampere Plasma Flow Switch Driven Liner Implosions," *Megagauss Technology and Pulsed Power Applications*, C. M. Fowler, R. S. Caird, and D. J. Erickson, eds., Plenum Press, New York, NY, 1987.

31. Peterkin, R. E., Jr., Buff, J., Frese, M. H., Roderick, N. F., and Payne, S. S., "MACH2 Simulations of Plasma Flow Switches with Shaped Electrodes," *Megagauss Technology and Pulsed Power Applications*, C. M. Fowler, R. S. Caird, and D. J. Erickson, eds., Plenum Press, New York, NY, 1987.

32. Turchi, P. J., Bird, G., Boyer, C., Conte, D., Davis, J., DeRaad, L., Fisher, G., Johnson, L., Latter, A., Seiler, S., Thomas, D., Tsai, W., and Wilcox, T., "Development of Coaxial Plasma Guns for Power Multiplication at High Energy," *Digest of Technical Papers: Third IEEE International Pulsed Power Conference*, T. H. Martin and A. H. Guenther, eds., 1–3 June 1981, Albuquerque, NM, IEEE, New York, NY, 1981.

33. Seiler, S., Davis, J. F., Turchi, P. J., Bird, G., Boyer, C., Donte, D., Crawford, R., DeRaad, L., Fisher, G., Latter, A., Tsai, W., Wilcox, T., "High Current Coaxial Plasma Gun Discharges through Structured Foils," *Digest of Technical Papers: Fourth IEEE Pulsed Power Conference*, M. F. Rose and T. H. Martin, eds., 6–8 June 1983, Albuquerque, NM, IEEE, New York, NY, 1983.

34. Turchi, P. J., "Magnetoacoustic Model for Plasma Flow Switching," *Digest of Technical Papers: Fourth IEEE Pulsed Power Conference*, M. F. Rose and T. H. Martin, eds., 6–8 June 1983, Albuquerque, NM, IEEE, New York, NY, 1983.

35. Ottinger, P. F., Turchi, P. J., Conte, D., and Shipman, J. D., Jr., "Transmission Line Code Modeling of the Plasma Flow Switch," *Digest of Technical Papers: Fifth IEEE Pulsed Power Conference*, M. F. Rose and P. J. Turchi, eds., 10–12 June 1985, Arlington, VA, IEEE, New York, NY, 1985.

36. Brackbill, J. U., "Numerical Magnetohydrodynamics for High-Beta Plasmas," *Methods in Computational Physics*, John Killeen, ed., Academic Press, New York, NY, 1976.

37. Krall, N. A. and Trivelpiece, A. W., *Principles of Plasma Physics*, Chapter 3, San Francisco Press, San Francisco, CA, 1986.

38. Cranfill, C. W., "EOSPAC: A Subroutine Package for Accessing the Los Alamos Sesame EOS Data Library," LA-9728-M, Los Alamos National Laboratory, Los Alamos, NM, August 1983.

39. Holian, K. S., ed., "T-4 Handbook of Material Properties Data Base, Vol. Ic: EOS," LA-10160-MS, Los Alamos National Laboratory, Los Alamos, NM, November 1984.

40. Degnan, J. H., Baker, W. L., Hackett, K. E., Hall, D. J., Holmes, J. L., Kriebel, J. B., Price, D. W., Reinovsky, R. E., Graham, J. D., Lopez, E. A., Alme, M. L., Bird, G., Boyer, C. N., Coffey, S. K., Conte, D., Davis, J. F., III, Seiler, S. W., and Turchi, P. J., "Experimental Results from SHIVA STAR Vacuum Inductive Store/Plasma Flow Switch Driven Implosions," *IEEE Transactions on Plasma Science*, PS-15, 6, 1987.

41. Reinovsky, R. E., Colclaser, R. G., Welby, J. M., and Lopez, E. A., "Energy Storage Transformer Power Conditioning Systems for Megajoule Class Flux Compression Generators," in *Megagauss Technology and Pulsed Power Applications*, Fowler, C. M., Caird, R. S., and Erickson, D. J., eds., Plenum, New York, NY, pp. 575-582, 1987.

42. Kiuttu, G. F., *Time- and Space-Resolved Soft X-Ray Spectroscopy of High Energy Density Plasmas*, Ph.D. dissertation, The University of New Mexico, Albuquerque, NM, 1986.

43. Rand, P. B. and Montoya, O. J., "Molded Ultra-Low Density Microcellular Foams," SAND86-0638, Sandia National Laboratories, Albuquerque, NM, July 1986.

44. Wong, S., Smiley, P., Sheridan, T., Levine, J., and Buck, V., "Balanced Puff Valve For Imploding Gas-Puff Experiments," *Rev. Sci. Instrum.*, Vol. 57, p. 1684, 1986.

45. Frese, M. H., "MACH2: A Two-Dimensional Magnetogydrodynamic Simulation Code For Complex Experimental Configurations," AMRC-R-874, Mission Research Corporation, Albuquerque, NM, in preparation.

46. Hartman, C. W. and Hammer, J. H., "Acceleration of a Compact Torus Plasma Ring, A Proposed Experimental Study," LLL-PROP-191, Appendix H, Lawrence Livermore National Laboratory, Livermore, CA, April 15, 1984.

47. Eddleman, J. L., private communication, June, 1987.

48. Buff, J., Frese, M. H., Giancola, A. J., Peterkin, Jr., R. E., and Roderick, N. F., "Simulations of a Plasma Flow Switch," in *IEEE Transactions on Plasma Science*, PS-15, 6, 1987.

49. Price, D. W., Baker, W. L., Beason, J. D., Degnan, J. H., Hall, D. J., Holmes, J. L., Graham, J. D., Lopez, E. A., Seiler, S. W., and Turchi, P. J., "Enhanced Load Current Delivery from the SHIVA STAR Vacuum Inductive Store/Plasma Flow Switch," *IEEE Transactions on Plasma Science*, PS-16, 4, 1988.

50. Hartman, C. W., and Hammer, J. H., "New Type of Collective Accelerator," *Phys. Rev. Lett.*, Vol. 48, No. 14, p. 929, April 1982.

51. Turner, W. C., Goldenbaum, G. C., Granneman, E. H. A., Hammer, J. H., Hartman, C. W., Prono, D. S., and Taska, J., "Investigations of the Magnetic Structure and the Decay of a Plasma-Gun-Generated Compact Torus," *Phys. Fluids* 26, p. 1965, July 1983.

52. Taylor, J. B., "Relaxation of Toroidal Plasma and Generation of Reverse Magnetic Fields," *Phys. Rev. Lett.* 33, p. 1139, 1974.

53. Frese, M. H. and Bida, T. A., "Task/Milestone Report; Demonstration of the Poloidal Field Capability of MACH2: Compact Toroid Simulations," AMRC-R-973, Mission Research Corporation, Albuquerque, NM, September 1987.

54. Roderick, N. F., "Anomalous Resistivity Considerations for Compact Torus Formation and Decay," MRC/ABQ-N-463, Mission Research Corporation, Albuquerque, NM, March 1990.

55. Milroy, R. D. and Brackbill, J. U. "Toroidal Magnetic Field Generation During Compact Toroid Formation in a Field-Versed Theta Pinch and a Conical Theta Pinch," *Phys. Fluids* 29, p. 1184, April 1986.

56. Alfvén, H., Lindberg, L., and Mitlid, P., *J. Nucl. Energy* 1, 116, 1960.

57. Rosenbluth, M. N., and Bussac, M. N., *Nucl. Fusion* 19, 489, 1979.

58. Hammer, J. H., "Reconnection in Spheromak Formation and Sustainment," UCRL-90109, Lawrence Livermore National Laboratory, Livermore, CA, December 1983.

59. Westerfield, J. M., unpublished.

60. Hall, D. J., unpublished.

61. Adaptable Laboratory Software, "ASYSTANT©," MacMillan Software Company, New York, 1986.

62. Degnan, J. H., Kiuttu, G. F., Richter-Sand, R. J., and Woodall, D. M., "Soft and Ultrasoft X-ray Measurements of Air Force Weapons Laboratory SHIVA Imploding Liner Plasmas," in *Low Energy X-ray Diagnostics*—1981, D. T. Attwood and B. L. Henke (eds.), pp. 264-269, American Institute of Physics, New York, 1981.

63. Woodall, D. M., Degnan, J. H., Kiuttu, G. F., Richter-Sand, R. J., Reinovsky, R. E., and Baker, W. L., "Grazing Incidence Spectrograph Measurements of SHIVA Imploding Liner Radiation Pulse," AFWL-NTYP-TN-80-107, Air Force Weapons Laboratory, Kirtland AFB, NM, 1980.

64. Samson, J. A. R., *Techniques of Vacuum Ultraviolet Spectroscopy*, Wiley, New York, NY, 1967.

65. Peterkin, R. E., Jr., "Compact Toroid Simulations with MACH2," MRC/ABQ-R-1130, Mission Research Corporation, Albuquerque, NM, December 1988.

66. Peterkin, R. E., Jr., Buff, J., Frese, M. H., Roderick, N. F., Clouse, C. J., Dietz, D., Hackett, K. E., Rowley, J. E., and Sovinec, C. R., *IEEE Conference Record—Abstracts, 1988 IEEE International Conference on Plasma Science*, 6–8 June, 1988, Seattle, WA, pp. 67–68, IEEE, New York, NY, 1988.

67. Peterkin, R. E., Jr., Buff, J., Frese, M. H., and Giancola, A. J., "MACH2: A Reference Manual—Third Edition," MRC/ABQ-R-1066, Mission Research Corporation, Albuquerque, NM, May 1988.

68. Chodura, R., *Nucl. Fus.* 15, p. 55, 1975.

69. Davidson, R. C., and Krall, N. A., *Nucl. Fus.* 17 (6) 1977.

70. Krall, N. A., "Low-Frequency Stability for Field Reversed Configuration Parameters," *Phys. Fluids* 30 (3), p. 878, 1987.

71. Perlstein, L. D. and Berk, H. L., *Phys. Rev. Lett.* 23, p. 220, 1969.

72. Davidson, R. C., Gladd, M. T., and Goren, Y., *Phys. Fluids* 21 (6), p. 992, 1978.

73. Gladd, M. T., and Krall, N. A., *Phys. Fluids* 29 (5), p. 1640, 1986.

74. Hoida, H. W., Barnes, C. W., Henins, I., Jarboe, T. R., Marklin, G., Buchenauer, C. J., and Knox, S. O., in *Proceedings of the 12th European Conference on Controlled Fusion and Plasma Physics*, European Physical Society, Vol. 9F, Part 1, p. 643, Petit-Lancy, Switzerland, 1985.

75. Jarboe, T. R., *Bull. Am. Phys. Soc.* 34, p. 1960, 1989.

76. Mayo, R. M., Choi, C. K., Levinton, F. M., Janos, A. C., and Yamada, M., *Phys. Fluids B* 2 (1), p. 115, 1990.

77. Degnan, J. H., Baker, W. L., Holmes, J. L., Price, D. W., Cowan, M., Graham, J. D., Lopez, E. A., and Roderick, N. F., *Fifth International Conference on Megagauss Magnetic Field Generation and Related Topics*, 3–7 July, 1989, Novosibirsk, Conference Proceedings (in press).

78. Kaye, R., Cnare, E. C., Cowan, M., Burgess, T., and Woodall, D. M., *IEEE Conference Record—Abstracts, Eighth IEEE International Conference on Plasma Science*, 18–20 May, 1981, Santa Fe, NM, pp. 62-63, IEEE, New York, NY, 1981.